

**CATALYTIC HYDROCRACKING OF WASTE
VEGETABLE OIL OVER TRANSITION METAL-BASED
CATALYSTS: SELECTIVE PRODUCTION OF JET FUEL
RANGE ALKANES**

Keldon Moodley

[BSc. (Eng)]

A dissertation submitted in the
School of Chemical Engineering
University of KwaZulu-Natal
Durban

In fulfilment of the requirements for the degree of
Master of Science in Engineering

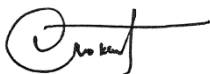
December, 2015

Supervisor: Dr. D. Lokhat

EXAMINER'S COPY

DECLARATION


As the candidate's Supervisor I agree to the submission of this dissertation for the degree of Master of Science in Chemical Engineering:



Dr. D. Lokhat

I, Keldon Moodley (Student number: 210501720) declare that

- (i) The research reported in this dissertation, except where otherwise indicated, is my original work.
- (ii) This dissertation has not been submitted for any degree or examination at any other university.
- (iii) This dissertation does not contain other persons' data, pictures, graphs or other information, unless specifically acknowledged as being sourced from other persons.
- (iv) This dissertation does not contain other persons' writing, unless specifically acknowledged as being sourced from other researchers. Where other written sources have been quoted, then:
 - a) their words have been re-written but the general information attributed to them has been referenced;
 - b) where their exact words have been used, their writing has been placed inside quotation marks, and referenced.
- (v) Where I have reproduced a publication of which I am an author, co-author or editor, I have indicated in detail which part of the publication was actually written by myself alone and have fully referenced such publications.
- (vi) This dissertation does not contain text, graphics or tables copied and pasted from the Internet, unless specifically acknowledged, and the source being detailed in the dissertation and in the References sections.

Signed: 

Date: 06/12/2015

Acknowledgements

First and foremost, I would like to thank my supervisor, Dr. David Lokhat, for providing this opportunity, and thereafter, sacrificing his time to share his knowledge, and offer support and guidance throughout this year.

I want to express my sincere thanks to my family, especially my parents, Dan and Ragani Moodley, both of whom always supported and encouraged me. Your love and care are greatly appreciated.

I would like to thank the technical staff, Mr. Danny Singh, Nomthandazo (Xoli) Hadebe and Thobekile Mofokeng of the Chemical Engineering Department of the University of KwaZulu-Natal. Your assistance throughout the year is immensely appreciated.

Lastly, I wish to thank my friends and colleagues, Eldon Naidoo, Janine Govender, Sasha Jadoo, Keroshan Govender and Bradley Paul for the help, support and advice during this work.

Abstract

The performance of transition metal-based catalysts on amorphous supports has been investigated for the high pressure (120 bar) hydrocracking of waste vegetable (cooking) oil in a fixed-bed tubular reactor between 400–450 °C. The study focused on the effect of the operating parameters (reaction temperature, type of transition metal catalyst and amorphous support, the sulphided state of the catalyst and the use of regenerated catalyst) on the yield of transportation fuel n-alkanes (C₅–C₁₈), and the primary product, kerosene (jet fuel) range n-alkanes using the One-Variable-At-A-Time approach. The objectives included characterising the feedstock and catalysts, determining the optimum catalyst and operating conditions to produce kerosene range n-alkanes and to estimate activation energies through a reaction kinetic study. Comparative studies of the results from commercially produced Ru/Al₂O₃ and Ni/Al₂O₃ catalysts and laboratory prepared Ni-Mo/SiO₂ and Co-Mo/SiO₂ were undertaken.

All tested catalysts were effective in achieving kerosene range n-alkanes in the liquid product while achieving oil conversions > 62 wt.%. While the laboratory catalysts only had liquid and gas products, the commercial catalysts also had a waxy residue product indicating a lower hydrotreating activity on the metallic sites. Furthermore, both laboratory catalysts had higher n-alkane yields indicating a higher activity for hydrocracking reactions on the acidic sites on the SiO₂ than the acidic sites on the Al₂O₃ support.

The best yield of kerosene range n-alkanes obtained from the experimental design was 5.84 wt.% using the fresh Ni-Mo/SiO₂ catalyst at 450 °C, with an oil conversion of 90.32 wt.%. An increase in oil conversion and liquid n-alkane products with an increase in reaction temperature for all tested catalysts indicated that hydroprocessing (hydrotreating and hydrocracking) reactions are favoured at higher temperatures. Furthermore, sulphiding the catalyst prior to use was found to greatly increase the catalyst activity in promoting hydroprocessing reactions.

Results from the use of regenerated catalysts show a small decrease in the yield of kerosene range n-alkanes when compared to the corresponding fresh catalyst. This suggests that regeneration of the spent catalyst and subsequent re-use may be a feasible option. A simple kinetic model of the hydroprocessing reactions was developed and kinetic parameters were identified by regression of the experimental data. The regenerated Ni/Al₂O₃ catalyst had the lowest estimated activation energy of 14.37 kJ/mol, while the fresh Ni-Mo/SiO₂ catalyst had the highest estimated activation energy of 51.75 kJ/mol from the studied catalysts.

Research outputs

Moodley, K., Govender, K., Kiambi, S.L. and Lokhat, D., “Catalytic hydrocracking of waste vegetable oil using a high pressure flow apparatus to obtain jet fuel range alkanes”, ICCBES, Kyoto, Japan, 7th-9th May 2015, pp. 922-929

Table of contents

List of figures	xii
List of tables	xvii
List of schemes	xxi
Nomenclature	xxii
Chapter 1 Introduction	1
1.1 Background	1
1.1.1 An alternative source of transportation fuel	2
1.1.2 Biofuels from waste vegetable (plant) oil	3
1.1.2.1 Hydroprocessing reactions	4
1.1.2.2 Hydroprocessing catalysts	4
1.1.3 The focus on aviation fuel	5
1.2 Significance of the study	6
1.2.1 Research aims	6
1.2.2 Research objectives	6
1.3 Report overview	7
Chapter 2 Literature review	9
2.1 Origin and early development of hydrocracking reactions	9
2.2 Current biofuel production processes	10

2.2.1 The Fischer-Tropsch synthesis of biomass	10
2.2.2 Conversion of carbohydrates to liquid fuels	11
2.2.3 Bio-Synfining process for synthetic paraffinic kerosene production	12
2.2.4 UOP LLC's green jet and diesel biofuels	13
2.3 Renewable sources for biofuels production	13
2.3.1 Vegetable oil as a feedstock	14
2.3.2 Investigation of used cooking oil as a feedstock	15
2.4 Reaction mechanisms for catalytic hydrotreating of liquid biomass	18
2.4.1 Saturation reactions	19
2.4.2 Hydrocracking	20
2.4.3 Heteroatom removal	21
2.4.4 Isomerisation reactions	24
2.4.5 Other proposed reaction mechanisms for hydroprocessing triglycerides	25
2.5 Reaction Kinetics	28
2.6 Hydroprocessing catalysts	29
2.6.1 Catalyst preparation	31
2.6.1.1 Drying	32
2.6.1.2 Calcination	32
2.6.2 Catalyst supports	32
2.6.3 Catalyst characterisation	32
2.6.3.1 BET Surface area measurements – BET method	33
2.6.3.2 Energy dispersive X-ray analysis	33
2.6.4 Catalyst pre-sulphiding	34
2.6.4.1 In situ sulphiding	34
2.6.5 Coke formation and regeneration	35
2.7 Hydroprocessing operating parameters	36
2.7.1 Reaction temperature	36
2.7.2 Hydrogen partial pressure	36

2.7.3 Hydrogen feed-rate	36
2.7.4 Liquid hourly space velocity	36
Chapter 3 Experimental design	39
3.1 One-Variable-At-A-Time (OVAT) method	39
3.2 Randomisation and replication	41
Chapter 4 Experimental equipment	42
4.1 Experimental equipment overview	42
4.2 The lab-scale hydrocracking apparatus	45
4.2.1 Oil feed storage tank	45
4.2.2 Oil feed pump	45
4.2.3 Reactor and electric furnace	46
4.2.4 The catalyst and packing material	47
4.2.5 Metering valve and collection vessels	48
4.2.6 Bubble flow meter	49
4.2.7 Gas analyser	50
4.2.8 The centrifuge	50
4.2.9 Gas chromatograph mass spectrometer	51
Chapter 5 Experimental methods	54
5.1 Catalyst preparation	54
5.1.1 Preparation of the Mo/SiO ₂ catalyst	54
5.1.2 Preparation of the Ni-Mo/SiO ₂ catalyst	55
5.1.3 Preparation of the Co-Mo/SiO ₂ catalyst	55
5.2 Catalyst chemical check for metal loading	56

5.2.1 Chemical check on Mo loading	56
5.2.2 Chemical check on Ni and Co loading	56
5.3 Catalyst characterisation	56
5.3.1 BET surface area analysis	56
5.3.2 Energy dispersive X-ray analysis	57
5.4 Catalyst loading and pre-treatment	57
5.5 Materials and operating procedure for the hydrocracking of waste vegetable oil	58
5.6 Product analysis	59
5.6.1 Mass of products	59
5.6.2 Product separation	59
5.6.3 Production identification and quantification (GCMS analysis)	60
5.7 Feed analysis	63
5.8 Catalyst regeneration	64
Chapter 6 Results and discussion	65
6.1 Results for preliminary experimental tests: Troubleshooting	65
6.1.1 Packing material	66
6.1.2 System pressure	66
6.1.3 Reaction temperature range	67
6.1.4 Liquid hourly space velocity	67
6.1.5 Catalyst sulphiding	67
6.2 Results for the hydroprocessing of waste cooking oil	68
6.2.1 Results for experiments using commercially produced fresh Ru/Al ₂ O ₃ catalyst	68
6.2.2 Results for experiments using commercially produced fresh Ni/Al ₂ O ₃ catalyst	73

6.2.3 Comparative study on the performance of the commercially produced fresh Ru/Al ₂ O ₃ and Ni/Al ₂ O ₃ catalysts in the hydroprocessing of waste cooking oil	76
6.2.4 Results for experiments using laboratory prepared fresh Ni-Mo/SiO ₂ catalyst	78
6.2.5 Results for experiments using laboratory prepared fresh Co-Mo/SiO ₂ catalyst	82
6.2.6 Comparative study on the performance of the laboratory prepared fresh Ni-Mo/SiO ₂ and Co-Mo/SiO ₂ catalysts in the hydroprocessing of waste cooking oil	86
6.2.7 Comparative study on the performance of the commercially produced fresh Ni/Al ₂ O ₃ and the laboratory prepared fresh Ni-Mo/SiO ₂ catalysts in the hydroprocessing of waste cooking oil	88
6.2.8 Results for experiments using commercially produced regenerated Ru/Al ₂ O ₃ catalyst	89
6.2.9 Results for experiments using commercially produced regenerated Ni/Al ₂ O ₃ catalyst	92
6.2.10 Comparative study of the performance of the commercially produced regenerated Ru/Al ₂ O ₃ and Ni/Al ₂ O ₃ catalysts in the hydroprocessing of waste cooking oil	96
6.2.11 Comparative study of the performance of the commercially produced fresh and regenerated Ru/Al ₂ O ₃ catalysts in the hydroprocessing of waste cooking oil	97
6.2.12 Comparative study of the performance of the commercially produced fresh and regenerated Ni/Al ₂ O ₃ catalysts in the hydroprocessing of waste cooking oil	98
6.3 Reaction kinetic study	99

Chapter 7 Conclusion and recommendations	105
References	107
Appendix A Pump calibration	114
A.1 Pump calibration flow rate test	114
A.2 Pump calibration time test	115
Appendix B Catalyst characterisation	116
B.1 Laboratory prepared catalysts	116
B.2 Commercially produced catalysts	117
Appendix C Waste cooking oil characterisation	119
Appendix D Sample calculations	120
D.1 Catalyst preparation calculations	120
D.2 Experimental analysis calculations	123
D.3 Reaction kinetic calculations	127
Appendix E Experimental data	130
Appendix F Calculated data	137

List of figures

Chapter 1

Figure 1-1 World crude oil consumption	1
Figure 1-2 Shell's world energy consumption outlook	2
Figure 1-3 Production of liquid fuels from biomass	3
Figure 1-4 Conventional production process of kerosene and other products	5

Chapter 2

Figure 2-1 Biomass to biofuel conversion via Fischer-Tropsch synthesis	11
Figure 2-2 Schematic representation of the reactor sequence and proposed chemistry to produce constituents of liquid transportation fuels from catalytic processing of sugars and polyols	12
Figure 2-3 Syntroleum's Bio-Synfining TM process	13
Figure 2-4 Chemical structure of triglyceride	14
Figure 2-5 Total ion chromatogram of the derivatised UCO	16
Figure 2-6 Diesel yield of hydrocracking fresh and used cooking oil	18
Figure 2-7 Reaction pathways for the conversion of triglycerides to alkanes	19
Figure 2-8 Schematic representation of the two different pathways for removal oxygen from triglyceride by hydrotreating	22
Figure 2-9 Heteroatom removal percent via hydrocracking of fresh and used cooking oil at three reaction temperatures	24
Figure 2-10 Expected mechanism of the simultaneous catalytic cracking and hydrogenation of palm oil over zeolite catalyst to produce nonane	25
Figure 2-11 Reaction pathways for hydroprocessing of triglycerides	27
Figure 2-12 Schematic diagram of the batch reactor	28

Figure 2-13 Typical hydrotreating catalysts a) before use and b) after use	31
Figure 2-14 Actual and predicted carbon formation on $\text{Al}_2\text{O}_3/\text{SiO}_2$ catalyst from cracking of n-hexadecane at 500 °C	36

Chapter 4

Figure 4-1 Scheme 1 of the experimental setup piping and instrumentation diagram	43
Figure 4-2 Scheme 2 of the experimental setup piping and instrumentation diagram	44
Figure 4-3 Waste vegetable oil storage tank	45
Figure 4-4 BECKMAN model 110A pump	46
Figure 4-5 Tubular reactor and opened clam shell electric furnace	46
Figure 4-6 Catalyst pellets	47
Figure 4-7 Glass beads used for packing	47
Figure 4-8 Schematic cross-sectional view of the tubular reactor	48
Figure 4-9 Glass product collection vessel	48
Figure 4-10 Bubble flow meter	49
Figure 4-11 MRU Vario Plus Gas Analyser	50
Figure 4-12 Centrifuge for product separation	51
Figure 4-13 2010 SHIMADZU GCMS-QP	51
Figure 4-14 Example TIC (Liquid product from experiment at 450 °C using fresh $\text{Ni}/\text{Al}_2\text{O}_3$ catalyst)	53

Chapter 5

Figure 5-1 Micrometrics ASAP 2020 gas adsorption analyser	57
Figure 5-2 ZEISS Ultra Plus Scanning Election Microscope	57
Figure 5-3 Separated liquid and wax product	60

Figure 5.4 GCMS temperature program for product analysis	61
Figure 5-5 GCMS temperature program for feedstock analysis	63

Chapter 6

Figure 6-1 Product yields for experiments over fresh Ru/Al ₂ O ₃ catalyst at different temperatures	69
Figure 6-2 Composition of the liquid obtained from experiments over fresh Ru/Al ₂ O ₃ catalyst at different temperatures	71
Figure 6-3 Yield of liquid n-alkanes in the transportation fuel range for experiments over fresh Ru/Al ₂ O ₃ catalyst at different temperatures	71
Figure 6-4 Product yields for experiments over fresh Ni/Al ₂ O ₃ catalyst at Different temperatures	74
Figure 6-5 Composition of the liquid obtained from experiments over fresh Ni/Al ₂ O ₃ catalyst at different temperatures	74
Figure 6-6 Yield of liquid n-alkanes in the transportation fuel range for experiments over fresh Ni/Al ₂ O ₃ catalyst at different temperatures	75
Figure 6-7 Oil conversion and liquid n-alkane product distribution for experiments over fresh Ru/Al ₂ O ₃ catalyst at different temperatures	76
Figure 6-8 Oil conversion and liquid n-alkane product distribution for experiments over fresh Ni/Al ₂ O ₃ catalyst at different temperatures	77
Figure 6-9 Product yields for experiments over fresh Ni-Mo/SiO ₂ catalyst at different temperatures	79
Figure 6-10 Composition of the liquid obtained from experiments over fresh Ni-Mo/SiO ₂ catalyst at different temperatures	81
Figure 6-11 Yield of liquid n-alkanes in the transportation fuel range for experiments over fresh Ni-Mo/SiO ₂ catalyst at different temperatures	81

Figure 6-12 Product yields for experiments over fresh Co-Mo/SiO ₂ catalyst at different temperatures	84
Figure 6-13 Composition of the liquid obtained from experiments over fresh Co-Mo/SiO ₂ catalyst at different temperatures	85
Figure 6-14 Yield of liquid n-alkanes in the transportation fuel range for experiments over fresh Co-Mo/SiO ₂ catalyst at different temperatures	85
Figure 6-15 Oil conversion and liquid n-alkane product distribution for experiments over fresh Ni-Mo/SiO ₂ catalyst at different temperatures	87
Figure 6-16 Oil conversion and liquid n-alkane product distribution for experiments over fresh Co-Mo/SiO ₂ catalyst at different temperatures	87
Figure 6-17 Product yields for experiments over regenerated Ru/Al ₂ O ₃ catalyst at different temperatures	91
Figure 6-18 Composition of the liquid obtained from experiments over regenerated Ru/Al ₂ O ₃ catalyst at different temperatures	91
Figure 6-19 Yield of liquid n-alkanes in the transportation fuel range for experiments over regenerated Ru/Al ₂ O ₃ catalyst at different temperatures	92
Figure 6-20 Product yields for experiments over regenerated Ni/Al ₂ O ₃ catalyst at different temperatures	94
Figure 6-21 Composition of the liquid obtained from experiments over regenerated Ni/Al ₂ O ₃ catalyst at different temperatures	94
Figure 6-22 Yield of liquid n-alkanes in the transportation fuel range for experiments over regenerated Ni/Al ₂ O ₃ catalyst at different temperatures	95
Figure 6-23 Oil conversion and liquid n-alkane product distribution for experiments over regenerated Ru/Al ₂ O ₃ catalyst at different temperatures	96
Figure 6-24 Oil conversion and liquid n-alkane product distribution for experiments over regenerated Ni/Al ₂ O ₃ catalyst at different temperatures	96
Figure 6-25: Linearized Arrhenius plots for the commercially produced fresh Ru/Al ₂ O ₃ and Ni/Al ₂ O ₃ catalysts	101

Figure 6-26: Linearized Arrhenius plots for the laboratory prepared fresh Ni-Mo/SiO ₂ and Co-Mo/SiO ₂ catalysts	102
Figure 6-27: Linearized Arrhenius plots for the commercially produced regenerated Ru/Al ₂ O ₃ and Ni/Al ₂ O ₃ catalysts	102

List of tables

Chapter 2

Table 2-1 Chemical structure of common fatty acids	14
Table 2-2 Fatty acid composition of various vegetable oils	15
Table 2-3 Linear equation, r-squared value and response factor for each component in the UCO sample	16
Table 2-4 Composition of fatty acids in UCO	17
Table 2-5 Fatty acid composition in UCO	17
Table 2-6 Properties of fresh and used cooking oil	23
Table 2-7 Strength of hydrogenation and hydrocracking function in dual-functional catalyst	30
Table 2-8 Typical adsorption temperatures for gases used in surface area Measurements	33
Table 2-9 Carbon formation as a function of particle size	36

Chapter 3

Table 3-1 Layout for experimental runs	40
--	----

Chapter 4

Table 4-1 Product analysis column characteristics and detector type	52
Table 4-2 Feed analysis column characteristics and detector type	52

Chapter 5

Table 5-1 Temperature program for liquid product analysis	60
---	----

Table 5-2 Relative Molar Response factors for different alkanes using xylene as the reference	62
Table 5-3 Temperature program for feed waste vegetable oil analysis	63

Chapter 6

Table 6-1 Product distribution & oil conversion for experiments over fresh Ru/Al ₂ O ₃ catalyst	69
Table 6-2 Product distribution & oil conversion for experiments over fresh Ni/Al ₂ O ₃ catalyst	73
Table 6-3 Product distribution & oil conversion for experiments over fresh Ni-Mo/SiO ₂ catalyst	78
Table 6-4 Product distribution & oil conversion for experiments over fresh Co-Mo/SiO ₂ catalyst	83
Table 6-5 Product distribution & oil conversion for experiments over regenerated Ru/Al ₂ O ₃ catalyst	90
Table 6-6 Product distribution & oil conversion for experiments over regenerated Ni/Al ₂ O ₃ catalyst	93
Table 6-7 Data obtained from the linearized Arrhenius plots	103

Appendix A

Table A-1 Results from pump calibration flow rate test	114
Table A-2 Results from pump calibration time test	115

Appendix B

Table B-1 BET surface area and Energy dispersive X-ray analysis results	116
Table B-2 Composition of Fe-Mo precursor from supplier	117
Table B-3 Composition of CoSO ₄ precursor from supplier	117
Table B-4 Ru/Al ₂ O ₃ characterisation data	117

Table B-5 Ni/Al ₂ O ₃ characterisation data	118
---	-----

Appendix C

Table C-1 Composition of waste cooking oil from GCMS analysis	119
---	-----

Appendix D

Table D-1 Molar flow rate of feed oil constituents	128
--	-----

Appendix E

Table E-1 Experimental data for fresh Ru/Al ₂ O ₃ catalyst	131
Table E-2 Experimental data for fresh Ni/Al ₂ O ₃ catalyst	132
Table E-3 Experimental data for fresh Ni-Mo/SiO ₂ catalyst	133
Table E-4 Experimental data for fresh Co-Mo/SiO ₂ catalyst	134
Table E-5 Experimental data for regenerated Ru/Al ₂ O ₃ catalyst	135
Table E-6 Experimental data for regenerated Ni/Al ₂ O ₃ catalyst	136

Appendix F

Table F-1 Calculated data at three reaction temperatures independent of catalysts	137
Table F-2 Calculated data for fresh Ru/Al ₂ O ₃ at 400 °C	138
Table F-3 Calculated data for fresh Ru/Al ₂ O ₃ at 425 °C	139
Table F-4 Calculated data for fresh Ru/Al ₂ O ₃ at 450 °C	140
Table F-5 Calculated data for fresh Ni/Al ₂ O ₃ at 400 °C	141
Table F-6 Calculated data for fresh Ni/Al ₂ O ₃ at 425 °C	142
Table F-7 Calculated data for fresh Ni/Al ₂ O ₃ at 450 °C	143

Table F-8 Calculated data for fresh NiMo/SiO ₂ at 400 °C	144
Table F-9 Calculated data for fresh NiMo/SiO ₂ at 425 °C	145
Table F-10 Calculated data for fresh NiMo/SiO ₂ at 450 °C	146
Table F-11 Calculated data for fresh CoMo/SiO ₂ at 400 °C	147
Table F-12 Calculated data for fresh CoMo/SiO ₂ at 425 °C	148
Table F-13 Calculated data for fresh CoMo/SiO ₂ at 450 °C	149
Table F-14 Calculated data for regenerated Ru/Al ₂ O ₃ at 400 °C	150
Table F-15 Calculated data for regenerated Ru/Al ₂ O ₃ at 425 °C	151
Table F-16 Calculated data for regenerated Ru/Al ₂ O ₃ at 450 °C	152
Table F-17 Calculated data for regenerated Ni/Al ₂ O ₃ at 400 °C	153
Table F-18 Calculated data for regenerated Ni/Al ₂ O ₃ at 425 °C	154
Table F-19 Calculated data for regenerated Ni/Al ₂ O ₃ at 450 °C	155
Table F-20 Calculated kinetic data	156

List of schemes

Chapter 2

Scheme 2-1 Saturation reaction of unsaturated carboxylic acid	19
Scheme 2-2 Conversion of cyclohexene to cyclohexane through hydrotreating reactions	20
Scheme 2-3 Conversion of benzene to cyclohexene through hydrotreating reactions	20
Scheme 2-4 Hydrocracking a triglyceride to form a fatty acid and propane	21
Scheme 2-5 Cracking reaction during hydroprocessing of pyrolysis oils	21
Scheme 2-6 Cracking reaction of long chain paraffins to smaller chain ones	21
Scheme 2-7 Deoxygenation reaction during hydroprocessing	22
Scheme 2-8 Decarbonylation reaction during hydroprocessing	22
Scheme 2-9 Decarboxylation reaction during hydroprocessing	22
Scheme 2-10 Examples of isomerisation reactions	24

Nomenclature

Notation	Description	Unit
A	Pre-exponential factor	$\text{m}^6/\text{mol/g/s}$
C_{io}	Initial concentration of species i	mol/m^3
C_i	Exit concentration of species i	mol/m^3
E_a	Activation energy	kJ/mol
F_{io}	Initial molar flow rate of species i	mol/min
F_i	Final molar flow rate of species i	mol/min
k	Reaction rate constant	$\text{m}^6/\text{mol/g/s}$
k'	Arbitrary constant	-
k''	Arbitrary constant	-
LHSV	Liquid hourly space velocity	$1/\text{hr}$
m_i	Mass of species i	g
\dot{m}_i	Mass flow rate of species i	g/min
n_i	Moles of species i	mole
\dot{n}_i	Molar flow rate of species i	mol/min
P	Pressure	Bar, Pa
\dot{q}_i	Gas volumetric flow rate of species i	m^3/min
R	Gas constant	J/mol/K
r_i	Reaction rate with respect to species i	mol/g/s
RMR_i	Relative molar response factor of species i	-
T	Temperature	$^{\circ}\text{C, K}$
t	Time	s, min, hr
\dot{V}_i	Liquid volumetric flow rate of species i	ml/min
W	Mass of catalyst	g
x_i	Mass fraction of species i	-
Greek letters		
ρ_i	Density of species i	g/ml

Chapter 1

Introduction

1.1 Background

Since its inception, transportation fuel production has relied heavily on crude oil as its raw material. However, as the reserve of crude oil is diminishing and the energy demand to meet the growth of the economy and population is persistently increasing, the price of fossil-based fuels will continually rise. Figure 1-1 shows the world consumption of crude oil from 1980 to 2012 in thousands of barrels per day. It can be seen that approximately 60 million barrels were used per day in 1980, while by 2012, that number increased to approximately 90 million barrels per day. The overall trend indicates a growing demand on crude oil as the raw material for energy products around the world, with transportation fuels being one of the largest consumers.

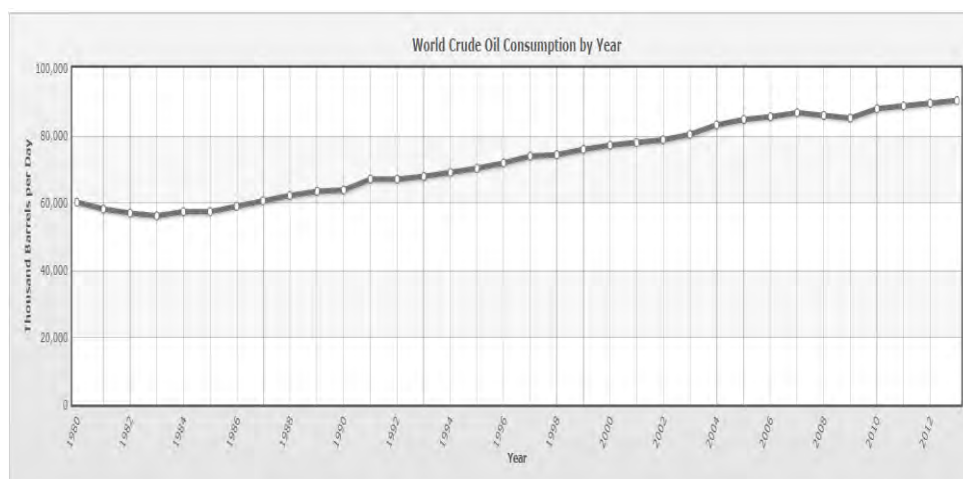


Figure 1-1 World crude oil consumption (Peng, 2012)

Furthermore, the combustion of fossil fuels and its derivatives result in severe environmental implications such as global warming (caused by the emission of the greenhouse gas carbon dioxide) and acid rain (related with NO_x and SO_x emissions) (Van Gerpen, 2005). In addition,

numerous governments are enforcing rigid regulations against harmful emissions from the burning of fossil fuels and their derivatives. These governments are also establishing policies which provide full and/or partial tax exemptions to large corporations and individuals as an incentive to promote the utilization of sustainable fuels. The European Union (EU) has set a target that 10% of the total transportation fuels will be biofuels by 2020 (Peng, 2012). As a result of the aforementioned facets, the investigation into an alternative source of transportation fuel has become compulsory in recent years.

1.1.1 An alternative source of transportation fuel

Over the past decade, many researchers have concentrated their efforts on developing biofuels from alternative and renewable sources to replace the large dependency on transportation fuels derived from crude oil. The efficient utilization of biomass (material derived from living or recently living organisms) for the production of transportation fuels is becoming increasingly important and necessary. Biofuels have the potential to contribute toward a large portion of the demand for transportation fuels, consequently reducing the current demand from crude oil derivatives. A ripple effect will be an increase in the preservation of crude oil as its depletion rate would decrease. Furthermore, there would be a reduction in the negative environmental impact as the combustion of biofuels has a neutral carbon dioxide balance, which would reduce the rate of global warming. The use of transportation biofuels can also improve rural environments, generate jobs and reduce the dependency on imported fuels (Sotelo-Boyás et al, 2008). Shell, one of the six oil and gas “supermajors” performed a study to predict the world’s energy consumption by the year 2050, the results of which are shown in Figure 1-2. While the prediction indicates that oil, gas and coal will still be the major contributors to the world’s energy supply, the energy supplied from biomass and other renewable sources will significantly increase.

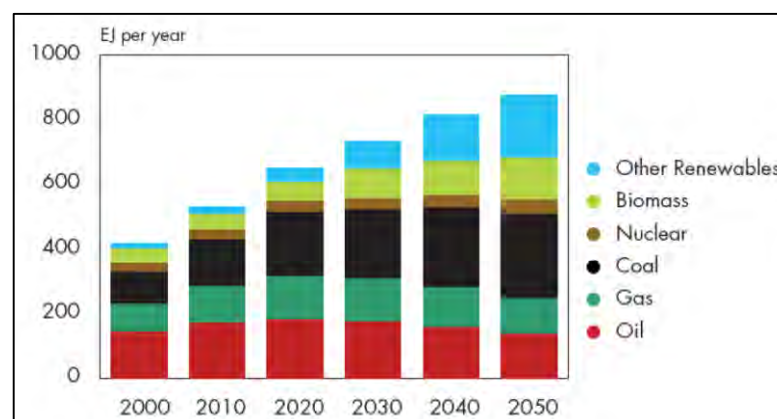


Figure 1-2 Shell’s world energy consumption outlook (Peng, 2012)

There are three types of processes that can currently be employed for the production of liquid fuels from biomass (Figure 1-3). The first process requires gasification of the biomass to produce

syngas, which is followed by the Fischer-Tropsch synthesis to produce alkanes. The second process utilizes pyrolysis and thermochemical liquefaction to produce bio-oils, which are subsequently further refined to produce alkanes. The last process employs hydrolysis of lignocellulose for sugar monomer production, which is further converted into ethanol and/or aromatic hydrocarbons through fermentation and/or dehydration (Huber and Dumesic, 2006).

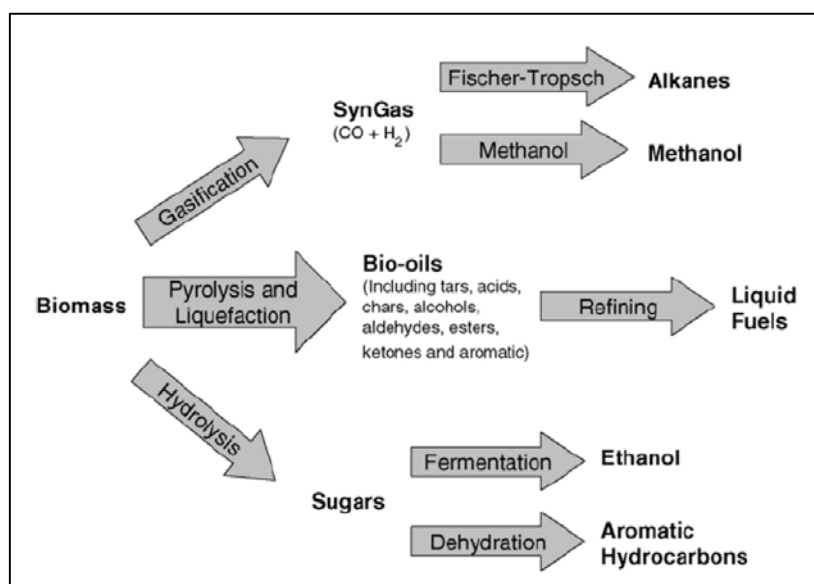


Figure 1-3 Production of liquid fuels from biomass (Peng, 2012)

Biomass can be classified according to the content of different carbohydrate and aromatic polymers (cellulose, hemicellulose and lignin) and other constituents such as starch, protein and oil. Most often, derivatisation and an analysis using HPLC is used to carry out this classification. Vegetable oils contain most of these constituents, however, in limited quantities. They are also more expensive than lignocellulosic biomass. However, biodiesel produced from transesterification of vegetable oils dominates 80% of the current biofuels market in Europe due to efficient conversion of triglycerides (Bendz, 2005). This suggests a major potential in vegetable oil as a feedstock for transportation fuels (not just biodiesel but aviation fuel and gasoline) and as such serves as a motivation for this study.

1.1.2 Biofuels from waste vegetable (plant) oil

While the possibility of producing biofuels from vegetable oils is very real, it needs to be remembered that these oils already serve other large commercial markets; most notably the health and beauty market (for repairing and rejuvenating hair and skin) and the food industry. Therefore, producing biofuels from fresh vegetable oil might solve one problem, but consequently cause prices to increase in other markets as the demand for these oils increases. Therefore, it was necessary to investigate yet another possibility; the production of biofuels from used/waste vegetable oil such as cooking oil. Even after multiple uses, the constituents of the cooking oil do

not change significantly, with an exception to increased heterogeneous food particulate matter and the oil becoming less hydrophobic. Thus, once thoroughly filtered, used cooking oil can be utilized as the feedstock in the production of biofuels. The major advantages being that the fresh vegetable oil supply and demand is not affected, and the cost of used cooking oil is substantially cheaper than its fresh counterpart.

1.1.2.1 Hydroprocessing reactions

Currently, the most successful type of biofuel production is biodiesel, which is produced from plant oils and/or animal fats. The process involves liquid-phased catalysed transesterification at low temperature. However, large investments are required for the production units in order to ensure high efficiency (Knothe, 2005).

Recent studies have investigated an alternative method for processing plant oils and animal fats into biofuels by using a catalytic hydrotreating process similar to the processes in the oil and gas industry (Huber et al, 2007). There are two main chemical steps that occur during the conversion of biomass-derived oils into biofuel products: oxygen removal (hydrodeoxygenation, hydrodecarbonylation and hydrodecarboxylation) and hydrocracking. The oxygen removal and the breakdown of carbon double or triple bonds is referred to as hydrotreating while the breaking of large carbon chains into smaller ones is referred to as hydrocracking. The two processes are included in a larger group of processes termed hydroprocessing (Rahmes, 2004).

1.1.2.2 Hydroprocessing catalysts

The hydroprocessing of vegetable oils and/or animal fats requires a dual function catalyst composed of a metallic portion and amorphous mixed oxides of acidic nature or proton exchanged crystalline zeolites. The metallic sites promote hydrogenation and dehydrogenation reactions while the acid sites promote isomerization and cracking reactions. This emphasises the need to design a catalyst which incorporates a balance between the metal composition and acidic sites to tailor the product selectivity, catalyst activity and stability (Morel et al, 1997).

Recent studies have identified two types of catalysts that are effective for hydroprocessing vegetable oils into biofuels: supported noble metal catalysts (most notably Palladium and Platinum) (Mäki-Arvela et al, 2011) and sulphided bimetallic catalysts on inert supports (usually Mo- or W-based sulphides promoted with Ni or Co supported on Al_2O_3 , SiO_2 or an $\text{Al}_2\text{O}_3/\text{SiO}_2$ combination) (da Rocha Filho et al, 1993). However, the major disadvantages of noble metal catalysts are the rarity and high price, making it an economically unfeasible option, as well as their susceptibility to catalyst poisons (Maxwell, 1987). Impurities (such as sulphur, heavy metals and oxygenated compounds) in the feedstock can cause severe catalyst deactivation (Choudhary

and Saraf, 1975). As such, a pre-hydroprocessing step is required to remove impurities from the feedstock which requires additional resources and time.

The conventional supported sulphided bimetallic catalysts as presently used for desulphurization of fossil diesel streams have high energy consumption rates as they need to be operated under high temperature and pressure, and consume a large amount of hydrogen (Egeberg and Knudsen, 2011). Majority of the products obtained over these catalysts are n-paraffins (n-C₁₅ – n-C₁₈) which solidify at low temperatures, so they are not suitable for high quality diesel use (Koivusalmi et al, 2008). However, it is already well established that the transesterification process to produce biodiesel is not energy intensive and has relatively high yields. As such this study focuses on hydroprocessing vegetable oils beyond the n-paraffin range and attempts to produce kerosene or jet fuel range n-alkanes (n-C₁₁ – n-C₁₃) by optimising the process conditions such as reaction temperature and pressure, the type of metallic or bimetallic catalyst and its support that is utilised, and the pre-sulphiding of the catalyst to ensure it provides good activity for hydroprocessing reactions.

1.1.3 The focus on aviation fuel

There have been many comprehensive studies on the production of biodiesel from biomass which has lead, not only to a solid foundational understanding of the process, but also its commercialisation. There a number of companies in Europe and North America which utilise biomass as a feedstock to produce biofuels, especially biodiesel. Some examples are Arizona Biodiesel and Amereco Biofuels Corp. with both companies utilising waste vegetable oil as their feedstock. These types of companies will invest in research to further optimise their production capabilities. In relation to biodiesel, there has been a small amount of research investigation into the production of jet (aviation fuel) from waste cooking oil. This provided further incentive for this study.

The conventional production process for kerosene or jet fuel (along with other products) from crude oil is shown in Figure 1-4. Many refineries worldwide have a similar production process.

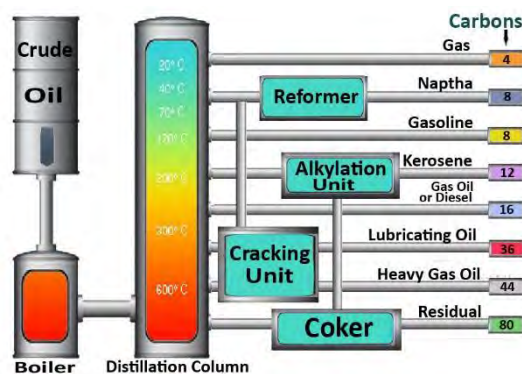


Figure 1-4 Conventional production process of kerosene and other products

Aviation fuel produced in this manner has been a major cause of decreasing air quality due to both ground level as well as higher altitude emissions of CO₂ from commercial, military and general flights (Dunn, 2001). Aircrafts produce up to 4% of the annual global CO₂ emissions from fossil fuels. Replacing petroleum derived jet fuel with the biomass derived counterpart helps to maintain the carbon balance on the earth and reduce greenhouse emissions consequently reducing global warming. Sustainable oils, a renewable fuels company, reported their results from a life cycle analysis (LCA) of jet fuel derived from camelina seed invented by the company. It showed the bio-jet fuel reduces carbon emissions by 84% compared to conventional petroleum jet fuel. This is a significantly high percentage reduction in emissions providing even further incentive to investigate used cooking oil as a feedstock for jet fuel. Lastly, most refineries that produce transportation fuels from crude oil already possess the equipment and infrastructure to implement the catalytic hydroprocessing of waste cooking oil, substantially reducing any possible capital costs (Bezergianni et al, 2009).

1.2 Significance of the study

1.2.1 Research aims

This study focuses on the investigation into the hydrocracking of waste vegetable oil (in particular, used cooking oil) over transition metal-based catalysts to produce jet fuel range n-alkanes. This included the laboratory synthesis of low cost catalysts and their subsequent comparison to commercially produced catalysts through hydrocracking performance tests. The comparability study revolves around the catalysts performance in the degree of hydrocracking of waste vegetable oil achieved and the yield of the desired product, jet fuel range n-alkanes. An additional part of the project was the investigation of the longevity of the commercial catalysts through a regeneration and re-use process. Lastly, there is little information in the literature regarding a kinetic model for the hydrocracking reactions of waste cooking oil to jet fuel range alkanes. Therefore, this study also aims to provide some insight into the kinetics regarding these reactions.

1.2.2 Research objectives

Before commencing with any experimental work, a comprehensive review of the literature has to be carried out to provide insight into hydrocracking reactions, waste cooking oil as a feedstock and the appropriateness of transition metal-based catalysts for these types of reactions. This review was also to provide understanding on catalyst preparations and characterization techniques as well as methods to analyse the feedstock and the products of the hydrocracking reactions, all utilised in this study. Analysing the results would enable the comparison of two commercially produced catalysts (Ru/Al₂O₃ and Ni/Al₂O₃) against two laboratory prepared catalysts (Ni-

Mo/SiO₂ and Co-Mo/SiO₂). The laboratory prepared catalysts were to undergo Energy dispersive X-ray and BET surface area analysis to determine their physical properties.

The experiments were designed in order to investigate how the combined effect of reaction temperature and type of catalysts employed influenced the performance parameters i.e. oil conversion and the yield of C₅-C₁₈ n-alkanes, in particular, kerosene (jet fuel) range n-alkanes (C₁₁-C₁₃). GCMS analysis, along with the employed internal standard method were to be utilised for the qualitative and quantitative analysis of the liquid product. The results would allow for the selection of the optimum operating conditions to achieve kerosene range n-alkanes.

The transition metal-based catalysts become fully active for hydroprocessing (hydrotreating and hydrocracking) reactions only after being brought into contact with sulphur, which converts the catalyst from a metal oxide to a metal sulphide. Pre-sulphiding using H₂S gas was to be employed in this study. In addition, a comparative investigation of the results obtained from non-sulphided catalyst would be used to draw conclusions about the increase in catalytic activity of sulphided catalysts. Furthermore, the catalysts ability to maintain its effectiveness was to be assessed via regeneration and re-use, and the results compared to that of the fresh catalyst.

Lastly, in order to further quantify the hydroprocessing activity of the various catalysts, a simple kinetic model was to be developed and kinetic parameters (including activation energy) were to be identified through regression of experimental data.

1.3 Report overview

In this chapter the reader has been afforded the opportunity to gain insight into the need for an alternate source of transportation fuel (other than crude oil and petroleum derivatives) and the possibility of using biomass, especially waste cooking oil, as an alternative. A justification into the study regarding the focus on jet fuel has been provided and the research aims and objectives have been subsequently delineated.

In Chapter 2, a comprehensive literature review provides understanding regarding hydroprocessing of waste vegetable oils. In particular it focuses on the constituents of the waste cooking oil feedstock, the transitional metal-based catalysts utilised (including the need for pre-sulphiding, catalyst regeneration and coke formation), the possible reaction mechanisms and kinetics involved, and the analytical techniques for catalyst and product analysis.

Chapter 3 focuses on the planning and design of the experimental procedure and product analysis. The One-Variable-At-A-Time approach and the significance of randomness in performing experiments is discussed.

Chapter 4 provides a detailed description of the experimental equipment utilised for this study. These include the catalyst characterisation equipment, the experimental apparatus assembled and commissioned for the hydrocracking reactions, as well as the storage vessels, product separation machinery, and gas and liquid analysis equipment.

The experimental methods employed in this study are discussed in Chapter 5. The synthesis and characterisation techniques of the catalyst are presented first followed by the subsequent catalyst loading and pre-sulphiding procedures. Thereafter a detailed account of the hydrocracking experiments including the materials used is discussed. The chapter concludes with a description on the methodology utilised for the feed and product analysis.

Chapter 6 contains the experimental results, which include preliminary troubleshooting, and a comprehensive discussion into the analytical findings. These include a comparison of the catalysts employed along with the implemented process conditions. Furthermore, a reaction kinetics study is discussed to provide a means of prediction for future experiments.

Conclusions drawn from this work, as well as future recommendations for this research are provided in Chapter 7.

Chapter

2

Literature review

2.1 Origin and early development of hydrocracking technology

Known as one of the oldest hydrocarbon conversion processes, hydrocracking technology was first developed for coal conversion between 1915 and 1945 in Germany. The Germans desired a steady supply of liquid fuel derived from domestic deposits of coal and thus began the research and development into hydrocracking reactions and processes (Scherzer and Gruia, 1996). The first plant for hydrogenation of brown coal was based on Leuna, Germany, and was considered the first commercial hydrocracking process. Between 1925 and 1930, a German and American company collaborated to develop a hydrocracking technology designed to convert heavier gas oils into lighter fuels (Heinemann, 1981). The United States also made attempts to develop a hydrocracking process in order to upgrade heavier petroleum fractions. These processes required high pressures (200-300 atm) and high temperatures ($> 375\text{ }^{\circ}\text{C}$) (Murphree et al., 1940). Tungsten sulphide was amongst the earliest most successful catalysts employed in the hydrocracking process (Scherzer and Gruia, 1996). Other early successful hydrocracking catalysts included iron or nickel supported on fluorinated montmorillonite and nickel supported on amorphous silica-alumina (Scherzer and Gruia, 1996). After World War II, with the availability of crude oil from the Middle East, there was practically no incentive to convert coal to liquid fuels. Newly developed catalytic cracking processes proved more economical for converting heavy petroleum fractions to gasoline (Scherzer and Gruia, 1996).

It wasn't until the late 1950s and early 1960s that saw the return and further development of hydrocracking technologies. Several factors contributed to the demand for hydrocracking processes. Automobile companies started to manufacture high performance cars whose engines required high-octane gasoline which was better achieved through hydrocracking (Scherzer and Gruia, 1996). In addition, the switch from steam to diesel engines on trains and the introduction of commercial jet aircrafts in the 1950s increased the demand for diesel fuel and low-freeze-point jet fuel. The rate of growth for hydrocracking technologies increased drastically as major oil and gas companies such as Chevron Research Company, Unocal and Universal Oil Products all announced new hydrocracking processes during this period. Nickel or nickel-tungsten on silica-alumina was the catalyst used in these processes (Sterba et al., 1960). By the mid-1970s, hydrocracking was considered a mature process but the rate of growth became moderate due to the high cost of hydrogen, which made hydrocracking a more expensive process than catalytic cracking for gasoline production.

In the 1980s and early 1990s the demand for middle distillates ($C_{11} - C_{18}$ saturated hydrocarbons) increased, causing a steady growth for hydrocracking processes around the world. New catalysts were also developed, designed to improve catalyst activity and selectivity. Some "flexible" catalysts were developed that made it possible to maximise the yield of different products by using the same catalyst at different operating conditions (Scherzer and Gruia, 1996).

Since hydrocracking is considered a mature and well developed technology, replacing the feedstock from crude oil to a sustainable and environment friendly alternative to produce biofuels appears to be the best option going forward, rather than replacing the entire process which will require large capital costs. It is for this reason that in the 21st century, oil and gas companies are investing resources and time into researching sustainable and renewable feedstocks such as vegetable oils and animal fats.

2.2 Current biofuel production processes

Although relatively new when compared to conventional fuel production processes, biofuel production processes are being researched and developed, and some have reached commercialisation. This section describes a few of those processes.

2.2.1 The Fischer-Tropsch synthesis of biomass

Both Syntroleum (de Klerk, 2007) and Sasol have independently developed a process to produce biofuels based on the gas-to-liquid (GTL) Fischer-Tropsch (FT) processes of cellulose plants. The biomass must first undergo a chemical conversion before the FT process. There exists a variety of possible conversion processes but usually gasification is the preferred method. This is

considered one of the best commercially available options to produce biofuel. Figure 2-1 is a general flow diagram of the conversion process.

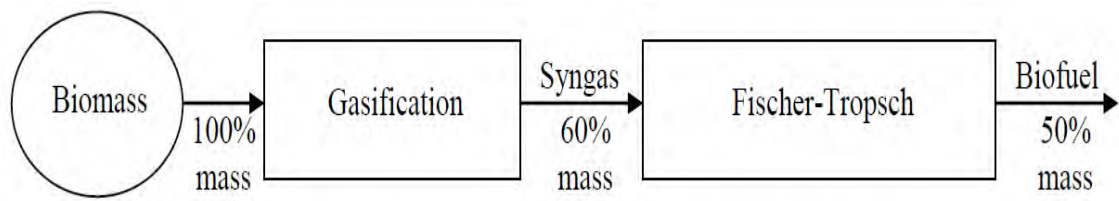


Figure 2-1 Biomass to biofuel conversion via Fischer-Tropsch synthesis (Freerks and Muzzell, 2004)

2.2.2 Conversion of carbohydrates to liquid fuels

As recent as 2008 a team of researchers reported a catalytic approach for the conversion of carbohydrates (sugars and polyols) to specific species of hydrocarbons which can be utilised as liquid transportation fuels. The methodology is modifiable and can be designed to produce shorter chain hydrocarbons and aromatic compounds in gasoline, or longer chain hydrocarbons in jet and diesel fuels. The process begins by converting the sugars and polyols over a Pt-Re catalyst to form primarily carboxylic acids, hydrophobic alcohols, ketones, and heterocyclic compounds. These are then passed through catalytic beds of either metallic catalysts on amorphous supports or zeolites at high temperature to produce a range of light hydrocarbons, aromatics and iso-paraffins as shown in Figure 2-2 (Kunkes et al., 2008).

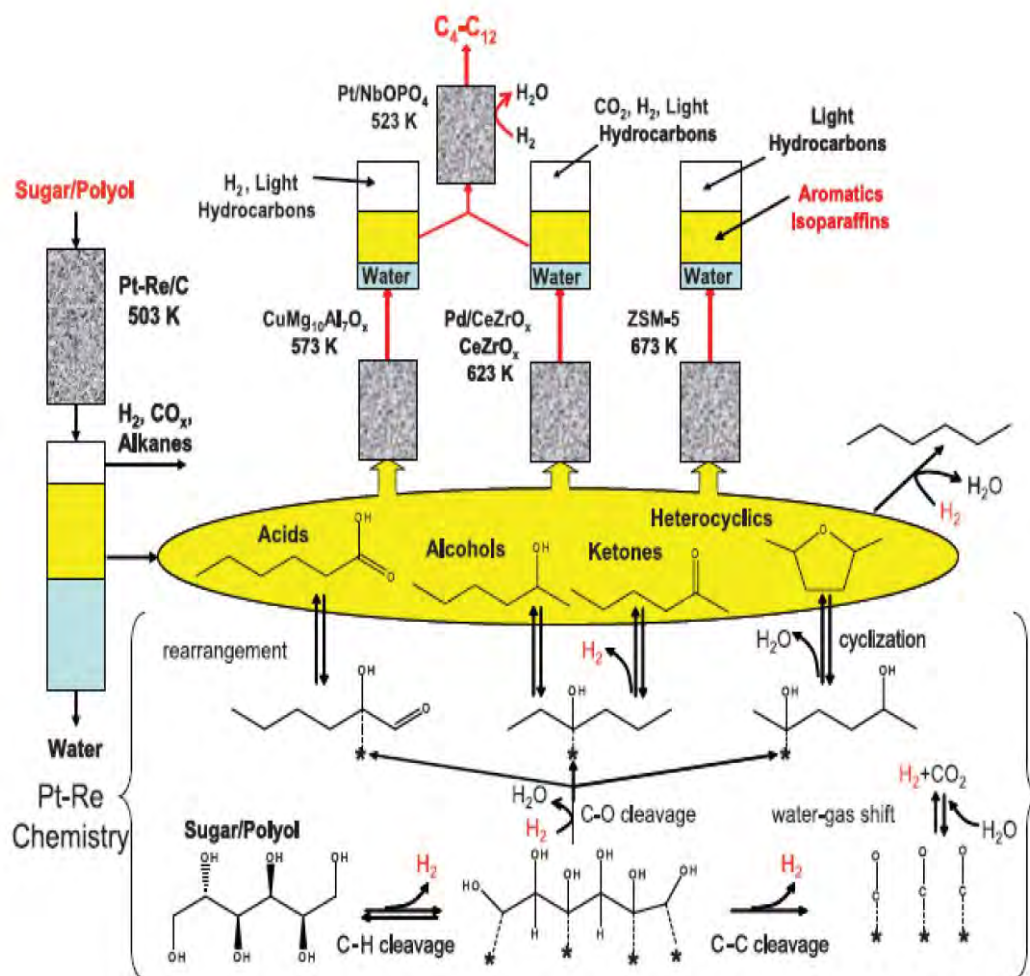


Figure 2-2 Schematic representation of the reactor sequence and proposed chemistry to produce constituents of liquid transportation fuels from catalytic processing of sugars and polyols (Kunkes et al., 2008)

2.2.3 Bio-Synfining process for synthetic paraffinic kerosene (SPK) production

Syntroleum, one of the company's using the FT process described in section 2.2.1, has also developed a low capital cost process termed Bio-SynfiningTM. The process uses bio-renewable feeds such as fats, greases, and algae oils to produce high quality synthetic paraffinic kerosene (SPK). Figure 2-3 depicts the schematic flow diagram for the process. The configuration is a simple single-train hydroprocessing unit which processes the biomass with heat and hydrogen using proprietary catalysts. The bio-feed requires pre-treatment, and is thereafter combined with the hydrocracker effluent which acts as the solvent/diluent for the exothermic hydrotreater reactions. After separation from the hydrogen and light hydrocarbons, the products are transferred to a fractionation unit.

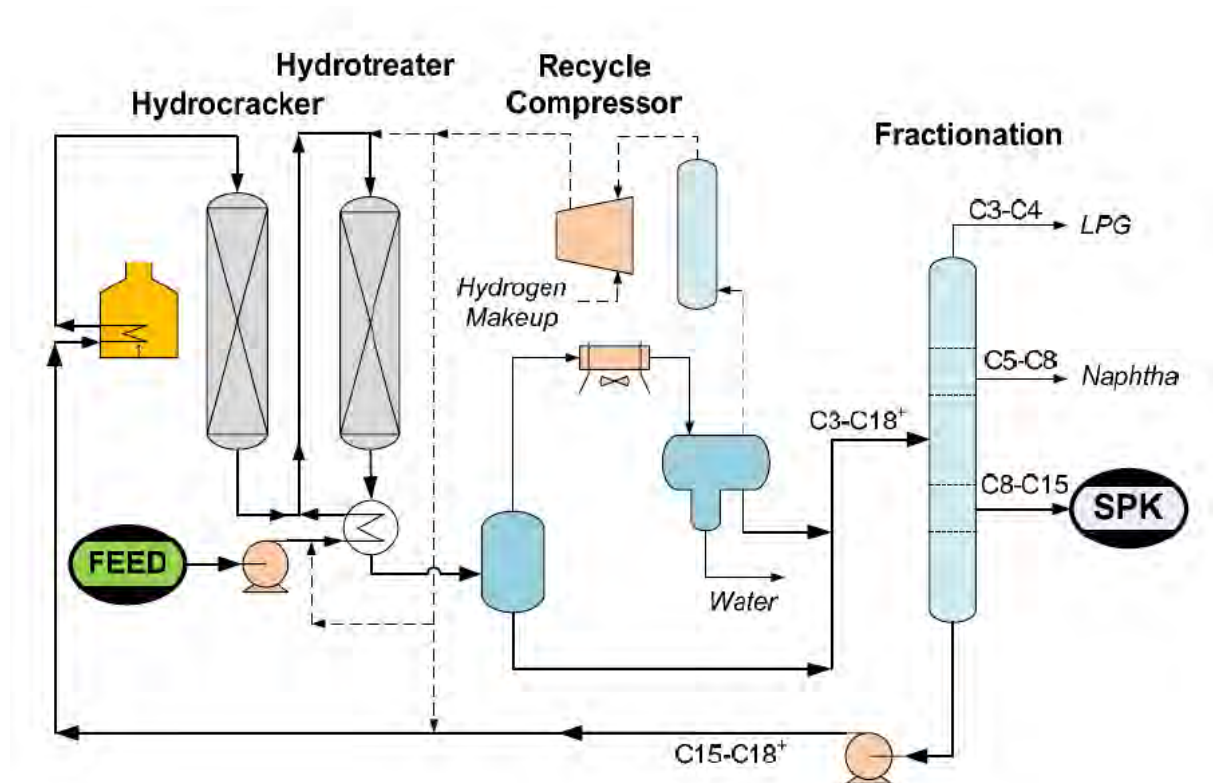


Figure 2-3 Syntroleum's Bio-SynfiningTM process (Freerks et al., 2004)

2.2.4 UOP LLC's green jet and diesel biofuels

A process was developed by UOP LLC, a Honeywell company, which utilises natural, renewable, fats and oils to produce green jet and diesel biofuels. However, certification and commercialisation are required before these fuels can be used on a widespread basis, which culminates into several years before this alternative fuel can be brought to the commercial market (Wang, 2012).

2.3 Renewable sources for biofuels production

Biomass derived oils can be obtained from many sources, such as animal fats, plants and microbial plants. Each source has advantages and disadvantages in terms of impurities, pre-treatment requirements, potential products, availability and cost. 1st generation feedstocks refers to crops whose sole purpose is to provide the oil as the feed material for transportation fuels. However, there is a controversial economic debate regarding 1st generation feedstocks commonly known as the "food versus fuel" conflict. In the interest of meeting the growing demand for biofuels while not compromising the value of food, land and water, there is large emphasis placed on research and process development which utilises 2nd generation feedstocks such as used cooking oil (UCO) (Wang, 2012).

2.3.1 Vegetable oil as a feedstock

Vegetable oils are ideal candidates for the production of biodiesel and biojet fuel since they are made up of 90 to 98% triglycerides (hydrophobic constituents of vegetable oils and animal fats), which contain a glycerol group that has three fatty acid chains attached to it as seen in Figure 2-4.

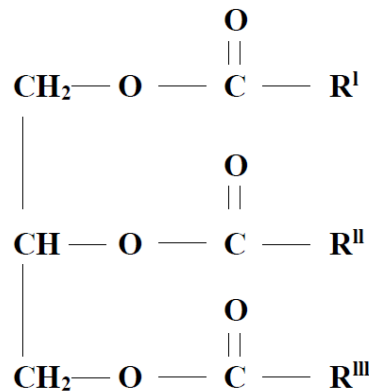


Figure 2-4 Chemical structure of triglyceride (Wang, 2012)

Triglycerides differ by the chain length and number of double bonds of the fatty acids as shown in Table 2-1. The side chains of triglycerides are either saturated, monounsaturated or polyunsaturated (Sotelo-Boyás et al., 2012). Fatty acids which are commonly found in vegetable oils are palmitic, stearic, linoleic and linolenic acids (Srivastava et al., 2000).

Table 2-1 Chemical structure of common fatty acids (Marckley, 1960)

Fatty Acid	IUPAC name	No. of carbon atoms and double bonds ^a	Chemical formula
Lauric	Dodecanoic	12:0	C ₁₂ H ₂₄ O ₂
Myristic	Tetradecanoic	14:0	C ₁₄ H ₂₈ O ₂
Palmitic	Hexadecanoic	16:0	C ₁₆ H ₃₂ O ₂
Stearic	Octadecanoic	18:0	C ₁₈ H ₃₆ O ₂
Arachidic	Eicosenoic	20:0	C ₂₀ H ₄₀ O ₂
Behenic	Docosenoic	22:0	C ₂₂ H ₄₄ O ₂
Lignoceric	Tetracosenoic	24:0	C ₂₄ H ₄₈ O ₂
Oleic	cis-9-Octadecanoic	18:1	C ₁₈ H ₃₄ O ₂
Linoleic	cis-9,cis-12-Octadecadienoic	18:2	C ₁₈ H ₃₂ O ₂
Linolenic	cis-9,cis-12,cis-15-Octadecatrienoic	18:3	C ₁₈ H ₃₀ O ₂
Erucic	Cis-13-Docosenoic	22:1	C ₂₂ H ₄₂ O ₂

[a] Indicates the number of carbon atoms and the number of carbon double bonds. For example, oleic acid contains 18 carbon atoms and 1 carbon double bond.

Table 2-2 indicates the breakdown in weight percentage of the different fatty acids found in various vegetable oils. It can be seen that most vegetable oils (including cooking oil) are made up primarily of unsaturated C₁₈ fatty acids.

Table 2-2 Fatty acid composition of various vegetable oils (Goering et al., 1982)

Vegetable oil	Fatty acid composition, wt.%									
	14:0	16:0	18:0	20:0	22:0	24:0	18:1	18:2	18:3	22:1
Corn (Maze oil)	0	11	2	0	0	0	28	58	1	0
Cottonseed	0	28	1	0	0	0	13	58	0	0
Crambe	0	2	1	2	1	1	19	9	7	59
Linseed	0	5	2	0	0	0	20	18	55	0
Peanut	0	11	2	1	2	1	48	32	1	0
Rapeseed	0	3	1	0	0	0	64	22	8	0
Safflower	0	9	2	0	0	0	12	78	0	0
H.O. Safflower	Trace	5	2	Trace	0	0	79	13	0	0
Sesame	0	13	4	0	0	0	53	30	0	0
Soy bean	0	12	3	0	0	0	23	55	6	0
Sunflower	0	6	3	0	0	0	17	74	0	0

The remainder (2~10%) of vegetable oils is made up of mono- and diglycerides, as well as free fatty acids (generally 1 to 5%), phospholipids, phosphatides, carotenes, tocopherols, sulphur compounds and traces of water (Wang, 2012).

Although these are potentially suitable feedstocks for hydrocracking to produce transportation fuels, the make-up of the vegetable oils listed in Table 2-2 were determined using 1st generation oils. This means that these oils were not used for any other purpose prior to the analysis of their constituents. This study however, focuses on the use of waste/used cooking oil (2nd generation) and it is therefore necessary to investigate the similarity of 2nd generation vegetable oils to its 1st generation counterpart. Understanding the constituents in used cooking oil will provide insight as to whether it is also a potentially suitable feedstock for biofuels production.

2.3.2 Investigation of used cooking oil as a feedstock

In order for used cooking oil to be a potentially suitable feedstock for biofuels, its chemical composition needs to be similar to that of the fresh vegetable oils shown in Table 2-2.

Abidin et al. (2012) performed a comprehensive study to determine the constituents of used cooking oil (supplied and filtered by Greenfuel Oil Co. Ltd.) as well as response factors for the major constituents. In order to determine the fatty acids in the used cooking oil, fatty acid methyl

esters (FAME) were prepared by using the fatty acids themselves, and thereafter quantification of the FAME was performed. The preparation of the FAME from the fatty acids was done by the popular methylation process. This method is well accepted due to the robustness and reproducibility of the chromatographic data. During analysis, it is assumed that the composition of the FAME is the same as the composition of the fatty acids in the feedstock. Using GCMS analysis, a total ion chromatogram was generated as seen in Figure 2-5.

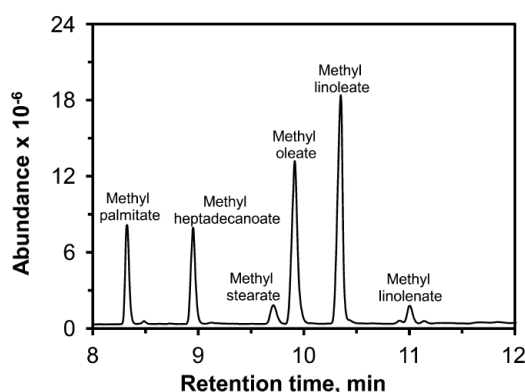


Figure 2-5 Total ion chromatogram of the derivatised UCO (Abidin et al., 2012)

Upon analysis on the generated chromatogram and previously prepared calibration curves for each constituent, both the response factors and the weight compositions of each fatty acid in the UCO was determined and are shown in Tables 2-3 and 2-4 respectively.

Table 2-3 Linear equation, r-squared value and response factor for each component in the UCO sample (Abidin et al., 2012)

Component	Linear Equation ^a	R-squared value	Response factor ^b
Methyl linoleate	$Y=0.9195X$	0.9974	0.9195
Methyl linolenate	$Y=0.9000X$	0.9918	0.9000
Methyl oleate	$Y=0.9789X$	0.9985	0.9789
Methyl palmitate	$Y=0.9311X$	0.9970	0.9311
Methyl stearate	$Y=0.9845X$	0.9982	0.9845

[a] The linear equation was determined from calibration curves. Y represents the area ratio of the component against the internal standard (heptadecanoate) and X represents the concentration ratio against the same internal standard.

[b] Units of concentration were g.L⁻¹ (Necessary for future calculations when using the linear equations)

Table 2-4 Composition of fatty acids in UCO (Abidin et al., 2012)

Fatty acid	Composition (wt. %)
Linoleic acid	43.85
Linolenic acid	4.65
Oleic acid	33.75
Palmitic acid	13.62
Stearic acid	4.13

In another study on the production of biodiesel from waste cooking oil performed by Chhetri et al. (2008), gas chromatography was used to analysis and quantify the constituents of waste cooking oil. The results of their analysis are presented in Table 2-5.

Table 2-5 Fatty acid composition in UCO (Chhetri et al., 2008)

Fatty acid	Composition (wt. %)
Myristic	0.11
Palmitic	5.18
Palmitoleic	0.51
Stearic	2.1
Oleic	59.7
Linoleic	19.31
Linolenic	6.82
Arachidic	0.61
Eicosenoic	1.21
Lignoceric	0.08
Others	4.36

In another study performed by Hanafi et al. (2015), very similar results to the previous studies mentioned were obtained from the analysis of waste cooking oil (obtained from local fast-food restaurants), with oleic and linoleic acids having the highest wt.% compositions of 20% and 68% respectively. Prior to analysis and subsequent experimental use, the oil was filtered through filter paper to remove solid impurities and was heated with stirring for 3h at 110 °C to remove moisture. Analysis of the oil was performed using an elemental analyser with channel control (Pw 1390-Philips) and a spectrometer model Pw 1410 (Hanafi et al., 2015).

Finally, in yet another study performed by Bezergianni et al. (2009), fresh and used cooking oil were catalytically hydrocracked in an attempt to produce biodiesel. The fresh oil was commercially produced sunflower oil while the used oil was obtained from local restaurants and households after being used extensively for frying. Figure 2-6 depicts the product yields of diesel at different reaction temperatures.

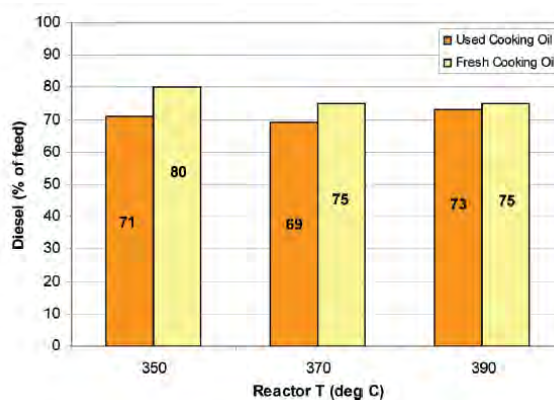


Figure 2-6 Diesel yield of hydrocracking fresh and used cooking oil (Bezergianni et al, 2009)

Their results indicate only a slight increase in diesel percentage of the initial feed for the fresh cooking oil compared to the used cooking oil. Since used cooking oil is substantially cheaper and does not contribute to the food versus fuel conflict, it appears to be an excellent sustainable alternative feedstock for transportation fuels.

Based on the fact that most fresh cooking oil is made up of C_{18} unsaturated fatty acids, and that three independent studies indicates a similar composition for used cooking oil, and similar yields of biodiesel were obtained with fresh and used cooking oil, it validates the use of used cooking oil as the feedstock for biojet fuel production in this study. Analysis on the feedstock for this study was performed and the results are presented in Appendix C. The used cooking oil in this study was also obtained from local restaurants and homes. The oil was filtered to remove solid food particles before being stored.

Lastly, in 2014/2015, the world consumed 173.27 million metric tons of cooking oil. This provides a clear indication of the vast amount of waste cooking oil that is potentially available as a feedstock.

2.4 Reaction mechanisms for catalytic hydrotreatment of liquid biomass

Several researchers have tried to elucidate the mechanism of the hydrocracking of vegetable oils into biofuels. However, due to the complexity of the reactions, the mechanisms and kinetics are still under investigation (Wang, 2012). Nevertheless, scientists generally acknowledge that the

triglycerides are first saturated on their side chain, which is then followed by the scission of the C-O bond, leading to the formation of diglycerides, monoglycerides, carboxylic acids and waxes (Huber et al., 2007). These are followed by decarboxylation, decarbonylation and hydrogenation/dehydration reactions and finally, isomerisation and cracking. The reaction pathways can be seen in Figure 2-7. Proposed reaction mechanisms from various studies are discussed in this section.

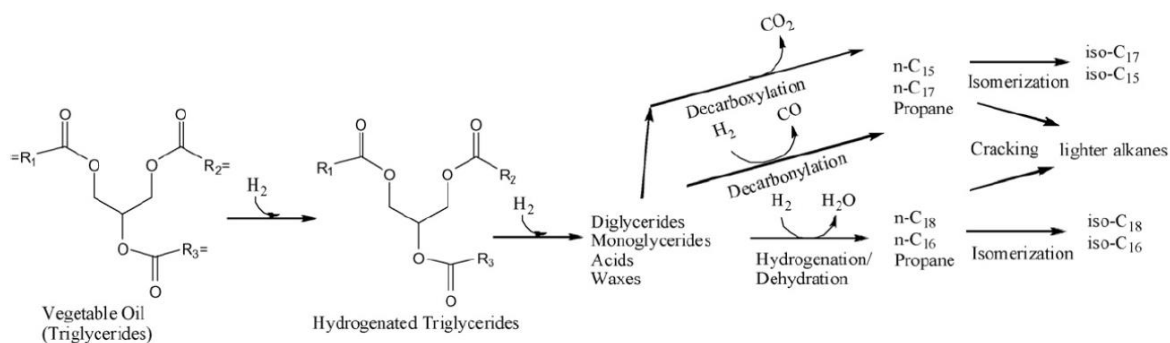


Figure 2-7 Reaction pathways for the conversion of triglycerides to alkanes (Huber et al., 2007)

In a fixed bed hydrotreating process, the reactions take place in a three-phase system: the liquid feed trickles down over the solid catalyst in the presence of a hydrogen-rich gas phase (Wang, 2012). Several types of reactions take place during the catalytic hydrotreatment of liquid biomass. These reactions depend on the type of biomass utilised, the operating conditions employed and the type of catalyst used. The types of reactions the liquid biomass undergoes during catalytic hydroprocessing include: a) saturation (hydrotreating), b) cracking (hydrocracking), c) heteroatom removal and d) isomerisation.

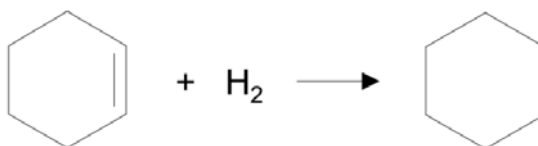
2.4.1 Saturation reactions

These reactions are described as hydrotreating or hydrorefining reactions as it involves non-destructive hydrogenation and is used to improve the quality of petroleum distillates without significantly altering the boiling point range (Sotela-Boyás et al., 2012). In these reactions the introduction of excess hydrogen allows for the breakage of C-C double bonds and their subsequent conversion to single bonds. A key reaction is the conversion of unsaturated carboxylic acids into saturated ones in feedstocks such as vegetable oils as depicted in Scheme 2-1 (Bezergianni, 2013).

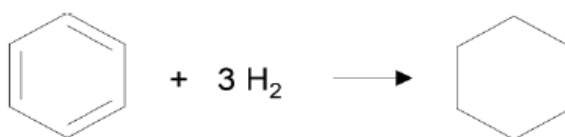


Scheme 2-1 Saturation reaction of unsaturated carboxylic acid (Bezergianni, 2013)

In the upgrading of pyrolysis oils, saturation reactions lead to the formation of naphthenes by converting unsaturated cyclic compounds and aromatics compounds as shown in Schemes 2-2 and 2-3 respectively.



Scheme 2-2 Conversion of cyclohexene to cyclohexane through hydrotreating reactions
(Bezergianni, 2013)



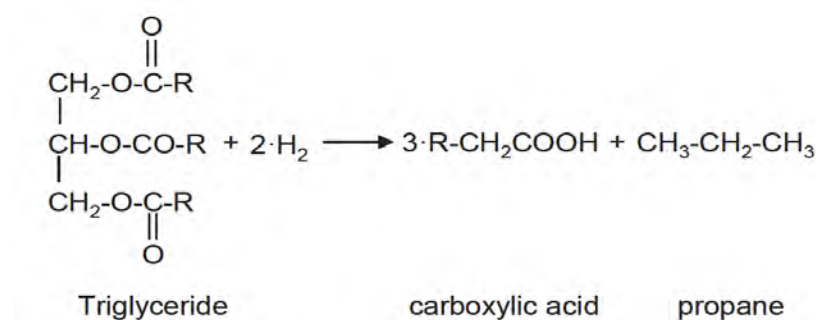
Scheme 2-3 Conversion of benzene to cyclohexane through hydrotreating reactions
(Bezergianni, 2013)

As a result of saturation reactions the produced saturated compounds are less active and less prone to polymerisation and oxidation reactions. This type of reaction aids in alleviating the sediment formation and corrosion appearing in engines.

In a study performed by Bezergianni et al. (2009), it was found that saturation reactions were not favoured by increased temperature, which was expected as saturation is a competing reaction mechanism to the cracking one. The degree of saturation is indicated by the bromine index in the feedstock and products. The higher the bromine index, the greater the number of unsaturated bonds.

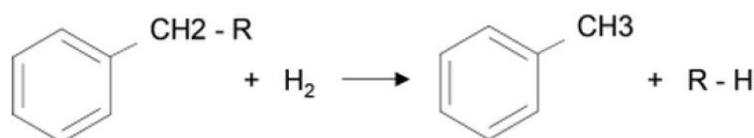
2.4.2 Hydrocracking

Hydrocracking reactions are necessary when it is desired to convert liquid biomass whose chemical structure is relatively large and complicated, into molecules of the size and boiling point range of transportation fuels i.e. gasoline ($C_5 - C_{10}$), kerosene ($C_{11} - C_{13}$) and diesel ($C_{14} - C_{18}$) (Bezergianni, 2013). A characteristic reaction that occurs during catalytic hydroprocessing of vegetable oils is the cracking of triglycerides into its consisting carboxylic acids (fatty acids) and propane as depicted in Scheme 2-4 (Donnis et al., 2009). This is a critical reaction in the hydroprocessing scheme as it converts the initial large triglycerides compounds of high boiling points ($>600\text{ }^{\circ}\text{C}$) into mid-distillate range compounds (gasoline, kerosene and diesel).



Scheme 2-4 Hydrocracking a triglyceride to form a fatty acid and propane (Donnis et al., 2009)

Other cracking reactions may occur, depending on the constituents of the feedstock. Scheme 2-5 depicts a cracking reaction which may occur during catalytic hydroprocessing of pyrolysis oils. Alternatively, Scheme 2-6 follows the deoxygenation of carboxylic acids on the produced long chain paraffinic compounds, leading to smaller chain paraffins. One such example is during the upgrading of Fischer-Tropsch wax (Bezergianni, 2013).



Scheme 2-5 Cracking reaction during hydroprocessing of pyrolysis oils (Bezergianni, 2013)



Scheme 2-6 Cracking reaction of long chain paraffins to smaller chain ones (Bezergianni, 2013)

2.4.3 Heteroatom removal

Heteroatoms refer to other atoms, other than carbon and hydrogen, which are often present in bio- and fossil-based feedstocks. These heteroatoms include sulphur, nitrogen and in the case of bio-based feedstocks, oxygen. It is necessary to try and eliminate or at least reduce these heteroatoms from the feedstock or eventual product to ensure the highest possible quality is achieved. Oxygen removal in particular is of utmost importance as the presence of oxygen reduces oxygen stability (due to carboxylic and carbonylic double bonds), increases acidity and corrosivity (due to the presence of water) and even reducing the heating value of the biofuels produced (Bezergianni,

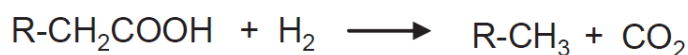
2013). The three main deoxygenation reactions that take place are deoxygenation, decarbonylation and decarboxylation as depicted in Schemes 2-7, 2-8 and 2-9 respectively (Donnis et al., 2009).



Scheme 2-7 Deoxygenation reaction during hydroprocessing (Donnis et al., 2009)



Scheme 2-8 Decarbonylation reaction during hydroprocessing (Donnis et al., 2009)



Scheme 2-9 Decarboxylation reaction during hydroprocessing (Donnis et al., 2009)

The above schemes were devised in a study by Donnis et al. (2009). A schematic representation of the two different mechanisms for the oxygen removal from the triglyceride is shown in Figure 2-8. The unbroken red lines indicate the hydrogenation/hydrodeoxygenation (HDO) reaction, in which it was proposed that the oxygen was removed as a form of water (the reaction is shown in Scheme 2-7). The blue lines represent the decarboxylation and decarbonylation reactions (the reactions are shown in Scheme 2-8 and 2-9). In this representation the triglyceride is converted into propane, carbon dioxide and/or carbon monoxide and into an n-alkane one carbon atom shorter than the total length of the original fatty acid.

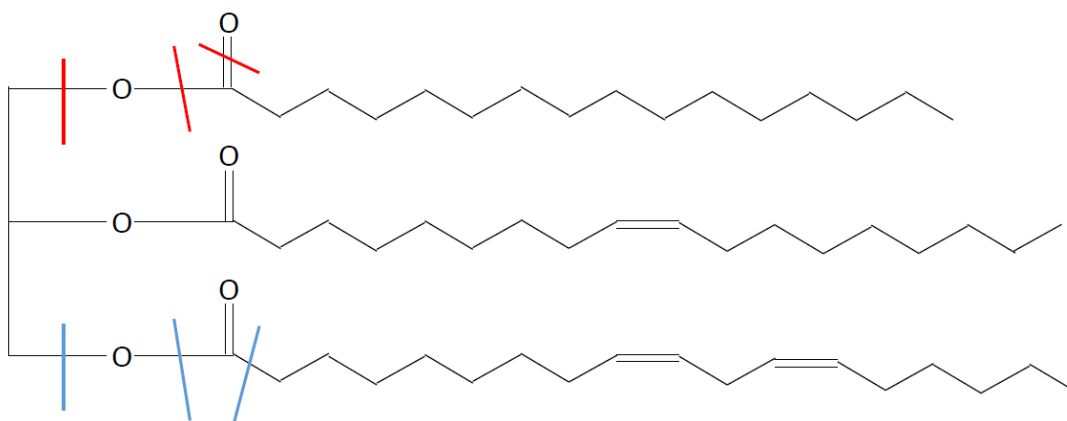


Figure 2-8 Schematic representation of the two different pathways for removal oxygen from triglyceride by hydrotreating (Wang, 2012)

The remaining heteroatoms (sulphur and nitrogen) are removed according to the well-known heteroatom removal mechanisms of the fossil fuels in the form of gaseous H_2S and NH_3 (Bezergianni, 2013).

In a study performed by Bezergianni et al. (2009), fresh and used cooking oil were catalytically hydrocracked. As part of the study heteroatoms compositions were measured in both feedstocks and their subsequent presence in the products were reported. The compositions of the oils (including the heteroatoms) are shown in Table 2-6.

Table 2-6 Properties of fresh and used cooking oil (Bezergianni et al., 2009)

	Fresh cooking oil	Used cooking oil
Density ($kg.m^{-3}$)	891.40	896.6
Sulphur (wppm)	0.90	38
Nitrogen (wppm)	0.69	47.42
Hydrogen (wt. %)	11.62	11.62
Carbon (wt. %)	76.36	76.74
Oxygen (wt. %)	12.02	11.64
Refractive index	1.45513	1.4511
Bromine index	49.20	46.60

The data provided in Table 2-6 shows that the used cooking oil has a slightly higher density than the fresh cooking oil. This is expected as the used cooking oil undergoes thermolytic, oxidative, and hydrolytic reactions (Bezergianni et al., 2009). The higher sulphur and nitrogen content in the used cooking oil was most likely caused by the hydrolysis and oxidation of existing sulphur and nitrogen compounds that were present in the fried foods. The study also indicated a difference in the bromine index with the value for fresh cooking oil being higher than the used cooking oil. This index indicates that the cooking oil increases in polarity with increased frying use (Guesta et al., 1993).

After the hydrocracking reactions, the products were analysed for the heteroatom contents since their removal is also a significant measure of the overall hydrocracking effectiveness (since heteroatoms are undesired in the final product). Figure 2-9 depicts the heteroatom removal as the percentage of sulphur, nitrogen and oxygen contained in the feed which has been removed during hydrocracking of the feedstock.

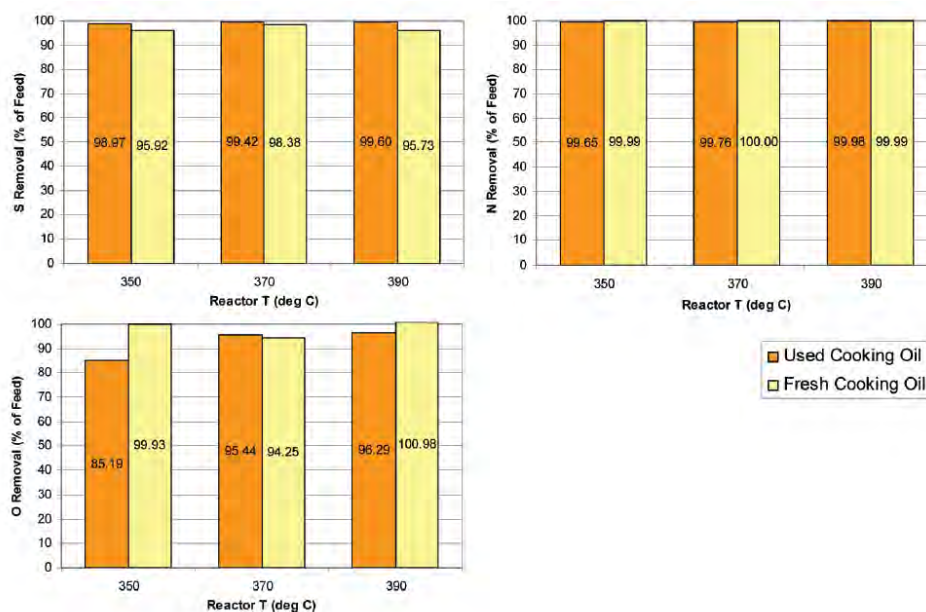
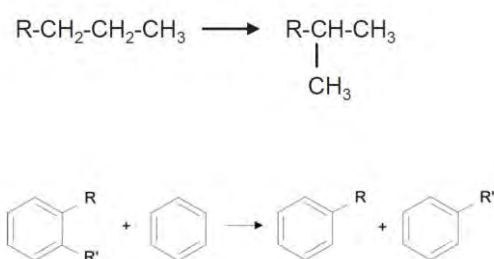


Figure 2-9 Heteroatom removal percent via hydrocracking of fresh and used cooking oil at three reaction temperatures (Bezergianni et al., 2009)

The results in Figure 2-9 showed that nitrogen was the most easily removed in for all three reaction temperatures for both feedstocks (> 99.5%). Sulphur was also effectively removed from both feedstocks, but achieved a higher removal percentage from the used cooking oil. Oxygen removal for both feedstocks performed similarly, even though the fresh oil contain less oxygen initially. These results validate sufficient heteroatom removal for the similar type of experiments discussed in this dissertation.

2.4.4 Isomerisation reactions

The straight chain paraffinic compounds resulting from the aforementioned Scheme 2-7 offer an increased cetane number, heating value and oxidation stability in the biofuels which contain them. However, they also degrade their cold flow properties. Cold flow properties can be improved by isomerisation reactions which normally take place in a second step/reactor as it requires a different catalyst. Some examples of isomerisation reaction are depicted in Scheme 2-10.



Scheme 2-10 Examples of isomerisation reactions (Bezergianni, 2013)

It can be seen that the triglyceride molecule was able to enter the zeolite catalyst pore first and then cracked. This was possible since its longitudinal section diameter (around 5.3 – 7.4 °Å) and chain length (around 30 – 45 °Å) was smaller than the catalyst pore (approx. 0.56 °Å, diameter). Thereafter the double bond in the nonene that was removed from the catalyst pore was saturated by the metallic sites of the catalyst to form nonane. However, while 37.97 wt. % of the product was nonane, 37.26 wt. % comprised of heptadecane with the balance being small amounts of C_{8,10,13,17} and 19 n-alkanes (< 8 wt.% each) (Wang, 2012). This shows that the experimental results did not match the proposed mechanism.

Another study conducted by Sotela-Boyás et al. (2012) proposed reaction pathways for triglyceride processing as depicted in Figure 2-11. This proposed mechanism indicates a path in which three triglycerides are converted into linear paraffins. In this case, the oil is considered to be composed of triolein, tripalmitin and trilinolein, three very large molecules. The first step suggests a formation of free fatty acids by scission of propane from the glycerol backbone of the triglyceride molecule present in the hydrogen. This results in the formation of oleic, palmitic and linoleic acids (Sotela-Boyás et al., 2012). The following steps follow the same saturation, cracking and heteroatom removal reactions described in sections 2.4.1 to 2.4.3.

Although the literature suggests similar reaction mechanisms and pathways for the hydroprocessing of triglycerides, there does not exist one proven mechanism that can describe the reactions with any type of triglyceride feedstock coupled with any type of hydroprocessing catalyst. The similarities in the literature does however provide an idea of the expected products from the types of experiments conducted in this study.

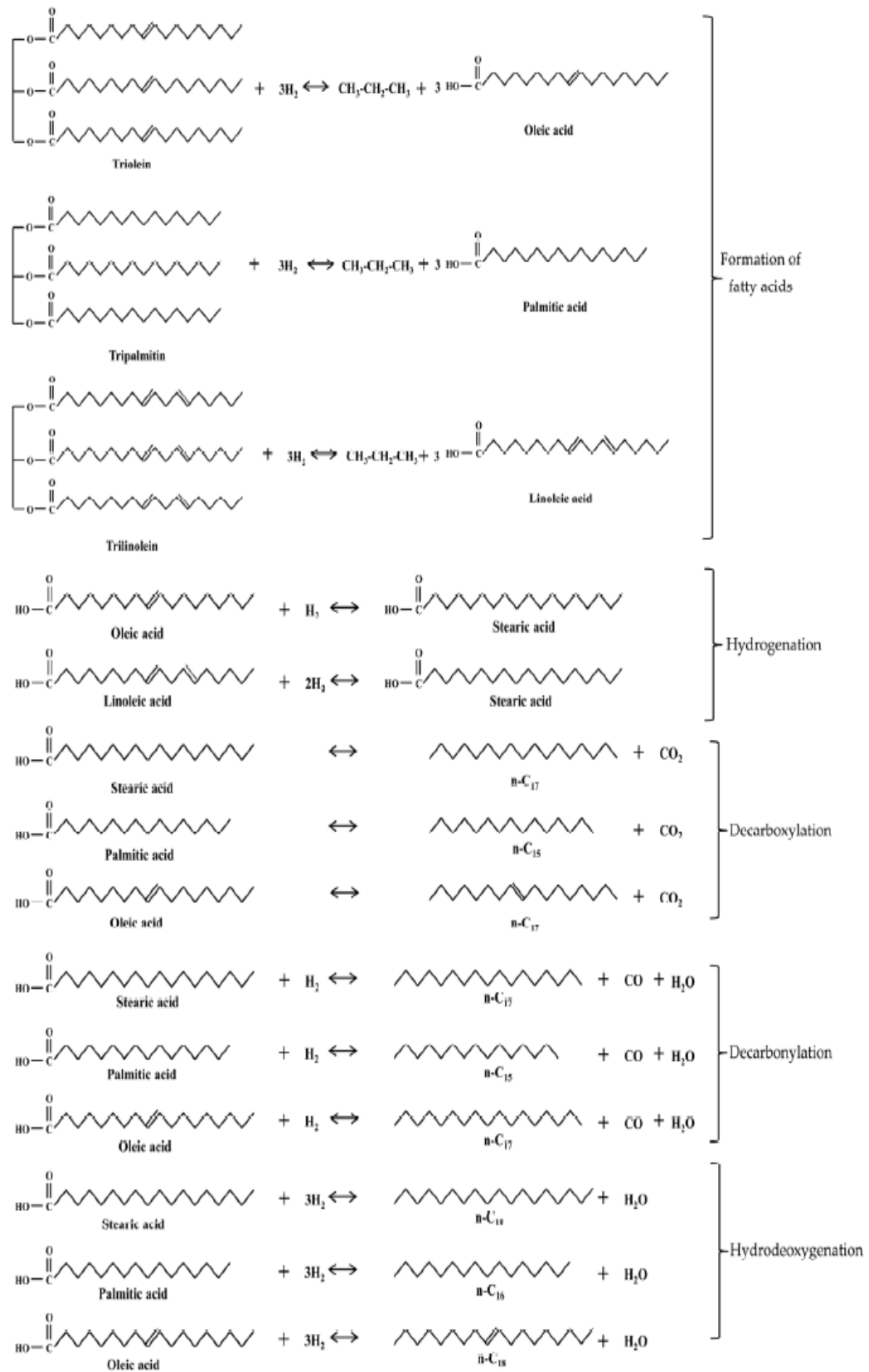


Figure 2-11 Reaction pathways for hydroprocessing of triglycerides (Sotela-Boyás et al., 2012)

2.5 Reaction kinetics

Like the reaction mechanism, the reaction kinetics for triglyceride conversion to biofuels via hydroprocessing has not been fully developed. The complexity in the reaction mechanisms makes it difficult to generate general rate equations for these reactions (Wang, 2012). Nevertheless, there have been some reaction kinetic studies that have focused on specific feedstocks, catalysts and operating conditions, while some have proposed kinetics by using a simplified version of the overall reaction scheme.

Smejkal et al. (2009) used thermochemical properties of reactive components to develop an equilibrium model for vegetable oil hydrogenation. The study utilised hydrotreating and hydrogenation catalysts (Ni-Mo/Al₂O₃ and Ni/Al₂O₃ respectively). The reaction enthalpy, ΔH_r^T (dependent on reaction temperature), can be calculated as follows (Smejkal et al, 2009):

$$\Delta H_r^T = \Delta H_r^\circ + \int_{298}^T C_{p,T} dT \rightarrow \Delta H_r^T = \Delta H_r^\circ + \overline{C_{p,T}}(T - 298) \quad (2-1)$$

Where ΔH_r° is the standard reaction enthalpy, $C_{p,T}$ is the heat capacity, and $\overline{C_{p,T}}$ is the average heat capacity.

The entropy of the reaction system can be calculated as follows (Smejkal et al, 2009):

$$\Delta S_r^T = \Delta S_r^\circ + \int_{298}^T \frac{C_{p,T}}{T} dT \rightarrow \Delta S_r^T = \Delta S_r^\circ + \overline{C_{p,T}} \ln\left(\frac{T}{298}\right) \quad (2-2)$$

The model predictions were in good agreement with the experimental data. Furthermore, the estimations suggest that the reaction was limited by hydrogen transfer (Smejkal et al., 2009).

Charusiri and Vitidsant (2005) performed a study whereby an attempt was made to develop a reaction rate expression based on the conversion of the biomass feedstock over time. Experiments were performed in a 70 cm³ batch micro-reactor using sulphated zirconia catalyst. A 2^k factorial experimental design was employed to investigate the parameters (reaction temperature, reaction time and initial hydrogen pressure) that affect the biofuel products. A material balance (Charusiri and Vitidsant, 2005) was developed from the schematic in Figure 2-12.

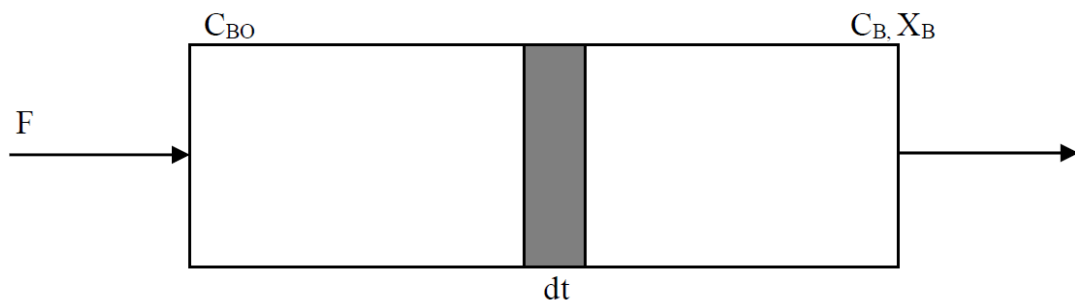


Figure 2-12 Schematic diagram of the batch reactor (Charusiri and Vitidsant, 2005)

$$-r_B = \left(-\frac{1}{V}\right) \left(\frac{dN_B}{dt}\right) \quad (2-3)$$

Supposing that N_{BO} is the initial amount of vegetable oil at time $t=0$, and that N_B is the amount of vegetable oil present at time t , the conversion of the feedstock in a constant volume system is given as follows (Charusiri and Vitidsant, 2005):

$$X_B = 1 - \frac{C_B}{C_{BO}} \quad (2-4)$$

At constant volume (Charusiri and Vitidsant, 2005):

$$-r_B = \frac{dC_B}{dt} = k_n C_B^n \quad (2-5)$$

If the first-order reaction is considered, the following is obtained after integration (Charusiri and Vitidsant, 2005):

$$\ln(C_B) = \ln(C_{BO}) - k_1 t \quad (2-6)$$

If the second-order reaction is considered, integration gives (Charusiri and Vitidsant, 2005):

$$\frac{1}{C_B} = \frac{1}{C_{BO}} + k_2 t \quad (2-7)$$

A plot of conversion versus time for all temperatures gave a straight line with a better regression constant ($R^2 \approx 1.00$) for the second-order than the first-order reaction. The study concluded that the system follows the second-order reaction. Finally, using the Arrhenius equation and plot of $\ln(k)$ versus $(1/T)$, the activation energy, E_a , was estimated to be 83.439 kJ.mol⁻¹ and the frequency factor, A , was estimated to be 914.886 s⁻¹.

Hanafi et al. (2005) performed a similar study to determine the reaction-order based on conversion of the feedstock. Waste cooking oil underwent hydrocracking over NiW/SiO₂-Al₂O₃ catalyst in a continuous system for one hour. The study investigated different temperatures and liquid hourly space velocities. Fourier transform infrared spectrometry (FTIR) analysis was employed on order to determine the conversion of the feedstock at different intervals during each one hour run. A plot of conversion versus time fitted well with the second-order reaction. The estimated activation energy was 56 kJ.mol⁻¹. Both studies, each utilising different bio-liquid feedstocks and catalysts, successfully concluded that the conversion of the used cooking oil follows the second order reaction.

2.6 Hydroprocessing catalysts

Hydroprocessing catalysts are dual-function catalysts. The concept of a dual-function catalyst having two distinctly different kinds of sites was introduced by Mills et al. (1953) and later expanded by Weisz (1962). These early studies showed that both metallic and acid sites must be

present on the catalyst surface in order to achieve all the desired hydroprocessing reactions, i.e. hydrogenation, dehydrogenation, hydrocracking etc. The acidic sites promote the cracking reactions as well as isomerisation reactions while the metallic sites promote the hydrogenation-dehydrogenation reactions.

The acidic sites are supports that consist of a) amorphous oxides (such as silica, alumina or silica-alumina), b) a crystalline zeolite (modified Y zeolite has been shown to perform better than X zeolite) plus a binder such as alumina, or c) a combination of crystalline zeolite and amorphous oxides. The metals can be a) noble metals (palladium, platinum) or b) non-noble metals from group VIA (molybdenum, tungsten) and group VIIIA (cobalt, nickel) (Scherzer and Gruia, 1996). Furthermore, hydrogenation supports subsequent cracking by forming an active olefinic intermediate compound via dehydrogenation (Bezergianni, 2013).

The composition of the metal in relation to the amorphous oxide support dictates the catalysts ratio between the cracking and hydrogenation functions. Catalyst activity and product selectivity can be optimised by adjusting the composition of the metal and support. The relative strength of different hydrogenation and hydrocracking functions in hydroprocessing catalysts are shown in Table 2-7.

Table 2-7 Strength of hydrogenation and hydrocracking function in dual-functional catalyst (Scherzer and Gruia, 1996)

Hydrogenation function	Co/Mo < Ni/Mo < Ni/W < Pt(Pd)
	Increasing hydrogenation activity
Hydrocracking function	Al ₂ O ₃ < Al ₂ O ₃ -halogen < SiO ₂ -Al ₂ O ₃ < zeolite
	Increasing hydrocracking activity (acidity)

For a hydroprocessing catalyst to be effective, it is necessary that a rapid molecular transfer exists between the acid sites and the metal sites in order to avoid undesirable side reactions. This can be achieved by having the metal sites in close proximity to the acid sites. Examples in the literature suggest that noble metal content for hydroprocessing catalysts usually compromise 1 wt. % or less, while non-noble catalysts are larger: 3-8 wt. % for cobalt or nickel oxides, and 10-30 wt. % for molybdenum or tungsten oxides. Besides the metal ratio and amount of metal used, other key factors regarding the metal component include the metal types, the degree of metal dispersion over the support, the metal-support interaction and the location of the metal on the support (Scherzer and Gruia, 1996).

Currently, the most commonly used commercial catalysts for hydroprocessing employ cobalt and molybdenum (Co-Mo) or nickel and molybdenum (Ni-Mo) in alumina substrate (Al_2O_3) as shown in Figure 2-13.



Figure 2-13 Co-Mo and Ni-Mo hydrotreating catalysts a) before use and b) Ni-Mo after use (Bezergianni, 2013)

It is crucial to ensure an appropriate hydroprocessing catalyst is selected as it plays a critical role in defining the hydroprocessing product yield and quality, as well as the operating cycle time of the process in the petroleum industry (Birchem, 2010). However, selection of a catalyst for hydroprocessing biomass feedstocks is particularly challenging and crucial for two reasons: a) the catalyst activity varies significantly, as commercial catalysts are designed for different feedstocks, such as feedstocks with high sulphur content etc., and b) there currently does not exist any hydroprocessing catalysts for lipid feedstocks and other intermediate products of biomass conversion processes (Bezergianni, 2013). However, there are on-going efforts that are geared towards developing hydroprocessing catalysts for converting/upgrading liquid biomass to biofuels (Tiwari et al., 2011)

2.6.1 Catalyst preparation

The key objective when preparing a catalyst is to ensure it has the correct combination of constituents to achieve high yield and selectivity, while having a reduced degradation and coking rate. This ensures a minimum amount of time and resources are required to produce the maximum amount of high quality product. There are two common methods employed to prepare catalysts: a) impregnation method and b) precipitation method, both of which require drying, calcining and reduction steps (Satterfield, 1991). The impregnation method is most commonly employed in the preparation of hydroprocessing catalysts. It is a simpler method, when compared to the precipitation method and is preferred when using an expensive metal component since only a small quantity of it is needed to be spread throughout the support. On the other hand, the precipitation method causes some of the metal ingredients to be enclosed by other present materials and is therefore unable to catalyse the desired reactions (Satterfield, 1991).

The two types of impregnation methods are ‘dry impregnation’ and ‘wet impregnation’. Wet impregnation is utilised when there is an interaction between the precursor and the support, and when the specific loading of the precursor is low (Pinna, 1998). Wet impregnation is utilised in this study to prepare the Ni-Mo/SiO₂ and Co-Mo/SiO₂ catalysts. Both of these catalysts required a Mo/SiO₂ precursor which was also prepared via the wet impregnation method. As such this method is often called the ‘sequential wet impregnation’ method.

2.6.1.1 Drying

Drying is a necessary step in the wet impregnation method as it removes excess water. This process usually occurs between 80 to 200 °C. The factors that need to be considered as they affect the distribution of the active sites are the drying temperature, the duration of drying and the rate of drying (Pinna, 1998). There are other complex factors that are difficult to take into account which include the rate of nucleation, degree of liquid saturation, pore size distribution and the degree to which the liquid paths between the pores are connected (Satterfield, 1991).

2.6.1.2 Calcination

Calcination is a heat treatment process whereby the catalyst is heated using air. The calcination temperature is usually around or slightly higher than the catalytic reaction temperature for which the catalyst is being prepared (Perego, 1997). Calcination eliminates chemically bonded water or atmospheric CO₂ allowing for the formation of an active phase metal oxide by decomposition of the precursor (Pinna, 1998).

2.6.2 Catalyst supports

The purpose of the catalyst support (or carrier) varies depending on the catalyst and the reactions occurring. Besides providing the acidic sites which promote hydrocracking reactions, the supports also provide a platform for the uniform distribution of the metal sites to achieve a larger surface area. Subsequently this helps prevent coalescing and/or agglomeration of the lower melting point metals (Stiles, 1987). For these reasons the selection of the support is a critical step, as the reaction is dependent on the acid sites on the support.

2.6.3 Catalyst characterisation

Catalyst characterisation techniques are utilised to determine different properties of the catalyst. It provides understanding into the catalyst’s behaviour and functionality during reactions allowing for optimisation for future catalyst preparations. The two types of catalyst analysis carried out in this study are the BET method for surface area measurements and Energy dispersive X-ray analysis for elemental information.

2.6.3.1 Surface area measurements – BET method

The BET method provides information on the textural properties of the catalyst such as the surface area, pore volume and pore width. This method is usually carried out in a gas analyser by the physical adsorption of gases that are non-polar, such as nitrogen (Anderson and Pratt, 1985). There are various other gases that could be used for the adsorption as shown in Table 2-8.

Table 2-8 Typical adsorption temperatures for gases used in surface area measurements (Anderson and Pratt, 1985)

Gas	Typical adsorption temperature (K)
Nitrogen	77
Argon	77
Xenon	90
Methane	90
n-Butane	27
Carbon dioxide	195

It is necessary to degas the catalyst sample prior to the physical adsorption procedure. The temperature and duration of the degassing process is specific to the catalyst sample and can be determined experimentally.

2.6.3.2 Energy dispersive X-ray analysis

Energy dispersive X-ray (EDX) analysis utilises the X-ray spectrum emitted by a solid sample which has been bombarded with a focused beam of electrons to obtain a localised chemical analysis. In principle, all elements from atomic number 4 (Be) to 92 (U) can be detected. Qualitative analysis involves the identification of the lines in the spectrum and is fairly straightforward owing to modern technology of X-ray spectra. Quantitative analysis requires measuring line intensities for each element in the sample and for the same elements in calibration standards of known compositions (Goldstein et al., 1992).

By scanning the beam and displaying the intensity of a selected X-ray line, element distribution images can be produced. In addition, images produced by electrons obtained from the sample reveal surface topography or mean atomic number differences according to the selected mode. The scanning electron microscope (SEM) is designed primarily for producing electron images, but can also be used for elemental mapping, and point analysis if an X-ray spectrometer is added (Goldstein et al., 1992).

2.6.4 Catalyst pre-sulphiding

Both commercially purchased and prepared metal catalysts are typically in their oxide form such as MoO_3 , CoO , and NiO etc. However, characterisation studies of hydroprocessing catalysts, performed under working conditions, indicate that these metals (Mo, Co, Ni, Ru, W etc.) are active as metal sulphides (Eijsbouts, 1997). Upon activation, the finely dispersed metal oxides are converted into well-dispersed metal sulphides such as MoS_2 , CoS_x , and NiS_x etc. However, there has been no clear agreement about the nature of the catalyst active phase. Furthermore, there is no accepted methodology pertaining to the optimisation of the catalyst activation process.

There has been numerous studies which have investigated the variables that affect the activation processes which include sulphiding gas composition, partial pressure of sulphur-containing species, heating schedule, final sulphiding temperature and various pre-treatment procedures in inert gas or hydrogen prior to sulphiding. Many authors have reported that sulphiding strongly influences the performance of hydroprocessing catalysts. There is much emphasis placed on the importance of fully sulphided structures for high activity, while noting that less desirable oxysulphides or incompletely sulphided species are formed at low sulphiding temperatures and after pre-reduction (John et al., 1996).

2.6.4.1 In-situ sulphiding

Traditionally, catalyst sulphiding has been performed in-situ by the addition of a sulphur compound to the circulating gas, or by doping a refinery stream with a sulphur compound (e.g. dimethyl disulphide) and circulating it through the catalyst bed. Along with in-situ sulphiding, environmental precautions must be taken. Many sulphiding chemicals are toxic and volatile with vapour pressures of up to a few hundred millibars at 20 °C. Therefore it is critical to ensure the system has no leakage and that the area is well ventilated (Vukovic et al., 2004).

Another important factor with regards to in-situ sulphiding is the time required to complete the process. Catalyst manufacturers recommend procedures which involve several temperature holds for extended periods which is very time-consuming. The entire duration of the sulphiding process can require several days.

The temperature profile under which the process takes place is another critical factor. Work performed by Prada et al (1989) on conventional Co-Mo catalyst showed that increasing the sulphiding temperature from 300 to 400 °C produced a major increase in the degree of sulphiding of the molybdenum species. Experimental temperature-programmed sulphiding studies suggest that metal reduction is initiated at 343 °C in the presence of hydrogen (Zeuthen and Blom, 1991). Pressure is believed to play no significant role in the sulphiding process.

2.6.5 Coke formation and regeneration

In catalytic hydroprocessing reactions, carbonaceous materials accumulate on the surface of the catalyst. The carbonaceous material is referred to as 'coke'. This process occurs according to the mechanism which involves the initial adsorption of either reactants or products, and thereafter followed by chemical reaction of the absorbed material to produce surface deposits of much lower volatility. This accumulation tends to lower the cracking activity of the catalyst. However, this material can be removed periodically by burning using oxygen, commonly called 'regeneration'. Coke formation results in the loss of desired product and subsequent regeneration is energy intensive and as such, factors leading to coke formation are of critical commercial importance (Eberly et al., 1966).

Since a wide range of reactions occur in hydroprocessing, a precise mechanism for coke formation has been difficult to establish, even in systems with pure compound feedstocks. However, there are certain generalisations that are made to provide more understanding and subsequently, predictability to the process. Common hydroprocessing catalysts usually have large surface areas and as a result, they adsorb hydrocarbons even at high temperatures (Eberly et al., 1961). Highly unsaturated, higher molecular weight hydrocarbons are adsorbed preferentially. This effect somewhat accounts for the fact that aromatics have the highest tendency for coke formation (Appleby et al., 1962). Coupled with adsorption, the aromatics can also undergo chemical reactions on the surface, such as condensation and hydrogen elimination. The hydrogen elimination reaction can proceed by olefins interacting with the adsorbed aromatics to form paraffins and hydrogen-deficient coke (Thomas, 1944).

A study performed by Voorhies (1945) concluded that carbon formation (wt. % on feed) increased exponentially with conversion level. Furthermore, when expressed as weight percent on catalyst (C), it followed the following equation (Voorhies, 1945):

$$C = at^n \quad (2-8)$$

Where a and n are constants and t is the cycle time. The n constant had a value around 0.5 indicating a diffusion-controlled process. Furthermore, no dependence on the feed rate was observed in the range of 0.6 to 1.2 (gas volume per liquid volume per hour) v./v./hr.

In order to determine the effect of particle size on coke formation in catalytic hydroprocessing, an experiment was conducted whereby n-hexadecane underwent hydrocracking reactions at 500 °C for 60 minutes over Al₂O₃/SiO₂ (13/87 wt.%) catalyst in a fixed bed which comprised of various particle sizes. After the experimental run, the particles were separated into fractions via screening and each fraction was analysed to determine the weight percent per carbon on catalyst

particle. Table 2-9 shows the results of the experiment which clearly indicate there is no noticeable difference in the amount of carbon found on each particle size range.

Table 2-9 Carbon formation as a function of particle size (Eberly et al., 1966)

Particle size range (μm)	990-2360	700-990	420-700	300-420	250-300	150-250	75-150
Wt. % carbon on catalyst	4.01	4.02	3.78	4.02	4.07	4.02	3.93

The results showed no discernible variation in wt. % of carbon on the catalyst over the entire particle size ranges indicating that coke formation is not dependent on particle size. Furthermore, this proved a uniform distribution of coke formation throughout the internal structure of the catalyst. This conclusion was also supported by a previous research on electron and light microscopical studies of carbonised catalysts (Haldeman et al., 1959).

The research by Eberly et al. (1966) also developed an equation to express the weight percent of carbon on the catalyst as a function of both cycle time and space velocity. Figure 2-14 shows experimental data (symbols) and predicted data (lines) for a range of experiments. The predicted data was produced using equation (2-9) (Eberly et al., 1966), which was generated by regression of the experimental data. This lead to the conclusion that coke formation in fixed beds for hydroprocessing reactions is a complex function of length of cracking cycle and the feed rate.

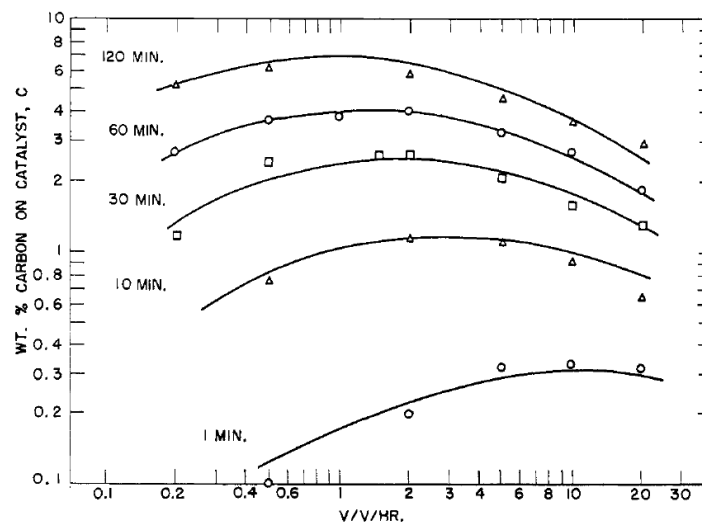


Figure 2-14 Actual and predicted carbon formation on $\text{Al}_2\text{O}_3/\text{SiO}_2$ catalyst from cracking of n-hexadecane at 500 °C (Eberly et al., 1966)

$$\log C = -0.2666 \log^2(v./v./hr.) + (0.5485 - 0.2666 \log[t] \cdot \log(v./v./hr.) + 0.7838 \log(t) - 0.7958 \quad (2-9)$$

2.7 Hydroprocessing operating parameters

It has been mentioned earlier that the choice of catalyst and the operating conditions affect hydroprocessing reactions. The key operating parameters of hydroprocessing reactions include the reaction temperature, hydrogen partial pressure, hydrogen feed-rate and the liquid hourly space velocity of the feedstock.

2.7.1 Reaction temperature

Catalytic hydroprocessing reactions operate between 290-450 °C. The temperature (or temperature range) is selected based on the type of catalyst/s and feedstock being processed, as well as the desired products. In industry, the temperature is initially kept low as the catalyst is in its early stages of catalyst life. As the reactions proceed, the reaction temperature is gradually increased to overcome the loss of catalyst activity (due to coking and deactivation) and to maintain both the yield and quality of the desired product (Bezergianni, 2013).

2.7.2 Hydrogen partial pressure

The hydrogen partial pressure has a significant effect on the hydroprocessing reactions as well as the catalyst deactivation. High hydrogen pressure promotes a greater degree of hydrocracking resulting in smaller chain hydrocarbons and is therefore suitable when kerosene and/or gasoline range is desired. Fortuitously, catalyst deactivation is also inversely proportional to hydrogen partial pressure which allows for extended use when smaller chain products are desired. However, high hydrogen partial pressure does require high operational costs, which rise even higher when high hydrogen consumption is necessary due to saturation reactions as is the case for highly unsaturated olefins or triglycerides. Therefore it is important to balance hydrogen partial pressure with catalyst activity and life expectancy in order to optimise the overall process (Bezergianni, 2013).

2.7.3 Hydrogen feed-rate

The hydrogen feed-rate also defines hydrogen partial pressure depending on the hydrogen consumption of each application. The hydrogen feed-rate favours both heteroatom removal and saturation reaction rates. However, once again, there is high operating costs associated with high hydrogen usage. As such, renewable energy sources for hydrogen production are being researched as a potential cost improvement (Bezergianni, 2013).

2.7.4 Liquid hourly space velocity

The liquid hourly space velocity (LHSV) is defined as the ratio of the liquid mass feed-rate (gr/h) over the catalyst mass (gr) and is expressed in hr^{-1} as shown in equation (2-10). LHSV is inversely

proportional to residence time of the liquid feed rate to the reactor. As such, if a high degree of cracking is required, a low LSHV should be utilized, which will allow for a greater residence time. Large LHSV imposes faster degradation of the catalyst, therefore in industrial applications the LHSV is maintained in as low values as practically possible (Bezergianni, 2013).

$$LHSV = \frac{\text{mass flow rate of liquid oil}}{\text{mass of catalyst}} \quad (2-10)$$

Chapter

3

Experimental design

3.1 One-Variable-At-A-Time (OVAT) method

The experimental plan was designed using the simple One-Variable-At-A-Time (OVAT) approach. In this method, only one factor (variable) is varied at a time while all other factors remain constant. This was an acceptable approach for this study since the reaction temperature was the only adjusted variable for each tested catalyst. If other factors were being tested, the OVAT approach should not be employed since it does not account for interaction between the various tested factors. Interaction between factors is evident when a factor affects the output differently at different levels of another factor (Montgomery, 1998). Therefore, in the case of multiple varied factors, results obtained from an OVAT approach may not be the optimum results achievable overall, unless all factors are completely independent of each other (Leardi, 2009).

DeCoursey (2003) suggests that all experiments should not be laid out prior to the start of experimental work. Preliminary runs should be carried out, and results analysed to serve as exploratory investigations. This provides greater understanding of the system and operating parameters while enabling troubleshooting, and results in a 'sequential' and 'evolutionary' experimental design (DeCoursey, 2003).

Since only one variable (reaction temperature) with three different levels are tested over six catalysts (four different catalysts with two regenerated) the total number of tests required is:

$$3^1 \times 6 = 18 \text{ Tests}$$

After preliminary tests (discussed in Chapter 4), the final layout of experiments were proposed. This layout can be seen in Table 3-1:

Table 3-1 Layout for experimental runs

Catalyst	Temperature (°C)	Pressure (Bar)	Liquid oil flow rate (ml/min)	H ₂ gas flow rate (ml/min)
Ru/Al ₂ O ₃ (F) ^a	425	120	0.1	500
	400			
	450			
Ni/Al ₂ O ₃ (F)	400	120	0.1	500
	450			
	425			
NiMo/SiO ₂ (F)	450	120	0.1	500
	425			
	400			
CoMo/SiO ₂ (F)	425	120	0.1	500
	450			
	400			
Ru/Al ₂ O ₃ (R) ^b	425	120	0.1	500
	450			
	400			
Ni/Al ₂ O ₃ (R)	425	120	0.1	500
	400			
	450			

[a] (F) – Indicates fresh catalyst

[b] (R) – Indicates regenerated catalyst

3.2 Randomisation and replication

Minimizing error due to interfering factors when conducting experimental runs is vital to attain accurate results. Randomisation and replication are two strategies that can be employed to minimize error.

In order to reduce the systematic error in measurements, randomisation of the order of experimental runs and product analysis techniques is employed. Systematic error arises from interfering factors such as machine wear, air temperature etc. Therefore, by employing the randomisation strategy when conducting experiments and analysis, the interfering factors are averaged out and the bias is minimized (DeCoursey, 2003). As such, as seen in Table 3-1, the reaction temperature for each experiment for each catalyst was selected at random rather than following a particular order such as lowest to highest or vice versa. Furthermore, all product analysis using the GCMS was performed in random order.

While experimental runs were performed once, all feedstock and product analysis techniques were performed in triplicate. This ensures the reproducibility of the results obtained from these analyses.

Chapter

4

Experimental equipment

4.1 Experimental equipment overview

The experimental procedure was categorised into three main sections; i) the catalyst preparation and pre-treatment, ii) the catalytic hydrocracking of waste cooking oil and, iii) the separation and analysis of the products obtained from the hydrocracking reactions.

The catalytic hydrocracking of waste vegetable oil was carried out in a lab-scale fixed bed reactor system designed and commissioned as part of the study. Figures 4-1 and 4-2 represent the two process instrumentation diagrams for the two experimental setups utilised in this study. Due to problems with line blockage during product collection, the low pressure glass separator (Scheme 1) was replaced by a high pressure stainless steel collection pot and the metering valve was placed after this collection vessel (Scheme 2). Product separation was carried out in a ROTOFIX 32 A Benchtop Centrifuge fitted with 6-place swing-out rotor and product analysis was performed using a 2010 SHIMADZU Gas Chromatograph Mass Spectrometer and a Thermo Finnigan Trace Gas Chromatograph coupled to a PolarisQ Mass Spectrometer. This chapter presents a detailed description of the experimental equipment utilized for this study.

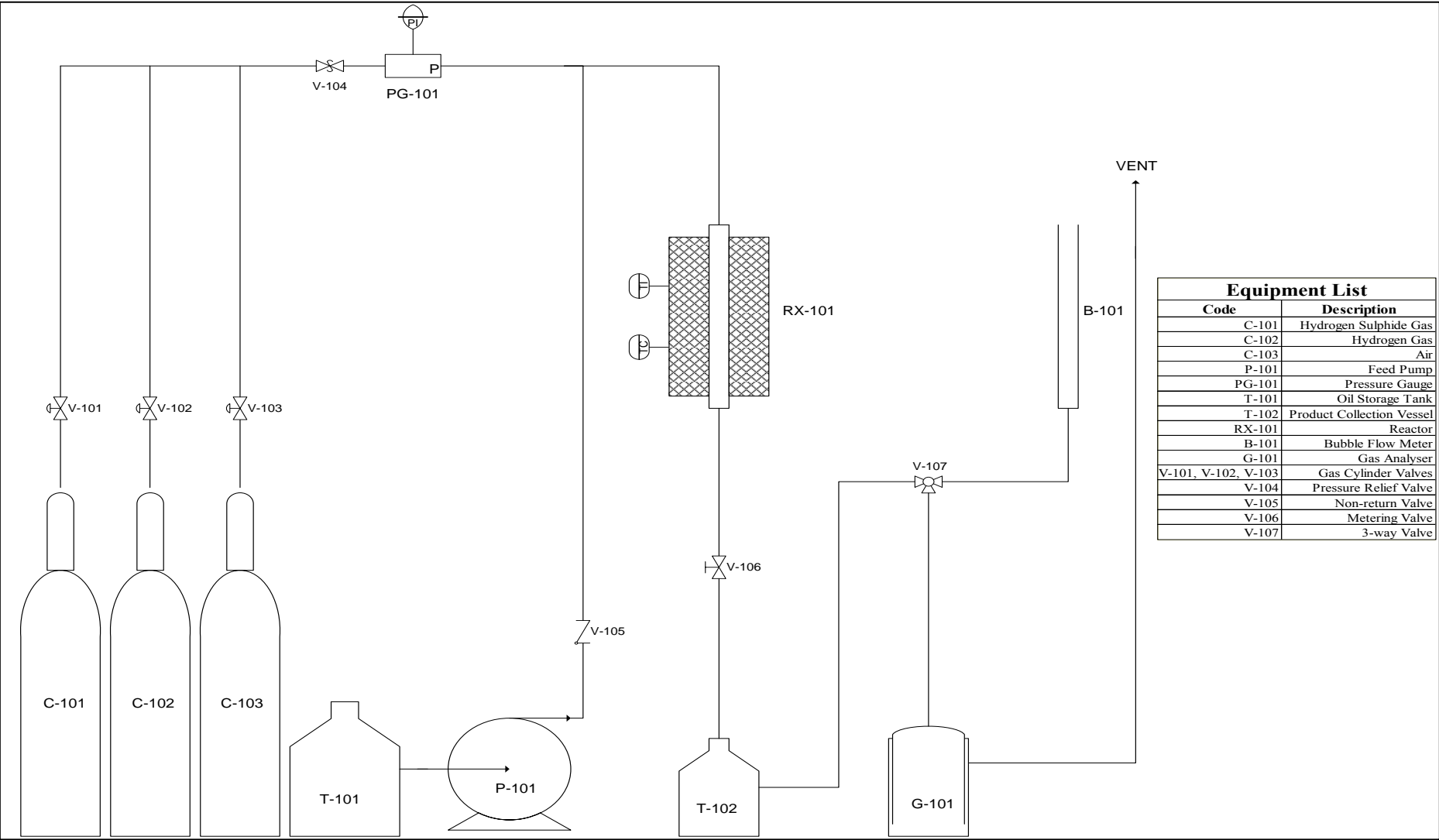


Figure 4-1 Scheme 1 of the experimental setup piping and instrumentation diagram

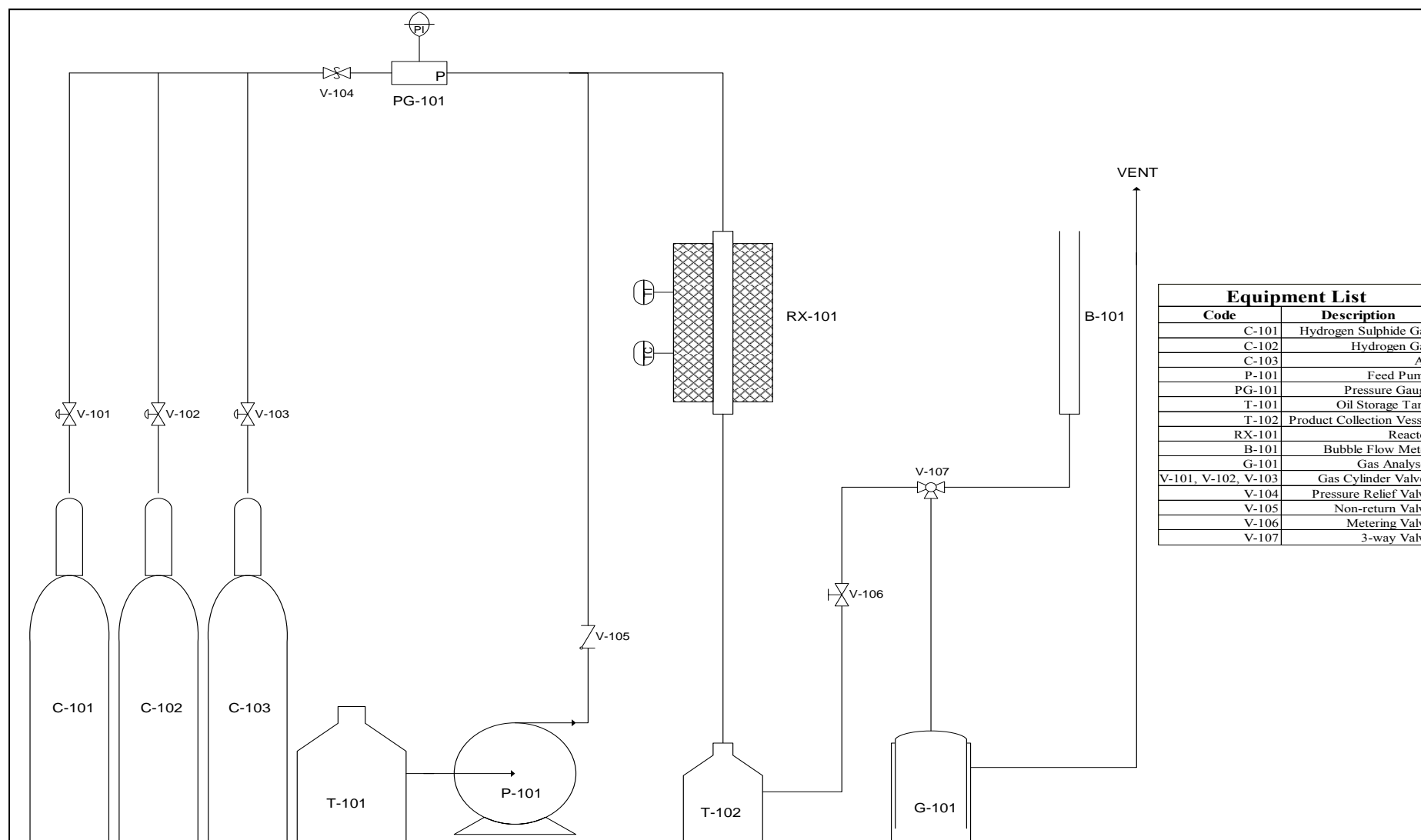


Figure 4-2 Scheme 2 of the experimental setup piping and instrumentation diagram

4.2 The lab-scale hydrocracking apparatus

The lab-scale fixed bed hydrocracking reactor system used in this study consisted of the equipment described below.

4.2.1 Oil feed storage tank

Figure 4-3 shows the stainless steel metal storage tank used to contain the waste cooking oil fed to the reactor. The storage tank was filled using a funnel through a ball valve on the lid of the tank. The tank was raised using a metal stand and oil was drawn to the reactor using a pump via a valve on the bottom of the tank.



Figure 4-3 Waste vegetable oil storage tank

4.2.2 Oil feed pump

The oil from the storage tank was fed to the reactor via a BECKMAN model 110A pump (Figure 4-4). The oil was pumped at room temperature. The volumetric flow rate setting ranged from 0.1 – 9 ml/min with increments of 0.1 ml/min. Calibration for the mass of oil fed per minute was carried out at higher flowrates (1-9 ml/min at 1 ml/min intervals) but extrapolation below 1 ml/min was unreliable. Therefore the density of the oil was used to calculate the total mass fed to the reactor over the duration of each experimental run. A non-return valve was fitted on the discharge side of the pump to prevent any oil or gas from flowing back into the pump.



Figure 4-4 BECKMAN model 110A pump

4.2.3 Reactor and electric furnace

The reactor was a 316 stainless steel tube (length = 40.4 cm, ID = 1.0 cm and OD = 1.4 cm) fitted with Swagelok tube reducing unions on either end. The tube was placed vertically into a clam shell electric furnace designed for heating tubular reactors (Figure 4-5). The vertical arrangement allowed the down flow of reactants and products via gravitational force. The feed line to the reactor was fitted with a pressure gauge to validate the system pressure over the entire duration of each experimental run. A pressure relief valve was also fitted onto the system as it served as a safety precaution. If the system pressure gradually or suddenly increased, the pressure relief valve would open, releasing the excess pressure to prevent damage to the equipment and possible injuries to the operator.



Figure 4-5 Tubular reactor and opened clam shell electric furnace

4.2.4 The catalyst and packing material

Since the most uniform temperature was in the middle of the tube, the catalyst only occupied the central space of the tubular reactor (bed length = 21.4 cm), while either end was packed with spherical glass beads ($D = 3\text{ mm}$). An example of the catalyst pellets and the glass beads are shown in Figure 4-6 and Figure 4-7 respectively.



Figure 4-6 Catalyst pellets



Figure 4-7 Glass beads used for packing

New glass beads were used each time new catalyst was loaded. A metal mesh was inserted at the exit of the reactor to prevent the packing and/or any small catalyst particles from blocking the reactor exit and being blown out of the tube. A metal rod was used to determine the total length of the reactor, and subsequently the height of the packing and the catalyst bed. Figure 4-8 shows a vertical cross sectional schematic view of the reactor tube with the catalyst, glass beads and metal mesh.

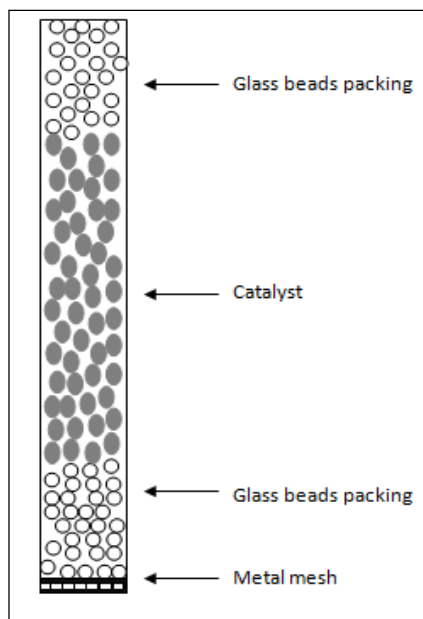


Figure 4-8 Schematic cross-sectional view of the tubular reactor

4.2.5 Metering valve and collection vessels

In the first setup (Scheme 1) the yellowish-grey coloured liquid and waxy product had to pass through a Swagelok bellow-sealed metering valve (SS-4BM) before entering the transparent glass collection vessel (Figure 4-9).



Figure 4-9 Glass product collection vessel

The valve maintained the system pressure and regulated the flow of gas leaving the system. As there had been no prior experiments of this type at the university to draw reference from, a transparent collection vessel enabled visual inspection of the product (and the amount formed) during the experimental run. However, during troubleshooting, an increase in the exit pressure to

the product vessel by adjusting the metering valve sometimes caused the plastic tubing connected to the collection vessel to rupture. For this reason, prior to the experimental run, it was important to set the valve to the appropriate position, and not to adjust it during the experimental runs. While the first set of experiments (commercial catalysts) were conducted using this scheme, a second scheme was developed to eliminate the possibility of ruptures around the collection vessel, consequently reducing the possibility of product loss and a failed experimental run, and avoiding a potential safety hazard.

In the second setup (Scheme 2), the metering valve was placed after the collection vessel, which was made from stainless steel, capable of withstanding high pressure. Visual inspection of the product was not possible with this vessel, however, it was not required as the previous setup had given insight into the amount of products formed. Using this setup meant that minor adjustments to the metering valve did not constitute a potential safety hazard.

4.2.6 Bubble flow meter

All gas leaving the system was either passed through a bubble flow meter (Figure 4-10) or through a gas analyser before being vented to the atmosphere. A 3-way valve was used to direct the gas through the desired equipment.



Figure 4-10 Bubble flow meter

The gas caused bubbles from a soapy solution to rise in the bubble flow meter glass tube, indicating a steady gas flow rate. During troubleshooting, no bubbles indicated a clog in the system, most commonly at the metering valve. The bubble flow meter was mounted close to the

reactor apparatus and as such, the gas was passed through the bubble flow meter for only a few seconds every 10 – 15 minutes to ensure steady gas flow and no clogging of the system. The remainder of the time the gas was passed through the gas analyser, and subsequently vented out the building and into the atmosphere to prevent large quantities of any unpleasant or unsafe substances inside the laboratory.

4.2.7 Gas analyser

During experimental runs, a MRU Vario Plus gas analyser (Figure 4-11) was used to identify the gases leaving the system. Although no collection and quantification of these gases were performed, the gas analyser provided insight into what gases were being produced from the hydrocracking reactions.



Figure 4-11 MRU Vario Plus Gas Analyser

4.2.8 The centrifuge

The liquid and waxy products from the collection vessel were separated using a ROTOFIX 32 A Benchtop Centrifuge fitted with 6-place swing-out rotor as seen in Figure 4-12. The centrifuge operates using the sedimentation principle in that centripetal acceleration causes denser substances to move outward in the radial direction while displacing less dense substances to the centre.



Figure 4-12 Centrifuge for product separation

4.2.9 Gas chromatograph mass spectrometer

The products from Scheme 1 were analysed using a 2010 SHIMADZU Gas Chromatograph Mass Spectrometer (GCMS-QP2010) in order to identify and quantify the liquid product obtained from the hydrocracking reactions (Figure 4-13). The hardware was connected to a computer which captured data using proprietary software, Lab Solutions®. This software enabled remote use of the hardware and allowed for product analysis. The GC consists of the injection port (fitted with an auto-injector) and a column within an oven, while the MS consists of an ion source, filter and injector.



Figure 4-13 2010 SHIMADZU GCMS-QP

The products from Scheme 2 were analysed using a Thermo Finnigan Trace Gas Chromatograph coupled to a PolarisQ Mass Spectrometer. It was operated in the same manner as the SHIMADZU GC-MS described above including the same column type and temperature program.

The waste vegetable oil used as the feed to the reactor was analysed using the same GCMS setup as the products from Scheme 2, however, a different column and temperature program was used.

The column characteristics for all three of the above mentioned analyses are given in Tables 4-1 and 4-2 below. The temperature programs are given in Chapter 5.

Table 4-1 Product analysis column characteristics and detector type

2010 SHIMADZU GCMS-QP and Thermo Finnigan Trace GC coupled with PolarisQ MS		
Column	Unit	Zebron ZB-5MS
Composition		5% Phenyl-Arylene, 95% Dimethylpolysiloxane
Temperature limits	°C	-60 to 350
Polarity		8 (non-polar)
Length	[m]	30
ID	[mm]	0.25
Film thickness	[μm]	0.25
Detector		TID

Table 4-2 Feed analysis column characteristics and detector type

Thermo Finnigan Trace GC coupled with PolarisQ MS		
Column	Unit	Supelco Nukol
Composition		Acid-modified poly(ethylene glycol)
Temperature limits	°C	-60 to 200
Polarity		Polar
Length	[m]	15
ID	[mm]	0.53
Film thickness	[μm]	0.5
Detector		TID

The different compounds in the injected sample are separated based on their volatility. The compounds retention time within the column increases with decreasing volatility. The output from the GC is a total ion chromatogram (TIC) displayed using the Lab Solutions® software. Each peak on the TIC (Figure 4-14) represents a different compound found in the sample. Using an internal standard, these peaks can be used to quantify the compounds found in the sample.

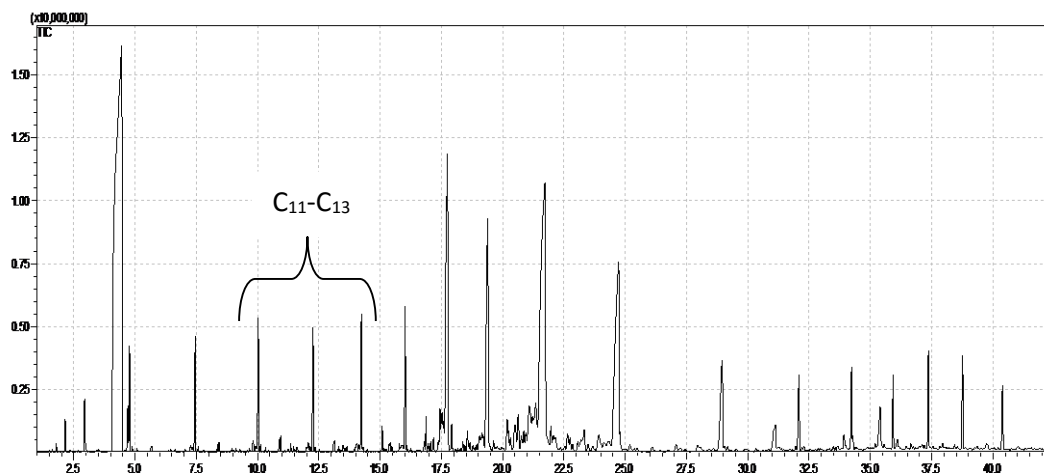


Figure: 4-14: Example TIC (Liquid product from experiment at 450 °C using fresh Ni/Al₂O₃ catalyst)

The ion source in the MS blasts the sample with electrons causing them to break and become positively charged ions. These ions travel through an electromagnetic field which filters the ions based on mass. Finally the detector counts the number of ions with a specific mass which generates a mass spectrum. Each compound has a unique mass spectrum and can therefore be compared against a database to identify it.

Chapter

5

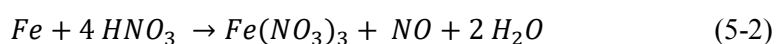
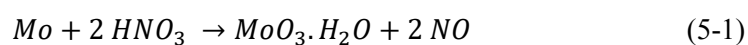
Experimental methods

5.1 Catalyst Preparation

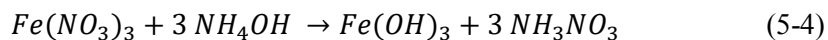
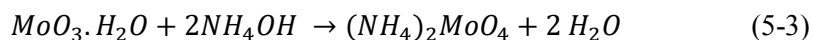
The study utilised four different catalysts. Two of the catalysts were commercially produced while the remaining two were prepared in the laboratory. The commercial catalysts were the ruthenium and nickel, both dispersed on alumina supports, while the prepared catalysts were that of molybdenum-nickel and molybdenum-cobalt, both dispersed on silica dioxide supports. In order to prepare these two catalysts, a sequential impregnation technique was used. It was necessary to first prepare a molybdenum silica dioxide catalyst. Once this was complete, the nickel (or cobalt) was loaded. More specifically, the wet impregnation method using salt solutions was utilised for both catalyst preparations. A detailed procedure of the catalyst preparation techniques are described below. The sample calculations can be found in Appendix D.

5.1.1 Preparation of the Mo/SiO₂ catalyst

In order to prepare the two catalysts; one comprising of 10.4 wt% Mo and 2.3 wt% Ni on SiO₂ and the other comprising of 9.8 wt% Mo and 2.5 wt% Co on SiO₂, a molybdenum-iron alloy (67.11% Mo) was digested in excess nitric acid according to:



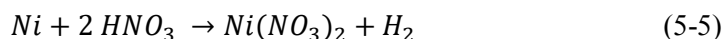
The next step was the addition of a slight excess of ammonium hydroxide to precipitate out the iron as $Fe(OH)_3$ and form ammonium molybdate:



Silica gel was dried at 100 °C for 2 hours and allowed to cool before weighing. An appropriate amount of ammonium molybdate was added to the silica gel together with a small amount of distilled water to form a slurry. The slurry was stirred vigorously overnight. The supernatant liquid was drawn off and the catalyst granules were then dried at 110 °C overnight. Calcination at 450 °C for 3 hours completed this preparation (Barath et al, 1999).

5.1.2 Preparation of the Ni-Mo/SiO₂ catalyst

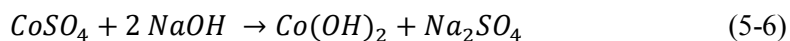
A stock solution of nickel nitrate was produced by digesting nickel shavings in concentrated nitric acid:



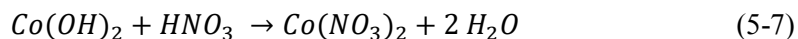
A weighed amount of the previously prepared Mo-SiO₂ catalyst was mixed with the $Ni(NO_3)_2$ solution to produce a slurry, which was allowed to stir vigorously overnight. The supernatant liquid was drawn off and the catalyst was dried at 110 °C overnight. Final calcination was carried out at 450 °C for 4 hours. The nitrate precursor was decomposed gradually to the metal oxide during the drying and calcination steps (Alouche et al, 2008).

5.1.3 Preparation of the Co-Mo/SiO₂ catalyst

An appropriate amount of cobalt sulphate was dissolved in distilled water. NaOH was added to form a precipitate of $Co(OH)_2$:



The precipitate was filtered, dried in an oven at 100 °C for 3 hours and weighed. The dried precipitate was dissolved in concentrated nitric acid to form cobalt nitrate:



A weighed amount of the previously prepared Mo-SiO₂ catalyst was mixed with the $Co(NO_3)_2$ solution to produce a slurry and allowed to stir vigorously overnight. The supernatant liquid was decanted and the catalyst was dried in an oven at 110 °C overnight. Finally, calcination was carried out at 450 °C for 4 hours.

5.2 Catalyst chemical check for metal loading

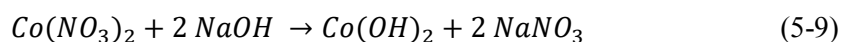
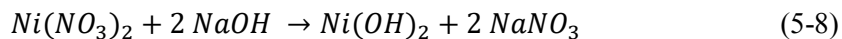
Chemical checks are carried out on the decanted supernatant liquids in order to ensure that all the desired metal has been loaded onto the support. These supernatant liquids are reacted with other chemicals to form precipitates which would contain any of the unloaded metal. Determining the mass of the unloaded metal indicates the success or failure of the catalyst preparation process. The chemical checks performed for each metal are described below.

5.2.1 Chemical check on Mo loading

An excess of FeCl_3 was added to the decanted supernatant liquid from the Mo-SiO₂ catalyst preparation to form a ferro-molybdenum oxide precipitate, $\text{MoO}_3 \cdot \text{Fe}_2\text{O}_3$. The precipitate was filtered, dried in an oven at 100 °C for 3 hours and weighed. The amount of molybdenum left in the liquid after the loading was then determined. A practically negligible amount of molybdenum was left in the precursor solution after loading, indicating that essentially all the molybdenum was loaded onto the silica oxide support.

5.2.2 Chemical check on Ni and Co loading

For both nickel and cobalt, the residual metal nitrate was reacted with NaOH to form insoluble metal hydroxides which were then filtered, dried at 100 °C for 3 hours and weighed to determine the actual loading:



Satisfactory loading was achieved when using the high stirring speeds during the impregnation step.

5.3 Catalyst Characterisation

Catalyst characterisations were performed in order to determine different properties of the catalyst. Characterisations were performed on the laboratory prepared catalysts while properties of the commercial catalysts were obtained from the supplier and/or literature (Appendix B).

5.3.1 BET surface area analysis

The textural properties of the catalysts in terms of the BET surface area, pore volume and pore width were determined using a Micrometrics ASAP 2020 gas adsorption analyser (Figure 5-1). Measurements were performed with nitrogen as the adsorbate at -196 °C. The samples were

degassed under nitrogen at 200 °C for 18 hours prior to analysis. All analyses were performed in triplicate.



Figure 5-1 Micrometrics ASAP 2020 gas adsorption analyser

5.3.2 Energy dispersive X-ray analysis

Energy dispersive X-ray (EDX) elemental analysis of the fresh catalyst was performed using a ZEISS Ultra Plus Scanning Election Microscope (SEM) (Figure 5-2), in the 10-20 keV range. All analyses were performed in triplicate.



Figure 5-2 ZEISS Ultra Plus Scanning Election Microscope

5.4 Catalyst loading and pre-treatment

Once the catalyst was prepared, ground down to a desirable size and weighed, it was loaded into the tubular reactor to form a fixed catalyst bed with glass beads packing on either end. It was then secured into the clam shell electric furnace where it would remain for catalyst pre-treatment, experimental runs and catalyst regeneration.

Catalyst pre-treatment was performed to ensure the catalyst was in the active state for hydrocracking reactions. In order to do this, the catalyst needed to be contacted with sulphur for a prolonged period of time to ensure that the metal components of the catalyst were converted to the active sulphides. For this study the in-situ method whereby hydrogen sulphide gas was passed over the catalyst bed was employed.

A 0.02 vol% sulphur gas is required to be contacted with the catalyst bed for activation. However, the hydrogen sulphide gas purchased from Afrox had a 0.05 vol% of sulphur. Therefore pure hydrogen gas (also purchased from Afrox) was used to further dilute the mixture to achieve a 0.02 vol% of sulphur in the hydrogen sulphide gas that was contacted with the catalyst bed.

Before pre-treatment was started, air was passed through the system and a soap solution was used to ensure there were no leaks at any mechanical joints in the setup. The clam shell electric furnace was set to room temperature. The calculated flow rates on the pure hydrogen and hydrogen sulphide gas to achieve a 0.02 vol% were set. The gas was allowed to pass over the bed for 10 minutes at room temperature and thereafter the temperature was ramped at a rate of 5° C/min to a maximum of 500° C. The gas continued to pass over the catalyst bed for another 8 hours at this maximum temperature to ensure complete catalyst activation for hydrocracking reactions. During pre-treatment, the exit gas was vented directly out of the building as hydrogen sulphide is flammable, toxic in large concentrations and has a very foul odour. Upon completion, the furnace was switched off and the gases were closed. The catalyst bed was now in the active state for the hydrocracking of waste vegetable oil.

5.5 Materials and operating procedure for the hydrocracking of waste vegetable oil

The primary feed material, waste vegetable oil, used for all experimental runs was obtained from local restaurants and homes. It was filtered under vacuum suction to remove any particulate matter during its cooking use. The hydrogen gas used for the dilution of hydrogen sulphide gas was also used in the hydrocracking reactions and had a purity of 99.999%.

With the tubular reactor in place and the catalyst pre-treatment completed, the clam shell electric heater was switched on and set to the desired reaction temperature (400, 425 or 450 °C). No adjustments were made to the reactor system after the pre-treatment procedure hence it was not necessary to re-check for possible leaks. Once the system reached and stabilised at the reaction temperature (a process that took approximately 20 minutes), the hydrogen gas was allowed to pass through the system increasing the pressure slowly until the reaction pressure of 120 bar was reached. The metering valve was opened and set to the appropriate position to ensure a steady gas

flow rate leaving the system as indicated by the bubble flow meter. The exit gas was then vented out of the building and the pump was switched on, pumping oil from the storage tank into the reactor at 0.1 ml/min, the lowest flow rate setting available. This was the start of the experimental run hence the time was recorded as the start time.

During the experimental run, it was important to monitor the system pressure and temperature as any undesired fluctuations could pose a potential safety hazard and/or damage to the equipment. It was also necessary to visually inspect the product being formed to ensure that the system was not clogged and that the collection vessel was big enough for the amount produced. The gas analyser was monitored to identify what gases were being produced inside the reactor and leaving the system. Lastly, it was important to direct the exit gas through the bubble flow meter every 10-15 minutes to ensure the gas was leaving the system at a steady rate, which further indicated no clogging (or product build-up) in the system.

At the end of the experimental run (2 hours for Scheme 1 and 3 hours for Scheme 2), the gases were closed, and the furnace and the pump were switched off. The remaining gas slowly exited and subsequently depressurized the system. Once the system was back to atmospheric pressure, the collection vessel containing the liquid and waxy product was removed and taken to the analytical lab for analysis. While not being used for analysis, the product was kept refrigerated in a sealed container.

5.6 Product analysis

5.6.1 Mass of products

The first step in analysing the product was to determine its combined mass i.e. the liquid and wax together. This was done by first weighing an empty bottle and thereafter weighing the bottle with the product inside it. This allowed for the determination of the total mass of the gas product formed during the experimental run (See equation 6-1). Due to the ease of product removal from the product vessel, there were negligible amounts of product loss and as such, product loss is not taken into account in the study.

5.6.2 Product separation

The next step was to separate the liquid product from the waxy product. This was done using a centrifuge described in section 4.2.8. The product was filled into one cylinder and water was filled into the cylinder directly across the product cylinder. This ensured the centrifuge maintained balance during the high speed rotation. The centrifuge was set to operate at 4000 rpm for 5 minutes. At the end of this process, the cylinder containing the product was removed. There were 2 distinct layers, the liquid product was displaced to the top while the denser wax product was

displaced to the bottom. The liquid was decanted into a glass bottle and weighed. The wax was removed using a spatula, placed into a glass bottle and also weighed. The separated liquid and wax product can be seen in Figure 5-3.



Figure 5-3 Separated liquid and wax product

5.6.3 Product identification and quantification (GCMS analysis)

Only the liquid product was analysed using the GCMS. The two GCMS units used for the analysis were the 2010 SHIMADZU Gas Chromatograph Mass Spectrometer (GCMS-QP2010) and the Thermo Finnigan Trace GC coupled to a PolarisQ MS. Their column characteristics were given in Tables 4-1 and 4-2 in section 4.2.9 respectively.

Both units utilised the same column temperature program as described in Table 5-1 and shown in Figure 5-4:

Table 5-1 Temperature program for liquid product analysis

2010 SHIMADZU GCMS-QP and Thermo Finnigan Trace GC coupled with PolarisQ MS			
			Hold time (min)
Program	T₁	70 °C	5
	rate1	8 °C/min	
	T₂	190 °C	10
	rate2	8 °C/min	
	T₃	270 °C	5
Detector temperature	[°C]	300	
Injector Temperature	[°C]	280	
Split Ratio		50:1	
Carrier gas (helium)	[ml.min ⁻¹]	46.5	

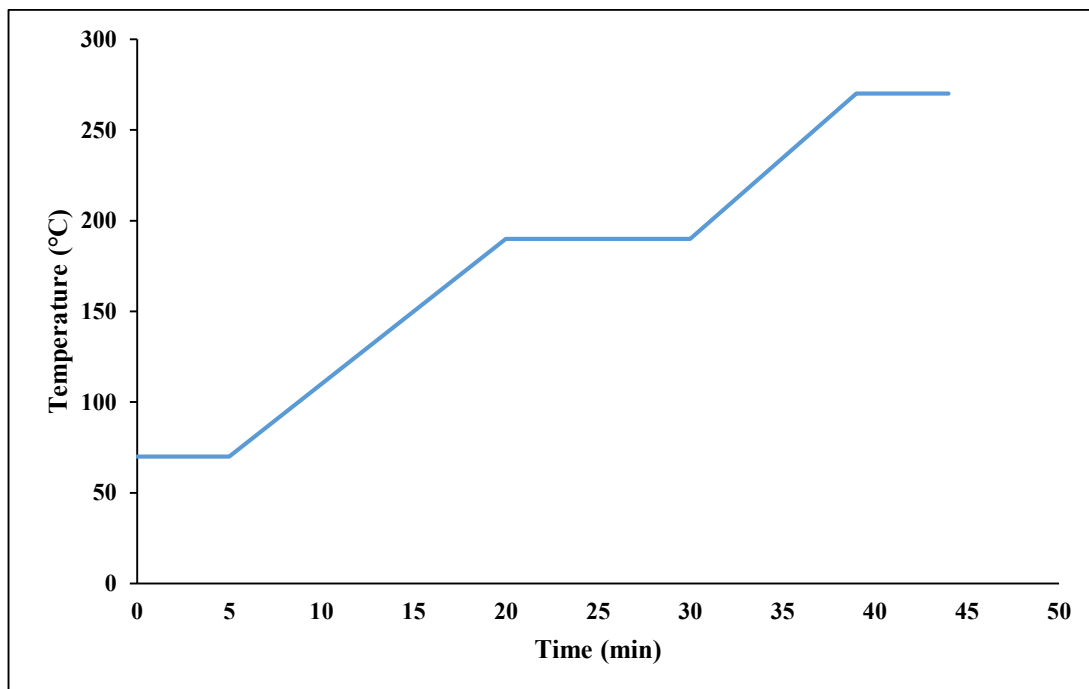


Figure 5.4 GCMS temperature program for product analysis

The internal standard method was used to quantify the liquid products formed. Xylene was selected as the reference component (component k) for this method as it was capable of dissolving all the liquid product to form one homogeneous substance. This method requires a relative molar response (RMR) factor for each component that exists in the liquid product. In order to determine this factor, a pure sample of each component in the liquid product is required. For each component (component i), a variety of solutions must be made up using a known number of moles of the component i (different amount for each solution) and a known number of moles of the reference component k (same amount for each solution). Each solution must be analysed using the GC to produce a total ion chromatogram (TIC). Each TIC will provide a peak for both the reference component, and the component for which the RMR is required. By plotting the area ratio against the mole ratio of each component i and the reference component k , a straight line should form whose gradient is the RMR for component i with respect to component k as follows:

$$RMR_{i,k} = \frac{n_i \cdot A_i}{n_k \cdot A_k} \quad (5-10)$$

However, not all the compounds were readily available and from those that were, some of the results proved to be inaccurate and unreliable, perhaps due to the age of the standards, contamination and low original purity. The n-alkanes have an unopened shelf life of three years and once opened, this decreases drastically into a few months. Most of available n-alkanes were obtained more than 3 years ago. The RMR data of Göröcs et al. (2013) was used for quantification.

The RMR for any n-alkane up to 20 carbon atoms can be determined via the regressed formula in equation (5-11) with $R^2 = 0.992$ (Göröcs et al., 2013):

$$RMR = 0.171n - 0.405 \quad (5-11)$$

where n = number of carbon atoms.

However, their study utilised naphthalene as the reference component and it was therefore necessary to implement a correction factor of 0.263 to account for xylene as the reference component in this study:

$$RMR = \frac{0.171n - 0.405}{0.263} \quad (5-12)$$

Table 5-2 below indicates the RMR for n-alkanes for a carbon atom range of 5-18, as found in the liquid products.

Table 5-2 Relative Molar Response factors for different alkanes using xylene as the reference (Göröcs et al., 2013)

Component	Number of carbon atoms	Relative Molar Response (RMR)
Pentane	5	1.71
Hexane	6	2.36
Heptane	7	3.01
Octane	8	3.66
Nonane	9	4.31
Decane	10	4.96
Undecane	11	5.61
Dodecane	12	6.26
Tridecane	13	6.91
Tetradecane	14	7.56
Pentadecane	15	8.21
Hexadecane	16	8.86
Heptadecane	17	9.51
Octadecane	18	10.16

Using a weighed sample of the liquid product, the mass fraction of each component can be obtained from the following equation by using the corresponding RMR factor and the area of the peak obtained from the TIC (Göröcs et al., 2013):

$$x_i = \frac{n_i \cdot M_i \cdot A_i}{\sum n_i \cdot M_i \cdot A_i} \quad (5-13)$$

This mass fraction from the analysed sample can be assumed to be the same for the total liquid product produced for a specific experimental run.

5.7 Feed analysis

It was important to identify the constituents of the waste oil being used as the feed to the reactor for the experiments. This was also performed using the Thermo Finnigan Trace GC coupled to a PolarisQ MS however, a different column was utilised. The column characteristics were described in section 4.3.9 and the temperature program is given in Table 5-3 and shown in Figure 5-5:

Table 5-3 Temperature program for feed waste vegetable oil analysis

Thermo Finnigan Trace GC coupled with PolarisQ MS			
Program	Hold time (min)		
	T ₁	100 °C	1
	rate1	8 °C/min	
	T ₂	220 °C	10
Detector temperature	[°C]	280	
Injector Temperature	[°C]	300	

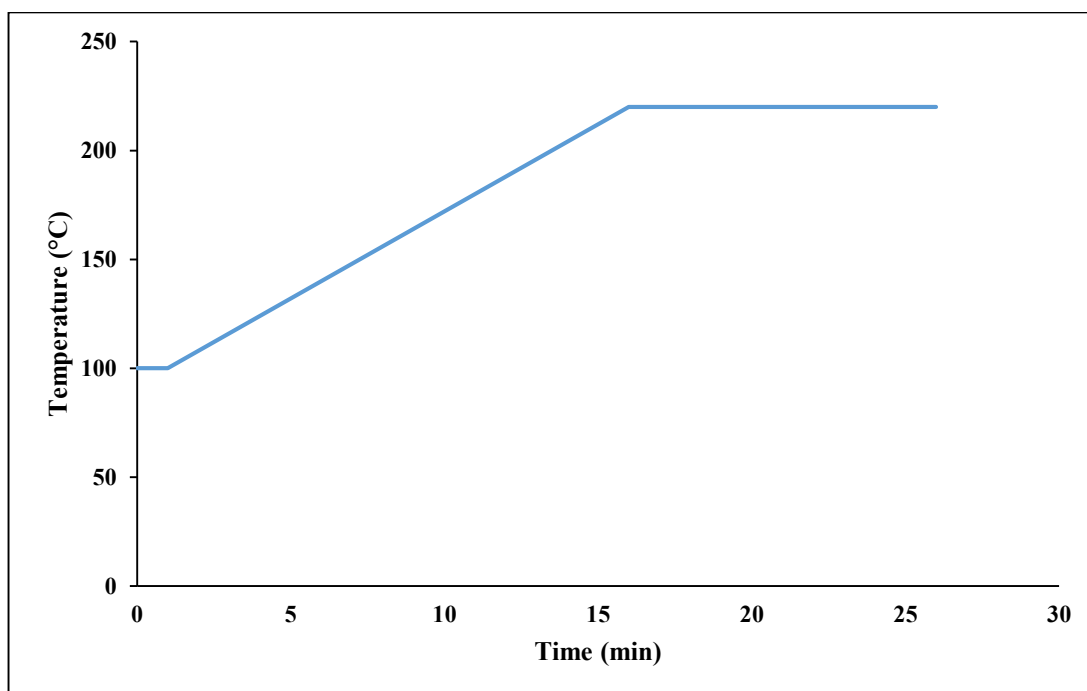


Figure 5-5 GCMS temperature program for feedstock analysis

10 mg of waste vegetable oil was combined with 10 ml of dichloromethane. The free fatty acids found in the waste vegetable oil (Appendix C) were quantified using authentic chromasolve standards from Sigma Aldrich.

5.8 Catalyst regeneration

Catalyst regeneration was performed on the commercial catalysts in order to determine if they maintained their activity even after several catalytic hydrocracking cycles. In order to burn off coke deposits from previous experimental runs, oxygen in the form of air was passed through the reactor and contacted the catalyst bed for 5 hours at 500 °C.

Chapter

6

Results and discussion

6.1 Results for preliminary experimental tests: Troubleshooting

Upon completion of the design and commissioning of the experimental apparatus, preliminary tests were performed to identify possible problem areas that required alteration. The preliminary tests were performed following the experimental setup in Figure 4-1 (Scheme 1: with the metering valve on the high pressure side). Initial operation conditions were a lower temperature range (350-400 °C) and a lower system pressure (40 bar) than the final employed conditions. These initial conditions were chosen based on a combination of the literature (Hancsó et al., 2014) and available resources at the time. Glass wool was initially selected for the packing material surrounding the catalyst in the tubular reactor. It was expected that the waste cooking oil would better spread over the entire inner diameter of the reactor tube due to the substantial air spaces in the fabric, thus allowing the oil to contact all of the catalyst in the fixed bed. All preliminary tests were performed using the commercial Ru/Al₂O₃ catalyst as there was a large amount already available at the university. The catalyst was not sulphided for these preliminary tests. The tests were carried out at a liquid oil volumetric flow rate of 0.2 ml/min. While 0.1 ml/min was the lowest available pump setting, 0.2 ml/min was selected in an attempt to produce a greater amount of product in a given time.

6.1.1 Packing material

While the hydrogen gas maintained the 40 bar system pressure (with a reaction temperature of 375 °C) and passed through the system without difficulty, the first encountered problem was that used cooking oil (UCO) took an extremely long time to pass through the glass wool packing. The first indication of the problem was that there was no product after two hours of run time (with UCO being pumped into the system over the entire duration of the run). The reason was discovered upon unpacking the reactor and finding the catalyst bed completely dry with a portion of the above glass wool soaked with the oil. Other available packing materials were considered, with solid spherical glass beads selected as the next best alternative. A dry test was performed by passing the oil through the glass beads in the reactor without catalyst at room temperature and no hydrogen gas. After 5 minutes, trickles of oil were present in the tube leading to the product collection vessel. This was a clear indication that the oil had passed through the system without problem, validating the choice to use glass beads in all subsequent experiments. Furthermore, upon inspection, it was noticed that virtually all the glass beads had been in contact with the oil, indicating a good distribution of the oil over the packing, which suggested a potentially good distribution of the oil over the catalyst bed. This further validated the use of glass beads as the packing material for this study.

6.1.2 System pressure

The next encountered problem was no liquid product, but only a thick grey waxy residue being formed. This resulted in the metering valve and exit line from the reactor being completely clogged. It was virtually impossible to remove the thick waxy residue from the 1/8" tubing (especially since it became harder as it cooled) and hence, new tubes were required. The metering valve had to be thoroughly cleaned before re-use. The system pressure of 40 bar was believed to be the reason for no liquid product since higher pressures favoured hydroprocessing reactions (Bezergianni, 2013). As a result, the system pressure was increased to 90 bar, however, the same result was experienced. The pressure was then increased to 120 bar, which was considered the highest safe operating conditions for the experimental equipment. As an additional safety precaution, a pressure relief valve was fitted to the system and would release any excess pressure above 140 bar. At 120 bar (and 375 °C), an appreciable amount of transparent yellow liquid product formed, however, large amounts of the grey waxy residue were also present. Mild clogging was still prevalent in the exit tubing and metering valve.

While increasing the reaction pressure to 120 bar helped reduce the production of waxy residue and subsequent clogging, it posed another problem regarding reactions using Scheme 1. At 120 bar, the metering valve could only be opened one turn to allow products to flow into the collection

vessel. If it was opened further, the high pressure would cause the transparent plastic tubing connected to the glass collection vessel to rupture, resulting in a loss of product as well as being a potential safety hazard. It was therefore vital to set the metering valve to the correct position using hydrogen at 120 bar before commencing with any experimental runs.

6.1.3 Reaction temperature range

Various literature (Bezergianni, 2013) had indicated that higher temperatures favoured hydrocracking reactions and as such, in an attempt to reduce the amount of waxy residue being formed, the range of reaction temperatures was increased from 350-400 °C to 400-450 °C. This increased temperature range was also expected to produce more kerosene and gasoline range products than the initial lower temperature range (since it favoured hydrocracking). An experiment conducted at 425 °C (and 120 bar) produced the highest amount of liquid relative to the waxy residue than any previous preliminary experiment. Qualitative analysis of this product using GCMS indicated gasoline, kerosene and diesel range n-alkanes to be present in the liquid product. It was therefore concluded that the higher temperature range would be utilised and studied.

6.1.4 Liquid hourly space velocity

Since a lower LHSV results in a greater residence time, which subsequently promotes the degree of hydrocracking occurring, the initial preliminary experiments carried out using a liquid oil volumetric flow rate of 0.2 ml/min was also considered to be contributing to the undesired low liquid to waxy residue formation. As such, this was decreased to 0.1 ml/min, which was the lowest available setting on the pump, in order to try and improve hydrocracking, and subsequently, the yield of liquid product. Test experiments performed at the 0.1 ml/min showed a greater yield of liquid products to the initial experiments carried out at 0.2 ml/min supporting the claim that higher residence times improve hydroprocessing reactions. As a result all experiments carried out in this study were performed at 0.1 ml/min.

6.1.5 Catalyst sulphiding

The final adjustable variable to try to improve the yield of liquid product while simultaneously reducing the formation of waxy residue was the pre-sulphiding of the catalysts. The catalyst was sulphided in-situ via a method adapted from various literature (Vukovic et al., 2004). A final preliminary test at 120 bar, 425 °C and sulphided Ru/Al₂O₃ catalyst was performed. Visual inspection of the product showed a substantial increase in yellow liquid product while a decrease in waxy residue, which was now creamy yellow in colour. The creamy yellow colour was probably as a result of the sulphur content on the surface of the catalyst from pre-treatment.

Finally, it was also noticed that the consistency of the waxy residue was softer and less prone to hardening under room temperature. This suggested that the catalytic activity of the catalyst increased greatly once sulphided and as such, all experimental runs would utilise sulphided catalysts bar one, which would be used to do a comparative study for the effects of sulphiding.

6.2 Results for the hydroprocessing of waste cooking oil

The following section contains the results for the hydroprocessing of waste cooking oil over transition metal-based catalysts. The main focus is a comparative study of the results which were used to determine which catalyst, under a specific set of operating conditions, produced the best yield of n-alkanes in the kerosene (jet fuel) range. Furthermore, results regarding the catalyst activity and effectiveness after regeneration are discussed. Finally, the importance of pre-sulphiding was also tested and a discussion is delineated in section 6.2.1. A few important assumptions were made in order to simplify the quantification of the products:

- The material balance

As it was difficult to collect and quantify the product gas, the mass of the product gas based on the oil feed was calculated as follows:

$$Mass_{gas\ produced} = Mass_{oil\ fed} - Mass_{liquid\ product\ and\ unreacted\ oil} - Mass_{solid\ product} \quad (6-1)$$

- Composition of liquid products

Qualitative analysis using the GCMS showed the liquid product contained a range of n-alkanes from C₅ to C₁₈ along with acids which are constituents of the waste cooking oil. As such the liquids in the product were categorised into n-alkanes and unreacted oil. In the rest of this dissertation, the term “liquid product” refers only to n-alkanes and not the unreacted oil.

All raw and calculated data in this chapter can be viewed in Appendices E and F respectively, with sample calculations shown in Appendix D.

6.2.1 Results for experiments using commercially produced fresh Ru/Al₂O₃ catalyst

The commercially produced Ru/Al₂O₃ catalyst was the first catalyst utilised in the study. It was decided to perform only the first experiment without sulphiding the catalyst. This was due to the fact that there was a possibility of the system experiencing some clogging due to waxy residue being formed. By doing this experiment first, results required to compare with sulphided catalysts were obtained. In addition, in the case that severe clogging was prevalent, any cleaning or replacement of the tubes and metering valve could be done for the last time, as clogging was not

expected to occur during experiments with sulphided catalysts. The experiment with un-sulphided catalyst was performed at 400 °C. The remainder of the experimental runs (at 425 and 450 °C) were performed after sulphiding the catalyst. Table 6-1 contains reactant and product data for experiments conducted using this catalyst. The figures that follow provide a graphical representation of calculated data based on Table 6-1.

Table 6-1 Product distribution & oil conversion for experiments over fresh Ru/Al₂O₃ catalyst

Reaction temperature	[°C]	400.0 ^a	425.0	450.0
Total oil fed	[g]	11.040	11.040	11.040
Liquid product	[g]	2.717	7.982	8.386
Solid product	[g]	8.063	2.310	1.693
Gas product	[g]	0.260	0.748	0.962
n-Alkanes in liquid product	[g]	2.476	7.889	8.252
• Gasoline range	[g]	0.028	0.266	0.317
• Kerosene (Jet fuel) range	[g]	0.052	0.337	0.493
• Diesel range	[g]	2.396	7.286	7.442
Unreacted oil in liquid product	[g]	0.241	0.093	0.133
Oil conversion (%)	[%]	97.82	99.16	98.79

[a] This experiment was performed with un-sulphided catalyst.

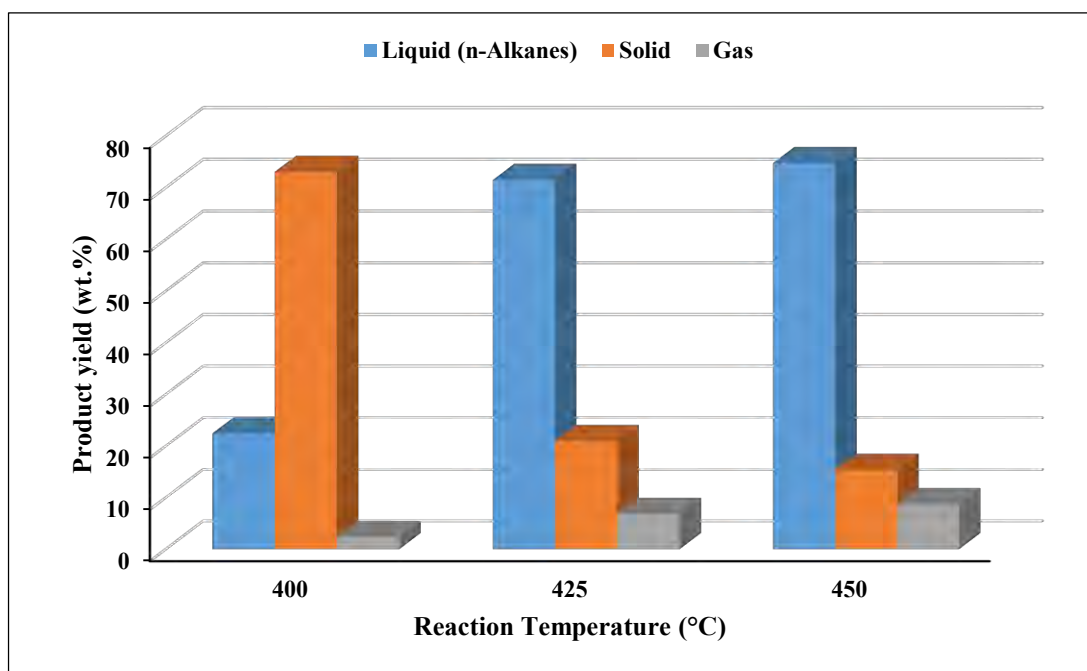


Figure 6-1 Product yields for experiments over fresh Ru/Al₂O₃ catalyst at different temperatures

It was evident from visual inspection of the product that there was a much greater amount of waxy residue relative to liquid (n-alkanes) being formed at 400 °C (using un-sulphided Ru/Al₂O₃ catalyst) compared to the opposite being observed at 425 °C and 450 °C (both using sulphided Ru/Al₂O₃ catalyst). Figure 6-1 clearly validates this observation as the product yield from un-sulphided catalyst at 400 °C comprised of 73.03% solids (waxy residue) and only 22.43% liquid. This is in stark contrast to the product yield from sulphided catalyst at 425 and 450 °C which comprised of 20.92% solids and 71.46% liquid, and 15.34% solid and 74.75% liquid respectively. The drastic difference in the low liquid to solid product ratio at 400 °C, coupled with the high liquid to solid product ratio at 425 and 450 °C was a clear indication of the increase in catalytic activity via sulphiding, for hydroprocessing reactions. While an increase in reaction temperature is also expected to favour hydroprocessing, a 25 °C difference would not constitute substantial reasoning for the vast difference in product distribution which further supports the claim that catalyst sulphiding is a necessary step in hydroprocessing waste cooking oil. This observation is especially important when noting that conversion of the oil was > 97% (Table 6-1) for all three experiments, but this can be misleading as in the case at 400 °C with the un-sulphided catalyst, where most of the product was undesired solid residue rather than the desired liquid n-alkanes. The gas analyser indicated that the gaseous products comprised of CO and CO₂, which was expected from the hydrotreating reactions as well as n-alkanes ≤ C₅.

This first set of experiments also provided an indication of the effect of reaction temperature on hydroprocessing reactions as seen in Figure 6-1 at 425 and 450 °C using sulphided Ru/Al₂O₃ catalyst. An increase in temperature resulted in a slight increase in the yield of liquid n-alkanes (from 71.46 to 74.75%) and gaseous products (from 6.78 to 8.71%) suggesting that hydroprocessing are favoured at higher temperatures.

In the paper by Huber et al. (2007) a sequential reaction mechanism was proposed for the conversion of triglycerides to alkanes. The vegetable oil is first hydrogenated to give diglycerides, monoglycerides and waxes. These species thereafter undergo decarboxylation, decarbonylation and further hydrogenation to yield diesel range alkanes. The heavier alkanes crack and isomerize to give lighter alkanes which constitute gasoline, kerosene and gas fractions.

In light of the results of this study it is clear that the first hydrogenation to wax products can be carried out over a low activity catalyst at relatively low reaction temperatures. However, the higher activation energies for subsequent steps demand a higher reaction temperature and a more active catalyst. Sulphiding of the metal catalyst produces a surface phase that is many times more active and selective than the original oxide state.

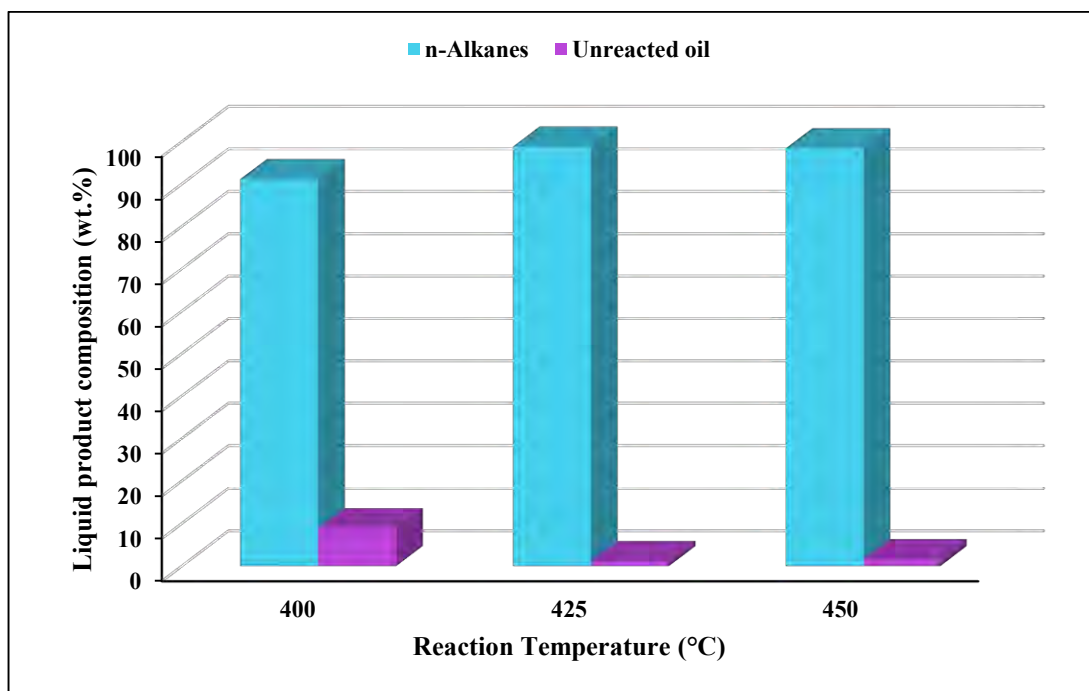


Figure 6-2 Composition of the liquid obtained from experiments over fresh Ru/Al₂O₃ catalyst at different temperatures

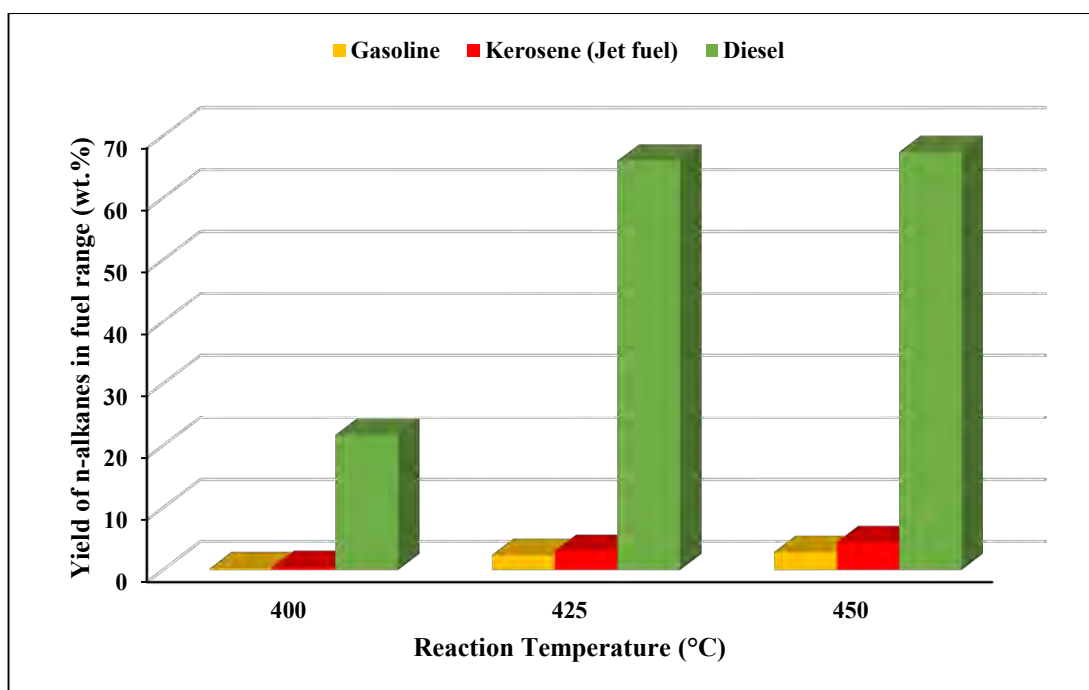


Figure 6-3 Yield of liquid n-alkanes in the transportation fuel range for experiments over fresh Ru/Al₂O₃ catalyst at different temperatures

Figure 6-2 shows the distribution of the liquid obtained from experimental runs. It can be seen that for all three reaction temperatures, the liquid contains primarily n-alkanes with very little

unreacted oil left over. Once again, at 400 °C the un-sulphided Ru/Al₂O₃ catalyst has a larger percentage of unreacted oil (8.86%) relative to reactions with sulphided Ru/Al₂O₃ catalyst at 425 and 450 °C (1.16 and 1.59% unconverted oil respectively). This suggests that the early hydroprocessing reactions (saturation reactions and other hydrotreating reactions such as decarboxylation and decarbonylation) are promoted in the presence of sulphided catalyst.

Figure 6-3 shows the break-down of the yield of liquid n-alkanes in the different transportation fuel ranges. For experiments at all three reaction temperatures, a large majority of the n-alkanes present are constituents for diesel fuel. This result was expected since the triglycerides are unsaturated long chain hydrocarbon molecules that first undergo saturation reactions, before cracking reactions break long chains into shorter ones. Furthermore, hydrocracking reactions are also very energy intensive reactions and they also require larger residence times. However, small quantities of gasoline and kerosene range n-alkanes were present for all three experiments suggesting that hydrocracking reactions were achieved. A distinct difference in the gasoline, kerosene and diesel range can be seen from the reaction with un-sulphided Ru/Al₂O₃ catalyst at 400 °C when compared to reactions at 425 and 450 °C using sulphided Ru/Al₂O₃ catalyst. This distinction serves as evidence that hydrocracking reactions are also promoted in the presence of sulphided catalysts.

The two sulphided catalysts show a slight increase in gasoline, kerosene and diesel range n-alkanes at 450 °C (2.88, 4.46 and 67.41% respectively), when compared to 425 °C (2.41, 3.05 and 66.00% respectively). This was a clear indication that hydrocracking reactions were favoured by increased temperatures, resulting in a higher number of saturated shorter chain n-alkanes relative to longer unsaturated ones. The fact that the yield of the diesel range n-alkanes did not decrease, along with only a slight, rather than a noticeable increase in the yield of the gasoline and kerosene range n-alkanes from the lower to the higher temperature, indicates that the rate of hydrotreating reactions was greater than the rate of hydrocracking reactions over the entire length of the catalyst bed.

Another vital observation regarding the high liquid n-alkane yields for the sulphided catalysts is that this indicates that the metallic sites were effective in catalysing the hydrogenation-dehydrogenation reactions. This is an important characteristic in hydroprocessing, especially when trying to achieve diesel range n-alkanes. On the other hand, the low yield for kerosene and gasoline range n-alkanes suggests that the acidic sites on the amorphous Al₂O₃ catalyst support may not be sufficiently effective for catalysing hydrocracking reactions in order to produce shorter chain n-alkanes.

Overall the fresh Ru/Al₂O₃ catalyst performed well in the hydroprocessing of waste vegetable oil producing large amounts of liquid n-alkanes (however most of which was diesel range) and achieved high oil conversion. A longer catalyst bed may provide the necessary residence time to further crack the long chain n-alkanes to produce more kerosene range n-alkanes. However, this may also contribute to more kerosene range n-alkanes cracking to form gasoline and liquid petroleum gas range n-alkanes.

The first set of experiments using fresh Ru/Al₂O₃ catalyst produced results that were in agreement with the literature regarding the effect of reaction temperature and sulphiding the catalyst on the products formed. These findings served as a basis for expected trends through the remainder of the study.

6.2.2 Results for experiments using commercially produced fresh Ni/Al₂O₃ catalyst

The second set of experiments were performed using commercially produced fresh Ni/Al₂O₃ catalyst. All experiments were performed after in-situ sulphiding. The results from these experiments were compared against the Ru/Al₂O₃ catalyst to determine which of the two commercially produced fresh catalyst performed better in producing liquid n-alkanes and more specifically, in the jet fuel range. Table 6-2 contains reactant and product data for experiments conducted using this catalyst. The figures that follow provide a graphical representation of calculated data based on Table 6-2.

Table 6-2 Product distribution & oil conversion for experiments over fresh Ni/Al₂O₃ catalyst

Reaction temperature	[°C]	400.0	425.0	450.0
Total oil fed	[g]	11.040	11.040	11.040
Liquid product	[g]	6.956	6.620	8.229
Solid product	[g]	2.954	2.468	0.867
Gas product	[g]	1.130	1.952	1.944
n-Alkanes in liquid product	[g]	3.951	4.233	5.843
• Gasoline range	[g]	0.178	0.263	0.461
• Kerosene (Jet fuel) range	[g]	0.240	0.279	0.572
• Diesel range	[g]	3.533	3.692	4.810
Unreacted oil in liquid product	[g]	3.005	2.387	2.386
Oil conversion (%)	[%]	72.78	78.38	78.38

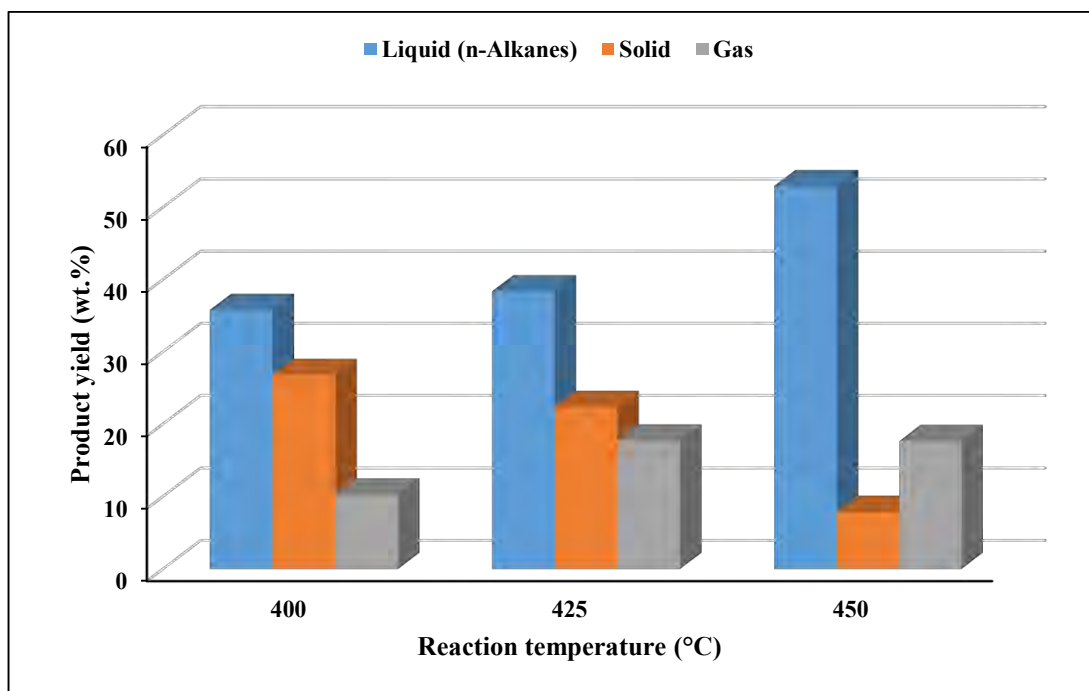


Figure 6-4 Product yields for experiments over fresh Ni/Al₂O₃ catalyst at different temperatures

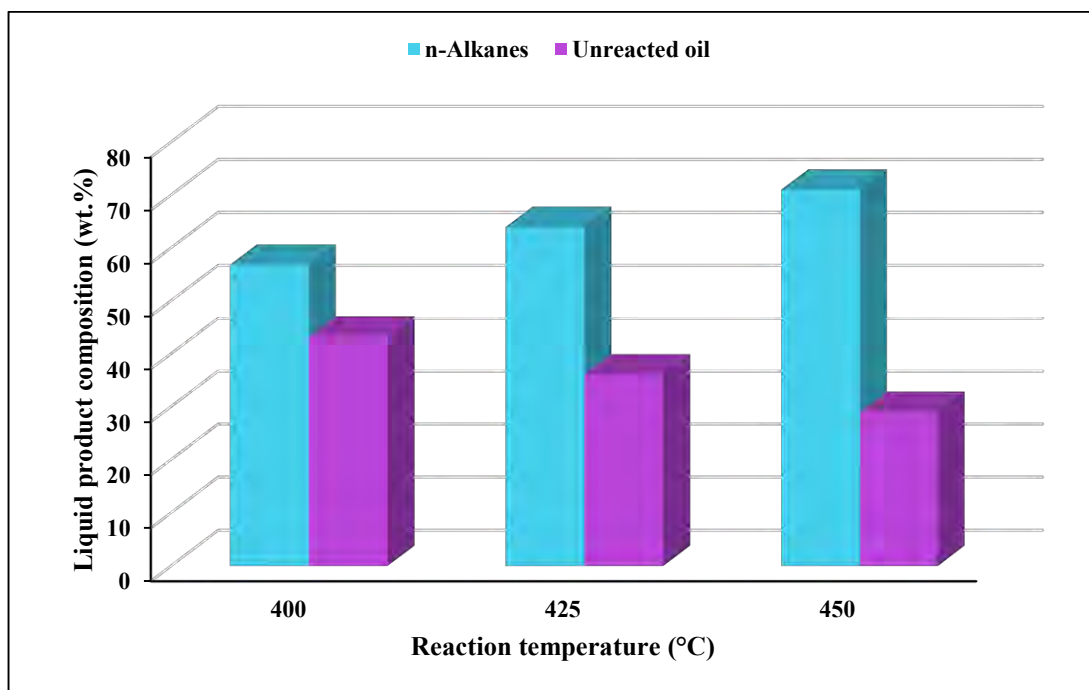


Figure 6-5 Composition of the liquid obtained from experiments over fresh Ni/Al₂O₃ catalyst at different temperatures

The Ni/Al₂O₃ catalyst underwent sulphiding treatment before any experiments were conducted making it possible to compare the results for all three reaction temperatures. From Figure 6-4, it can be seen that as reaction temperature increased from 400 to 425 and finally to 450 °C the liquid

n-alkanes in the product increased from 35.79 to 38.35 and finally to 52.92% respectively. The large increase in the yield of n-alkanes from 425 to 450 °C suggests that hydrocracking may be significantly favoured as temperature increases linearly. Furthermore, as temperature increased (400, 425 and 450 °C), gaseous product increased (10.24, 17.68 and 17.61% respectively) and solid product decreased (26.76, 22.36 and 7.85% respectively) validating that hydroprocessing reactions are favoured at higher temperatures.

The data represented in Figure 6-5 shows that the liquid obtained from all three experiments contained more n-alkanes relative to unreacted oil. As temperature increased (400, 425 and 450 °C), liquid n-alkane product increased (56.80, 63.95 and 71.00%) and unreacted oil decreased (43.20, 36.05 and 29.00). This expected result very clearly shows how temperature favours hydroprocessing of waste cooking oil into liquid n-alkanes. However, the low yield of liquid n-alkanes (all < 53%) and the large amounts of unreacted oil (all $\geq 29\%$) for all three experiments suggests that the fresh sulphided Ni/Al₂O₃ catalyst may not have a large enough percentage of active metallic sites for hydrotreating reactions to convert unsaturated triglycerides into saturated n-alkanes.

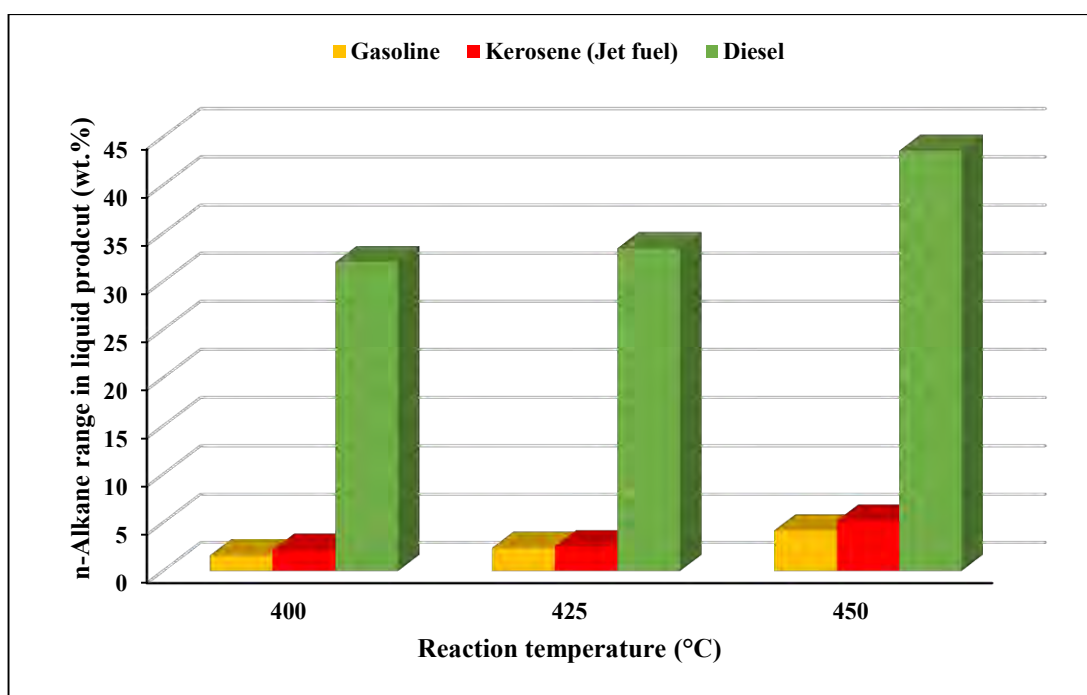


Figure 6-6 Yield of liquid n-alkanes in the transportation fuel range for experiments over fresh Ni/Al₂O₃ catalyst at different temperatures

As expected, all three experiments (400, 425 and 450 °C) with fresh sulphided Ni/Al₂O₃ catalyst resulted in higher yields of diesel range n-alkanes (32.00, 33.44 and 43.57%), compared to much smaller yields of gasoline (1.61, 2.38 and 4.17%) and kerosene (2.18, 2.52 and 5.19%) as seen in

Figure 6-6. It is observed that an increase in reaction temperature from 400 to 425 °C resulted in a very small increase in the yield of diesel (1.44%), kerosene (0.34%) and gasoline (0.77%). However, an increase in the reaction temperature from 425 to 450 °C shows a significantly larger increase in the yields of diesel (10.13%), kerosene (2.67%) and gasoline (1.79) range n-alkanes. This, like in the case of the Ru/Al₂O₃, suggests that a linear increase in the reaction temperature, may promote an exponential growth in the degree of hydrocracking reactions. However, excessively increasing the reaction temperature requires large amounts of energy which may make the process unfeasible. In addition, the catalyst can deactivate at extremely high temperatures causing a severe lack of catalytic activity and subsequently, poor hydroprocessing of waste cooking oil. As it was with the Ru/Al₂O₃ catalyst, no decrease in the yield of diesel range n-alkanes along with no very noticeable increase in the yield of gasoline and kerosene range n-alkanes as reaction temperature increased, suggests that the rate of the hydrotreating reactions were greater than the hydrocracking reactions along the entire length of the catalyst bed.

6.2.3 Comparative study on the performance of the commercially produced fresh Ru/Al₂O₃ and Ni/Al₂O₃ catalysts in the hydroprocessing of waste cooking oil

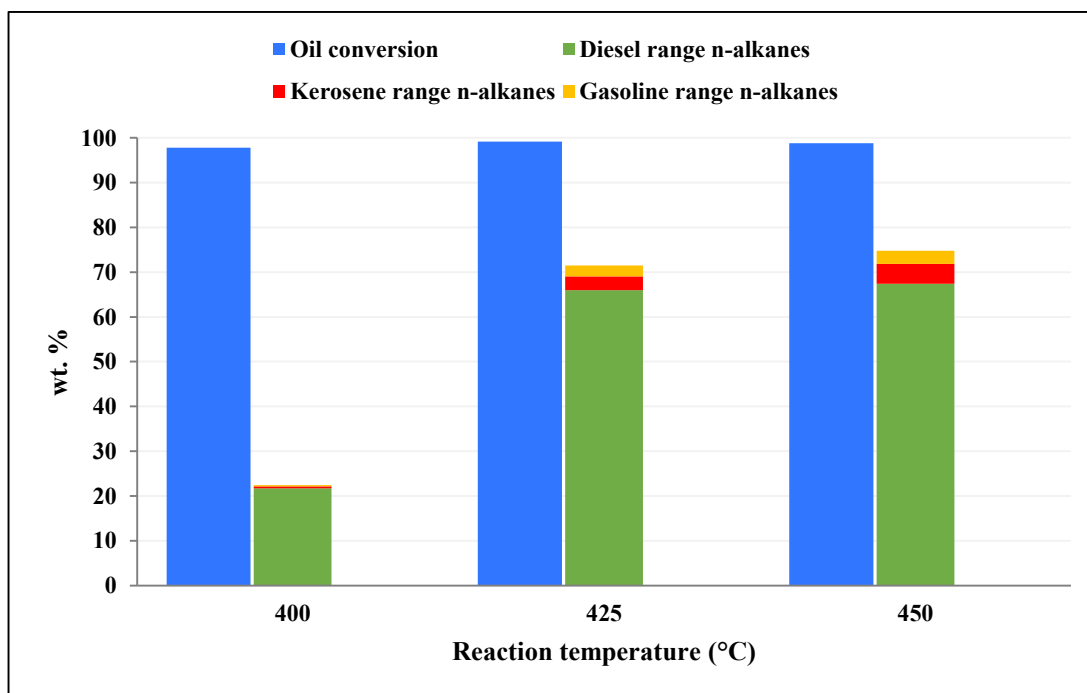


Figure 6-7 Oil conversion and liquid n-alkane product distribution for experiments over fresh Ru/Al₂O₃ catalyst at different temperatures

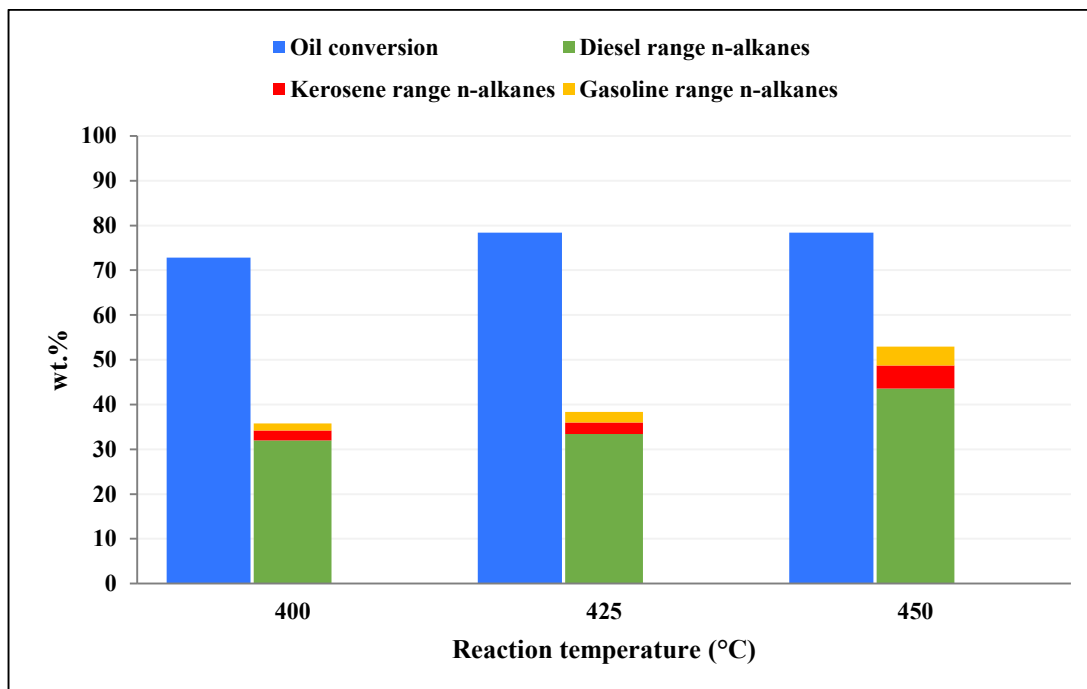


Figure 6-8 Oil conversion and liquid n-alkane product distribution for experiments over fresh Ni/Al₂O₃ catalyst at different temperatures

The results for the two catalysts indicate that both were successful in catalysing hydroprocessing reactions to produce liquid n-alkanes in the transportation fuels range. However, the performance of the catalysts were not identical. As such, a comparative study of the results will enable the selection of which of the two achieved a greater degree of hydroprocessing of waste cooking oil.

In order to determine which commercially produced catalyst performed better in the hydroprocessing of waste cooking oil, the following data were compared: oil conversion, yield of liquid n-alkanes and the percentage of each transportation fuels n-alkane range in the liquid n-alkanes. Figure 6-7 and 6-8 represent this data for the Ru/Al₂O₃ and Ni/Al₂O₃ catalyst respectively. Only results from experiments at reaction temperatures of 425 and 450 °C for the two catalysts were compared since the Ru/Al₂O₃ catalyst was un-sulphided at 400 °C, while the Ni/Al₂O₃ catalyst was sulphided at that temperature.

While very similar trends are observed for both catalysts at both temperatures, the total oil conversion for the Ru/Al₂O₃ catalyst is much greater than in the case of the Ni/Al₂O₃ catalyst (approx. 20% for both temperatures). Furthermore, the total liquid n-alkanes produced is also larger at both temperatures. This indicates that the Ru/Al₂O₃ catalyst performed better at saturation and hydrogenation-dehydrogenation reactions than the Ni/Al₂O₃ catalyst. However, upon analysis of the composition of the liquid n-alkane product, it was interesting to note that gasoline and kerosene composition increased and diesel composition decreased from the

Ru/Al₂O₃ to the Ni/Al₂O₃ catalyst. This observation indicates that while the Ru/Al₂O₃ catalyst performed better at hydrotreating reactions, the Ni/Al₂O₃ catalyst performed better at hydrocracking reactions. However, the difference between the two catalysts with respect to hydrocracking reactions was not large (the biggest increase was a difference of 3.82% for kerosene range n-alkanes composition from Ru/Al₂O₃ catalyst to Ni/Al₂O₃ catalyst at 450 °C).

Based on the comparisons analysed above, it is clear that the Ru/Al₂O₃ catalyst has performed better than the Ni/Al₂O₃ catalyst in the overall hydroprocessing of waste cooking oil. However, if greatest kerosene range n-alkane yield is the sole desired outcome, the fresh Ni/Al₂O₃ catalyst should be considered.

6.2.4 Results for experiments using laboratory prepared fresh Ni-Mo/SiO₂ catalyst

Experimental runs for the laboratory prepared catalysts followed Scheme 2 (Figure 4.2) and were three hours long. The new metal collection vessel was larger than the previous glass vessel, allowing for the collection of more product. Furthermore, since these catalysts were not regenerated and re-used for additional experiments, their extended use did not have any subsequent effects on other experiments.

The third set of experiments were carried out over the laboratory prepared fresh Ni-Mo/SiO₂ catalyst. The preparation method of this catalyst is outlined in Chapter 5 (Section 5.1), with catalyst characterisation results and sample calculations for preparation available in Appendices B and D respectively. The catalyst was sulphided in-situ prior to any experimental runs. Table 6-3 contains reactant and product data for experiments conducted using this catalyst. The figures that follow provide a graphical representation of calculated data based on Table 6-3.

Table 6-3 Product distribution & oil conversion for experiments over fresh Ni-Mo/SiO₂ catalyst

Reaction temperature	[°C]	400.0	425.0	450.0
Total oil fed	[g]	16.560	16.560	16.560
Liquid product	[g]	11.300	9.800	8.520
Solid product	[g]	0.000	0.000	0.000
Gas product	[g]	5.260	6.760	8.040
n-Alkanes in liquid product	[g]	7.301	7.039	6.917
• Gasoline range	[g]	0.972	1.195	1.268
• Kerosene (Jet fuel) range	[g]	0.736	0.940	0.967
• Diesel range	[g]	5.593	4.904	4.682
Unreacted oil in liquid product	[g]	3.999	2.761	1.603

Oil conversion (%)	[%]	75.85	83.33	90.32
--------------------	-----	-------	-------	-------

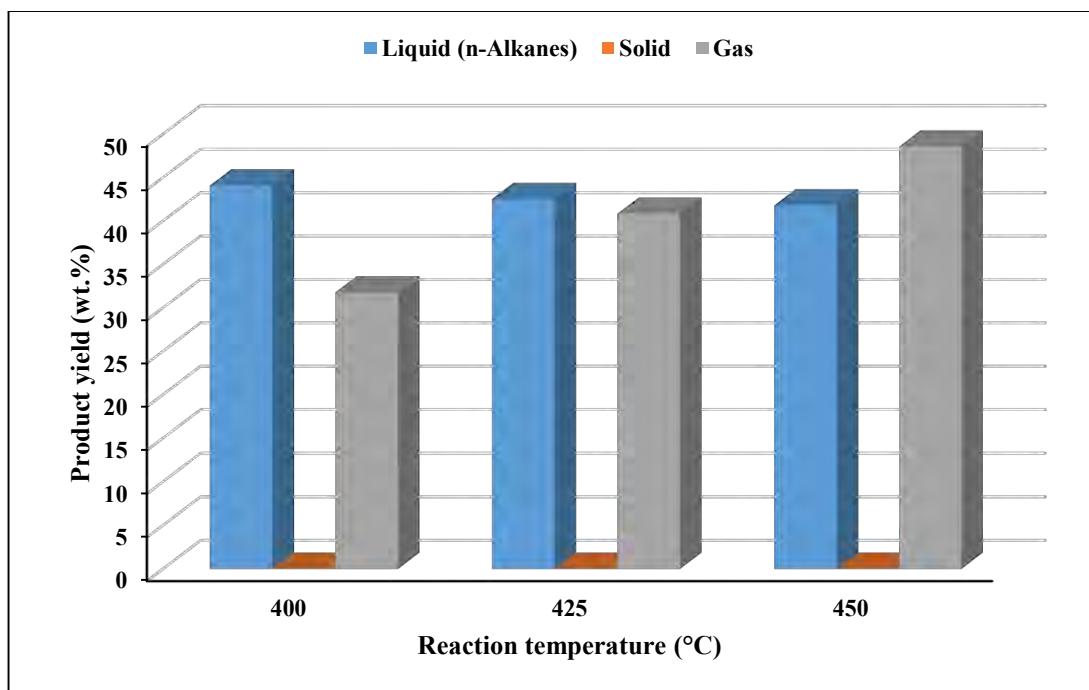


Figure 6-9 Product yields for experiments over fresh Ni-Mo/SiO₂ catalyst at different temperatures

Upon visual inspection of the product in the metal collection vessel, no waxy residue (solid) was present (even at room temperature). This indicated that any converted oil formed products that are in the liquid and gas phase at room temperature and atmospheric pressure. As such, no solid mass is present in the results in Table 6-3 and subsequently, only liquid (n-alkanes) and gas wt.% yields are seen in Figure 6-9.

In order for no solid product to be present and for the liquid to contain only n-alkanes and unreacted oil, any converted oil would have needed to undergo complete hydrotreating reactions (complete saturation reactions, as well as complete hydrogenation-dehydrogenation reactions). This means all C-C double bonds were broken into C-C single bonds and all oxygen atoms were removed from the converted oil molecules in the form of CO, CO₂ and H₂O. Furthermore, it meant that virtually no C₁₉₊ n-alkanes were present in the product as these molecules are solid at room temperature and atmospheric pressure. This suggests that any C₁₉₊ n-alkanes formed during the initial hydrotreating reactions were subsequently broken down into smaller straight chain n-alkanes via hydrocracking reactions before leaving the reactor system. In addition, analysis revealed that the lowest oil conversion for this catalyst was 75.85% (at 400 °C) which indicates that the lack of solid product was not a result of poor oil conversion. As a result, the only

conclusion is that any oil converted underwent complete hydrotreating reactions as well as some hydrocracking reactions before leaving the reactor. This indicates that the metallic sites on the catalyst were very active in promoting hydrotreating reactions.

Figure 6-9 shows very distinct trend in that as the reaction temperature was increased (400, 245 and 450 °C), the liquid (n-alkane) yield decreased (44.09, 42.51 and 41.77%), and the gaseous product yield increased (31.76, 40.82 and 48.55%). This was an indication that the increase in reaction temperature was favouring hydrocracking reactions causing longer chain liquid n-alkanes to break down and form gaseous smaller chain n-alkanes such as pentane, butane and propane. In addition to increased temperatures favouring hydrocracking, the high yields of gas products is also an indication that the acidic sites on the amorphous SiO₂ support were very active in promoting hydrocracking reactions. Furthermore, this result coupled with the complete hydrotreating reactions removing all oxygen atoms to produce CO and CO₂, provide good justification for the large amount of gas produced and is consistent with the lack of solids present in the product.

Figure 6-10 shows that as reaction temperature increases (400, 425 and 450 °C), the composition of n-alkanes in the liquid increased (64.41, 71.83 and 81.18%), and the composition of unreacted oil decreased (35.39, 28.17 and 18.82%). This trend is in agreement with the fact that hydroprocessing of waste vegetable oil is an energy intensive process requiring higher temperatures to improve conversion. The low amounts of unreacted oil present in the liquid (especially at 450 °C), along with the lack of solid products, suggest the Ni-Mo/SiO₂ catalyst was very successful in achieving high conversion and excellent hydrotreating. However, the product distribution into n-alkanes for the different transportation fuels must be analysed to determine the success in achieving jet fuel range n-alkanes.

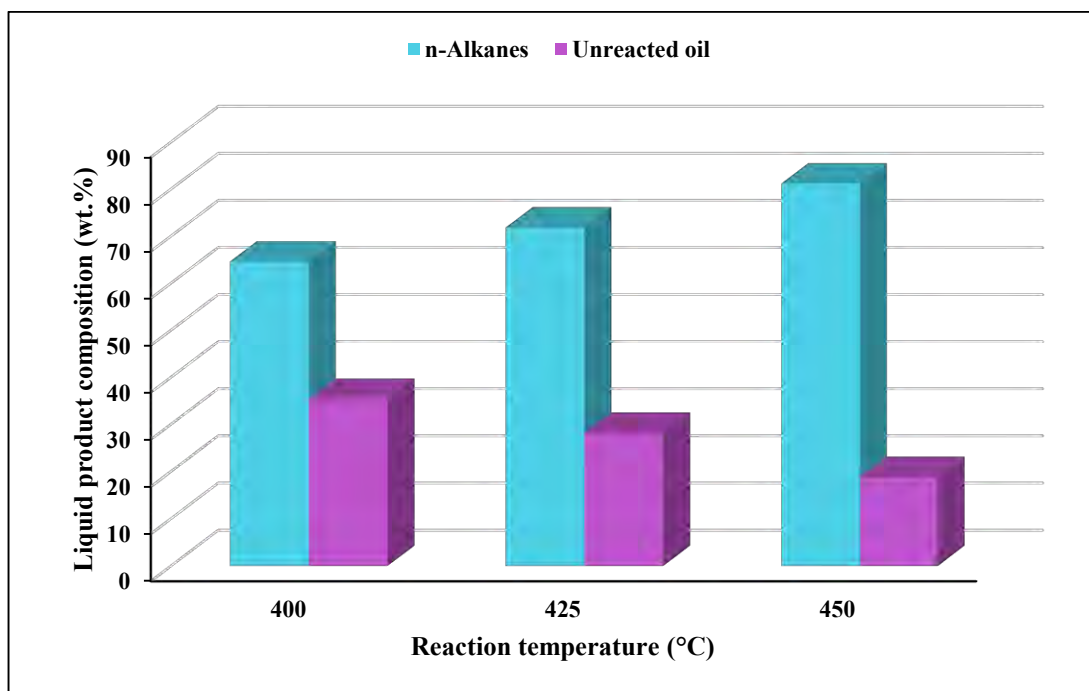


Figure 6-10 Composition of the liquid obtained from experiments over fresh Ni-Mo/SiO₂ catalyst at different temperatures

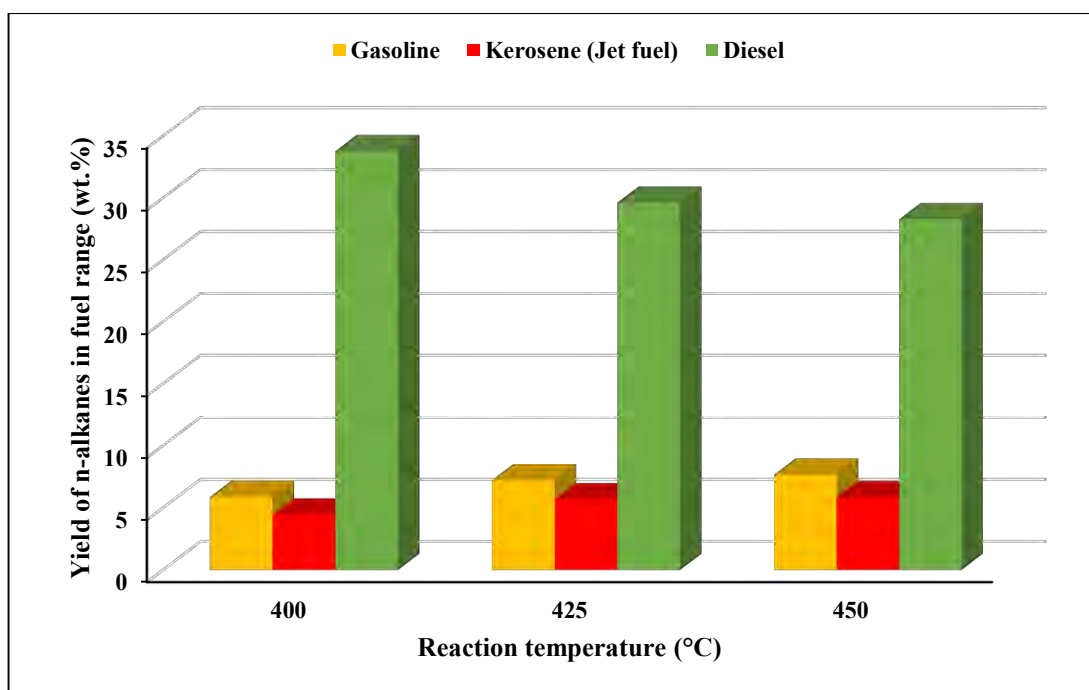


Figure 6-11 Yield of liquid n-alkanes in the transportation fuel range for experiments over fresh Ni-Mo/SiO₂ catalyst at different temperatures

Once again, as expected, the greatest n-alkane yield lies in the diesel range. As explained earlier, this is due to the fatty acids undergoing hydrotreating reactions first, before any hydrocracking can occur. Furthermore, the breaking down of unsaturated C-C bonds to form saturated C-C bonds requires less energy than breaking down longer saturated C-C bonds into smaller saturated C-C bonds. This means hydrotreating reactions have a lower activation energy allowing it to start earlier than hydrocracking reactions while they compete over the same catalyst.

The results observed in Figure 6-11 are consistent with the increase in reaction temperature (400, 425 and 450 °C) in that the yield of the n-alkanes in the diesel range decreased (33.77, 29.62 and 28.27%) due to greater hydrocracking at higher temperatures, there was an increase in the yields of gasoline (5.87, 7.22 and 7.65%) and kerosene (4.44, 5.67 and 5.84%) ranges. Furthermore, with the increase in reaction temperature, the decrease in the yield of the diesel range n-alkanes, along with the noticeable increase in the gasoline and kerosene range n-alkanes suggest that the rate of hydrocracking reactions were greater than that of hydrotreating reactions over the length of the catalyst bed.

A key observation noticed for this catalyst is that the yield of n-alkanes in the gasoline range is greater than the yield in the kerosene range for all three reaction temperatures. This is an indication that the majority of the n-alkane molecules that undergo hydrocracking from the diesel range into the kerosene range are further breaking down into the gasoline range. Beyond that, the high gas product yields suggest that a substantial percentage of gasoline range n-alkanes are being broken down to form gaseous n-alkanes. This suggest that the catalyst has a very high hydrocracking activity and a larger catalyst bed (and subsequently and increased residence time) might have led to substantially more kerosene and gasoline range n-alkanes with a noticeable decrease in the diesel range components. However, since this study focuses on achieving jet fuel range n-alkanes, hydrocracking reactions that goes beyond this range forming more compounds in the gasoline range are undesired.

Overall this sulphided catalyst (Ni-Mo/SiO₂) has performed exceptionally in hydrotreating and hydrocracking reactions. It followed the trends in literature as well as those from this previously studied catalysts in this research. It had excellent liquid n-alkane and gas yields without any waxy residue forming. Furthermore, good conversion of waste cooking oil was achieved.

6.2.5 Results for experiments using laboratory prepared fresh Co-Mo/SiO₂ catalyst

The fourth set of experiments were carried out over the laboratory prepared fresh Co-Mo/SiO₂ catalyst. The preparation method of this catalyst is outlined in Chapter 5 (Section 5.1), with catalyst characterisation results available in Appendix B. The catalyst was sulphided in-situ prior to any experimental runs. The results from this catalyst were used to perform a comparative study

with the results from the other laboratory prepared catalyst (Ni-Mo/SiO₂) in order to determine which performed better in the hydroprocessing of waste vegetable oil to produce jet fuel range n-alkanes. Table 6-4 contains reactant and product data for experiments conducted using this catalyst. The figures that follow provide a graphical representation of calculated data based on Table 6-4.

Table 6-4 Product distribution & oil conversion for experiments over fresh Co-Mo/SiO₂ catalyst

Reaction temperature	[°C]	400.0	425.0	450.0
Total oil fed	[g]	16.560	16.560	16.560
Liquid product	[g]	11.340	10.250	9.420
Solid product	[g]	0.000	0.000	0.000
Gas product	[g]	5.220	6.310	7.140
n-Alkanes in liquid product	[g]	5.935	5.714	4.991
• Gasoline range	[g]	0.703	0.738	0.921
• Kerosene (Jet fuel) range	[g]	0.745	0.722	0.627
• Diesel range	[g]	4.486	4.254	3.443
Unreacted oil in liquid product	[g]	5.405	4.536	4.429
Oil conversion (%)	[%]	67.36	72.61	73.25

As was the case with the Ni-Mo/SiO₂ catalyst, visual inspection of the product in the metal collection vessel indicated that no waxy residue (solid) was present (even at room temperature). Once again, this indicated that any converted oil formed products that are in the liquid and gas phase at room temperature and atmospheric pressure. As such, no solid mass is present in the results in Table 6-4 and subsequently, only liquid (n-alkanes) and gas wt.% yields are seen in Figure 6-12. Substantial reasoning for the lack of solid products was provided in section 6.2.4 for experiments over the Ni-Mo/SiO₂ catalyst. Since the reasoning is the same for this catalyst it will not be discussed again.

The product yields for the Co-Mo/SiO₂ catalyst as seen in Figure 6-12 follow the same trend as seen in section 6.2.4 for the Ni-Mo/SiO₂ catalyst, in that as the reaction temperature increased, (400, 425 and 450 °C) the liquid n-alkane yield decreased (35.84, 34.50 and 30.14%) and the gas product yield increased (31.52, 38.10 and 43.12%). Once again, this is in agreement that hydroprocessing is favoured at higher temperatures. However, the highest combined yields of liquid n-alkanes and gas product (which is also the oil conversion) is 73.25% (at 450 °C). Being the lowest conversion of all four fresh catalysts, this is an early suggestion that the metallic sites

on the catalyst are not as sufficient as the other catalysts in promoting the initial hydrotreating of waste cooking oil. The high gas yields are attributed to complete hydrotreating reactions causing the removal of oxygen atoms in the form of gaseous CO and CO₂ as well the formation of short chain n-alkanes such as propane, butane and pentane as a result of the hydrocracking reactions.

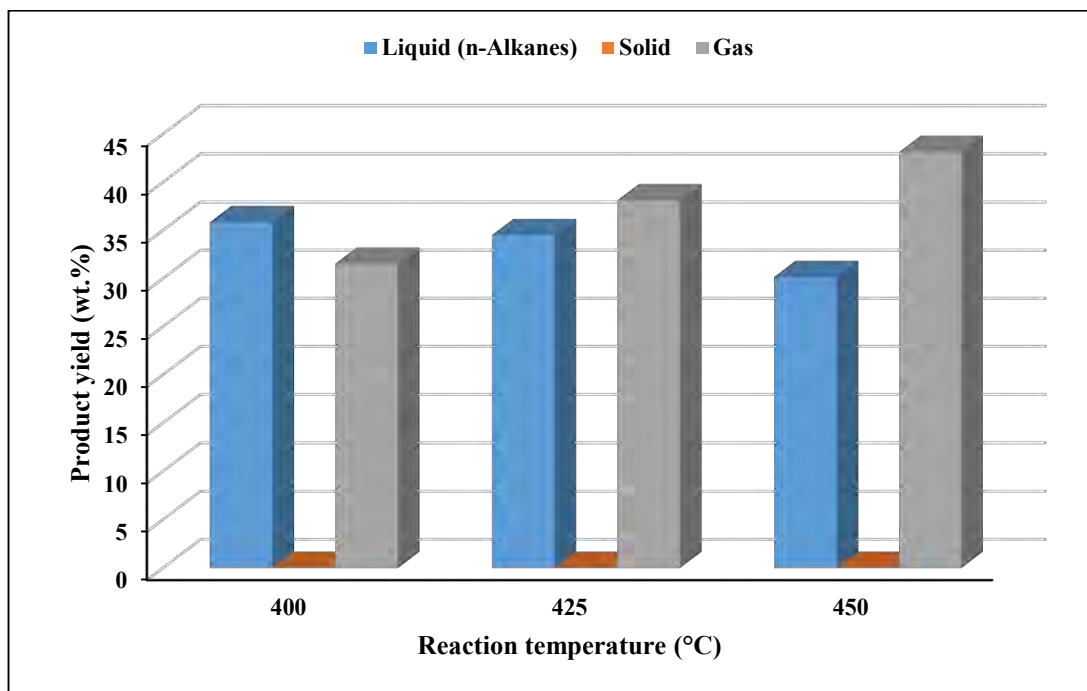


Figure 6-12 Product yields for experiments over fresh Co-Mo/SiO₂ catalyst at different temperatures

As seen in Figure 6-13, unlike the previous catalysts, the expected temperature trend is not observed for this catalyst. As the reaction temperature is increased (400, 425 and 450 °C) the n-alkanes in the liquid obtained initially increases and then decreases (52.34, 55.74 and 52.98%) while the amount of unconverted oil initially decreases and then increases (47.66, 44.26 and 47.02%). This was the first case whereby the least amount of unconverted oil in the liquid was not at the highest reaction temperature. This suggests that the optimal temperature for hydroprocessing waste cooking oil using Co-Mo/SiO₂ catalyst lies between 400 and 450 °C. This might be an indication that the catalyst is beginning to deactivate at elevated temperatures. The high percentage of unconverted oil present in the liquid for all three experiments further supports the claim that the catalyst was not highly effective in promoting initial hydrotreating reactions to convert the oil into long chain saturated n-alkanes.

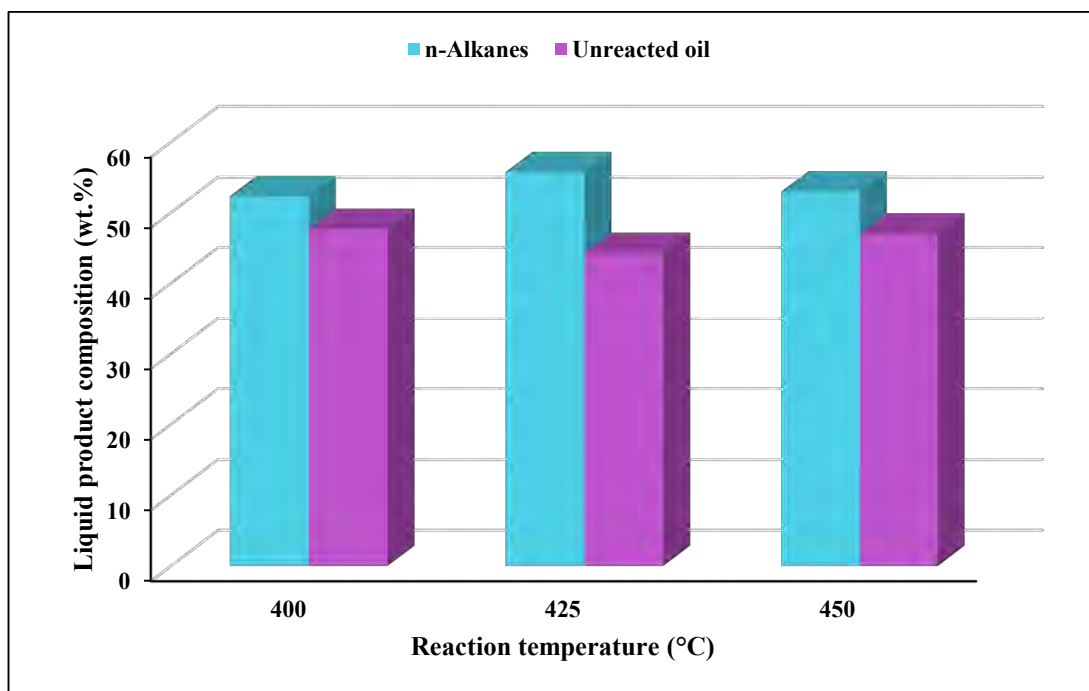


Figure 6-13 Composition of the liquid obtained from experiments over fresh Co-Mo/SiO₂ catalyst at different temperatures

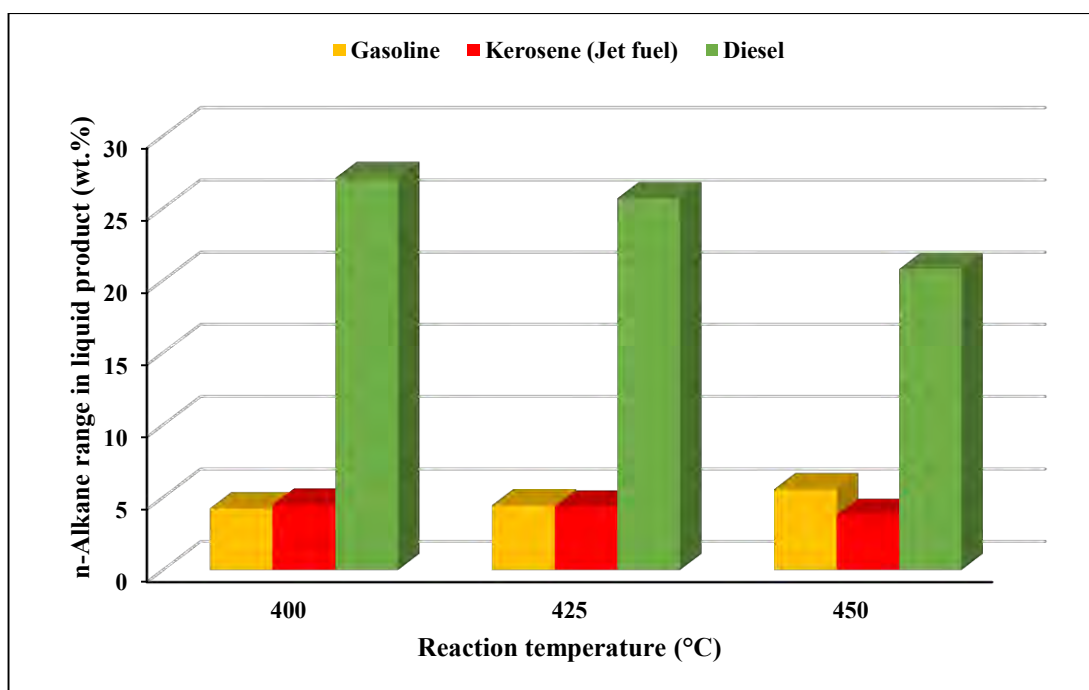


Figure 6-14 Yield of liquid n-alkanes in the transportation fuel range for experiments over fresh Co-Mo/SiO₂ catalyst at different temperatures

Figure 6-14 shows, as expected, the diesel range n-alkanes are majority of the liquid n-alkanes produced. Also, the hydrocracking temperature trend is observed in that as temperature increased (400, 425 and 450 °C), the yield of n-alkanes in the diesel range decreased (27.09, 25.69 and 20.79%) while combined yields of the n-alkanes in the gasoline and kerosene range increased (8.75, 8.82 and 9.35%). However, while the kerosene range n-alkane yield was higher than the gasoline counterpart at 400 °C, the gasoline range had a higher yield at 425 and 450 °C (gasoline range: 4.46 and 5.56%, kerosene range: 4.36 and 3.79%). This result coupled with the high gas yields indicates that the hydrocracking reactions were well promoted by the acidic sites on the amorphous SiO₂ support. Furthermore, as was the case with the Ni-Mo/SiO₂ catalyst, with the increase in reaction temperature, the decrease in the yield of the diesel range n-alkanes, along with the noticeable increase in the gasoline and kerosene range n-alkanes suggest that the rate of hydrocracking reactions were greater than that of hydrotreating reactions over the length of the catalyst bed.

Overall this catalyst (Co-Mo/SiO₂) had poor oil conversion suggesting the metallic sites did not sufficiently promote the initial hydrotreating reactions that convert fatty acids into liquid n-alkanes. The lack of solid product suggests that any oil involved in hydrotreating conversion reactions were processed fully into saturated n-alkanes. The catalyst showed good hydrocracking activity in that more kerosene and gasoline range n-alkanes, along with more gas product, formed at higher temperatures.

6.2.6 Comparative study on the performance of the laboratory prepared fresh

Ni-Mo/SiO₂ and Co-Mo/SiO₂ catalysts in the hydroprocessing of waste cooking oil

As was the case with the commercially produced catalysts, both laboratory catalysts were successful in the hydroprocessing of waste cooking oil to produce transportation fuel n-alkanes, and more specifically, in the kerosene (jet fuel) range. However, a comparative study with regards to oil conversion and n-alkane product distribution was performed to determine which of the two laboratory prepared catalysts performed better overall.

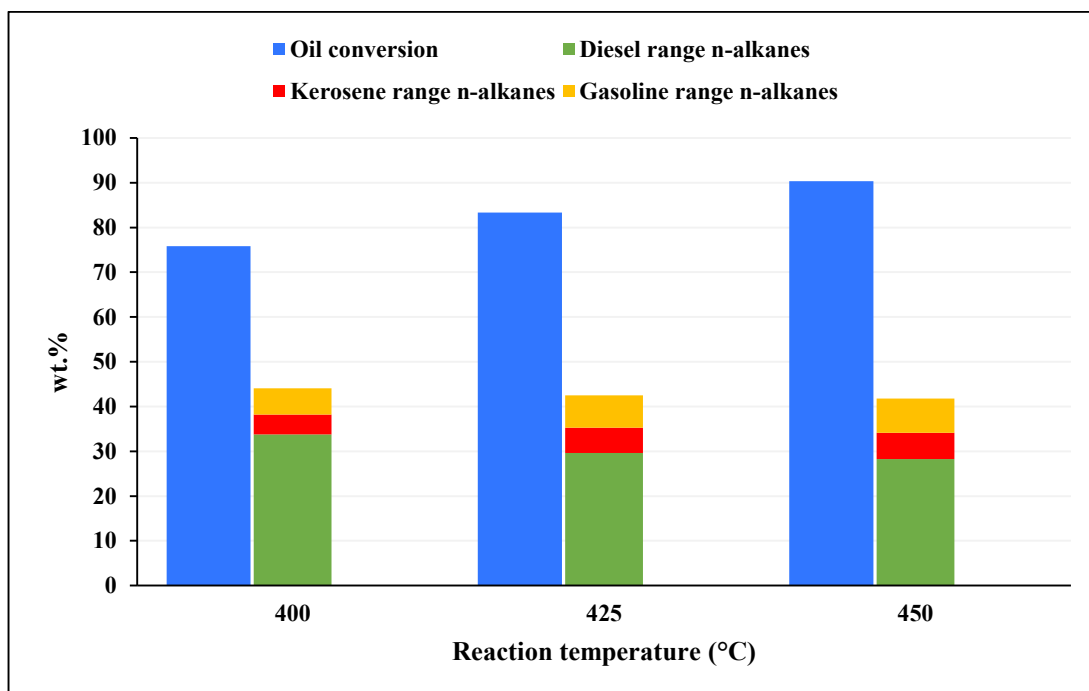


Figure 6-15 Oil conversion and liquid n-alkane product distribution for experiments over fresh Ni-Mo/SiO₂ catalyst at different temperatures

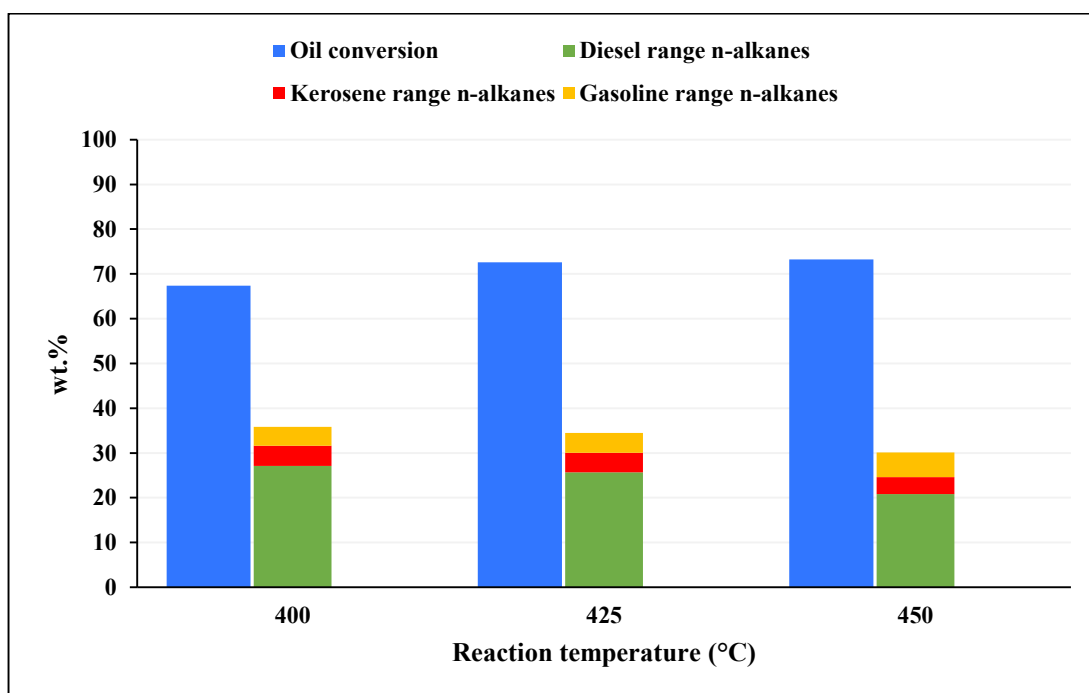


Figure 6-16 Oil conversion and liquid n-alkane product distribution for experiments over fresh Co-Mo/SiO₂ catalyst at different temperatures

Figures 6-15 and 6-16 display the oil conversion and liquid n-alkane product distribution from the hydroprocessing of waste cooking oil for Ni-Mo/SiO₂ and Co-Mo/SiO₂ catalyst respectively.

Since no solid products were obtained during all experimental runs for both catalysts, the oil conversion represented the combined yield of liquid n-alkanes and gaseous products only. As such oil conversion was a good representation of the performance of these laboratory prepared catalysts with regards to their hydrotreating and hydrocracking activity.

The oil conversion for the Ni-Mo/SiO₂ catalyst ranged from 75.85 to 90.32% performing substantially better than the Co-Mo/SiO₂ catalyst whose highest conversion was 73.25% (which was lower than the lowest oil conversion using Ni-Mo/SiO₂ catalyst). In addition, the total liquid n-alkane yield for all experiments was higher for the Ni-Mo/SiO₂ than the Co-Mo/SiO₂ catalyst. Like oil conversion, the lowest yield of liquid n-alkanes for the Ni-Mo/SiO₂ catalyst (44.09% at 400 °C) was higher than the highest yield of liquid n-alkanes for the Co-Mo/SiO₂ catalyst (35.84% at 400 °C).

Analysis of the liquid n-alkane distribution indicates that the Ni-Mo/SiO₂ catalyst had higher yields for all diesel and gasoline range n-alkanes when compared to the Co-Mo/SiO₂ catalyst. It is worth noting that both catalysts for all experiments show a very similar composition of kerosene range n-alkanes in the n-alkane liquid product. However, at 400 °C, the Co-Mo/SiO₂ had an almost negligible 0.04% higher kerosene yield than the Ni-Mo/SiO₂ catalyst while at the other two temperatures the Ni-Mo/SiO₂ catalyst had kerosene range yields greater than 1% when compared to the CoMo/SiO₂ catalyst.

Taking all of these observations into account, the Ni-Mo/SiO₂ catalyst has undisputedly performed better than the Co-Mo/SiO₂ catalyst in the hydroprocessing of waste cooking oil to produce n-alkanes in the transportation fuels range and in specific, jet fuel range n-alkanes.

6.2.7 Comparative study on the performance of the commercially produced fresh Ni/Al₂O₃ and the laboratory prepared fresh Ni-Mo/SiO₂ catalysts in the hydroprocessing of waste cooking oil

A final comparative study was performed regarding only fresh catalysts to determine whether the best commercially produced catalyst or the best laboratory prepared catalyst performed better during these experiments. The key outcome was the yield of jet fuel range n-alkanes. A quick comparison of the results displayed in Figures 6-8 and 6-15 (which represent the product distribution and oil conversion of the commercially produced Ni/Al₂O₃ and the laboratory prepared Ni-Mo/SiO₂ catalyst respectively), shows that the Ni-Mo/SiO₂ catalyst has performed substantially better. At all reaction temperatures, the kerosene range n-alkane yield was higher for experiments using Ni-Mo/SiO₂ catalyst when compared to the Ni/Al₂O₃ catalyst. Furthermore, higher oil conversions were achieved and no waxy residue was visible in the products.

It is also worth noting that the same conclusion can be drawn when comparing the laboratory prepared Co-Mo/SiO₂ catalyst to the commercially produced Ni/Al₂O₃ catalyst. As such a final ranking of the fresh catalysts performance with respect to the production of jet fuel range n-alkanes via the hydroprocessing of waste cooking oil can be concluded. The laboratory prepared fresh Ni-Mo/SiO₂ catalyst performed the best followed by the other laboratory prepared fresh Co-Mo/SiO₂ catalyst. Third best was the commercially produced fresh Ni/Al₂O₃ catalyst and finally the commercially produced fresh Ru/Al₂O₃ catalyst.

This concluded all experiments using fresh catalyst. The remainder of the study utilises regenerated commercial catalysts to analyse their sustainability in maintaining effectiveness in hydroprocessing reactions to produce jet fuel range n-alkanes.

6.2.8 Results for experiments using commercially produced regenerated Ru/Al₂O₃ catalyst

The literature is largely devoid of research testing the performance of used catalyst which has undergone regeneration via oxygen burning to remove carbonaceous material. As such, this study aimed to provide some insight into the sustainability of the effectiveness of transition metal-based catalysts for the hydroprocessing of waste vegetable oil. These experiments were performed with the commercially produced catalysts only.

Upon completion of the three experimental runs using the fresh Ru/Al₂O₃ catalyst, oxygen burning was performed to remove any carbonaceous material that may have formed and be present on the catalyst from previous experiments. This, along with the subsequent catalyst sulphiding was performed in-situ and as such, the reactor system was not opened and the catalyst was not removed. After these processes, three experimental runs were performed with the same operating conditions in all previous experiments. In order to perform an accurate comparison with the fresh commercial catalysts, these experimental runs were also two hours long using Scheme 1. The results from this catalyst would be compared to the results from its fresh counterpart as well as the other regenerated catalyst. Table 6-5 contains reactant and product data for experiments conducted using this catalyst. The figures that follow provide a graphical representation of calculated data based on Table 6-5.

Table 6-5 Product distribution & oil conversion for experiments over regenerated Ru/Al₂O₃ catalyst

Reaction temperature	[°C]	400.0	425.0	450.0
Total oil fed	[g]	11.040	11.040	11.040
Liquid product	[g]	5.635	6.285	6.987
Solid product	[g]	4.213	3.216	3.095
Gas product	[g]	1.192	1.539	0.958
n-Alkanes in liquid product	[g]	1.482	2.383	3.845
• Gasoline range	[g]	0.037	0.129	0.557
• Kerosene (Jet fuel) range	[g]	0.072	0.141	0.337
• Diesel range	[g]	1.373	2.113	2.911
Unreacted oil in liquid product	[g]	4.153	3.902	3.142
Oil conversion (%)	[%]	62.39	64.66	71.54

Table 6-5 shows the oil conversion ranges from 62.39 to 71.54%. While it is not exceptionally high, the regenerated catalyst still seems to be capable of promoting the initial hydrotreating reactions. The trend relating hydroprocessing to reaction temperature is consistent with the results since as temperature was increased (400, 425 and 450 °C), the solid yield decreased (38.16, 29.13 and 19.61%) while the liquid n-alkane (13.43, 21.59 and 34.83%) and gas (10.80, 13.94 and 17.11%) product increased suggesting an improved rate of hydroprocessing reactions at higher temperatures (as seen in Figure 6-17). While there are larger wax yields, the highest liquid n-alkane yield was only 34.83% suggesting that the catalyst did not perform particularly well with the latter hydrotreating reactions to remove all C-C double bonds and oxygen atoms via CO and CO₂ gas formation.

The liquid composition from the experiments showed the expected trend in that an increase in temperature (400, 425 and 450 °C) resulted in an increase in the n-alkane composition (26.31, 37.92 and 55.04%) while it also resulted in the subsequent decrease in the composition of unreacted oil (73.69, 62.08 and 44.96%) (Figure 6-18). However, two out of the three experiments resulted in a higher composition of unreacted oil than liquid n-alkanes in the liquid product suggesting poor conversion to n-alkanes. This is in agreement with the highest liquid n-alkanes yield being only 34.83%.

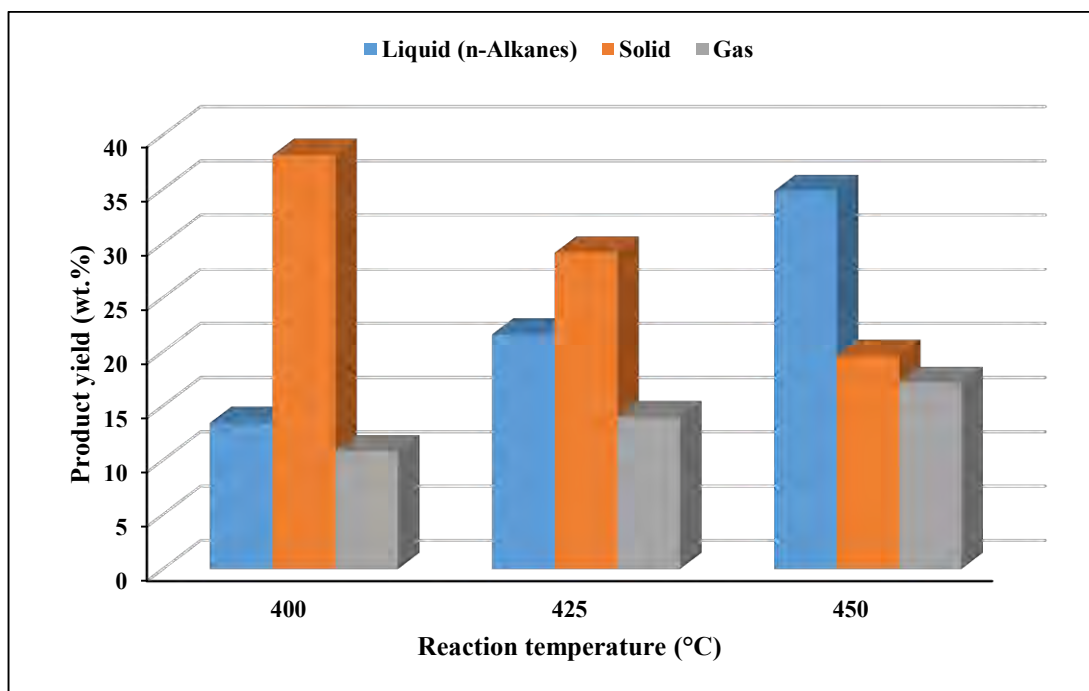


Figure 6-17 Product yields for experiments over regenerated Ru/Al₂O₃ catalyst at different temperatures

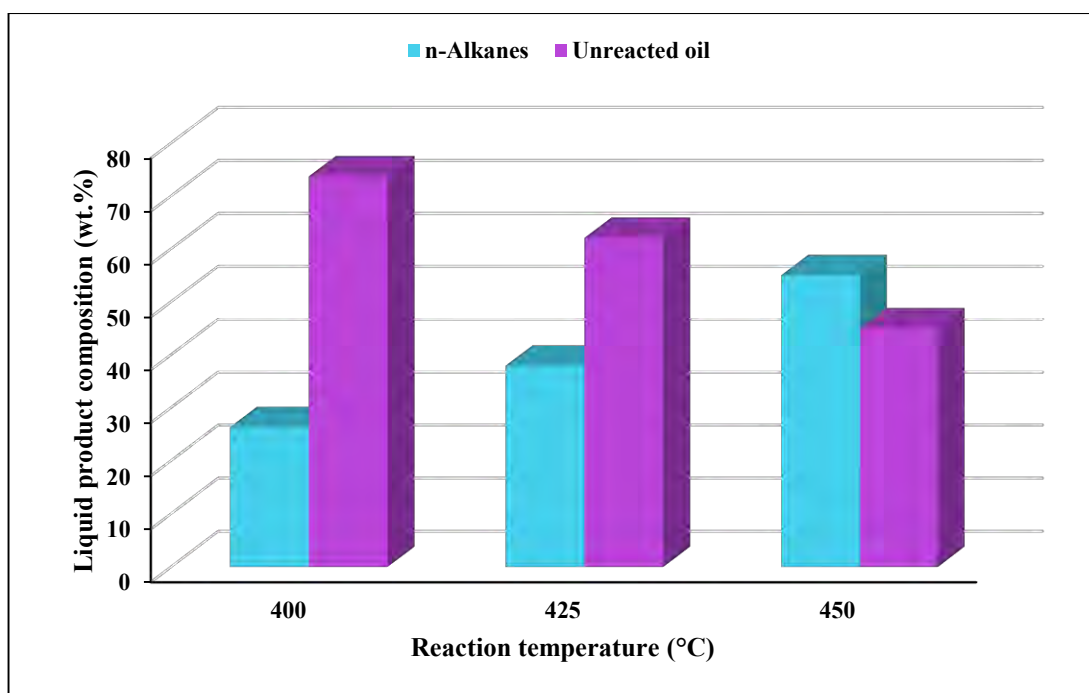


Figure 6-18 Composition of the liquid obtained from experiments over regenerated Ru/Al₂O₃ catalyst at different temperatures

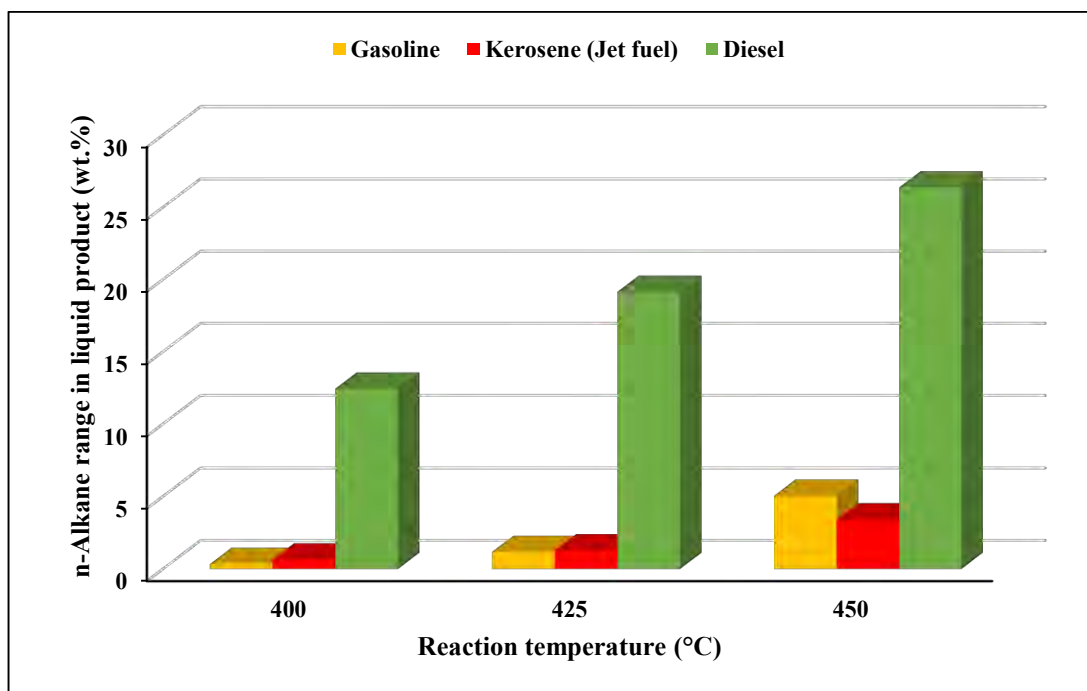


Figure 6-19 Yield of liquid n-alkanes in the transportation fuel range for experiments over regenerated Ru/Al₂O₃ catalyst at different temperatures

While the overall yield of liquid n-alkanes was low for all reaction temperatures, the yields of the gasoline and kerosene range n-alkanes showed only a slight decrease from the fresh catalyst (Figure F-19). As the reaction temperature was increased (400, 425 and 450 °C) so too did the yield for n-alkanes in the diesel (12.44, 19.14 and 26.37%), kerosene (0.65, 1.28 and 3.42%) and gasoline (0.34, 1.17 and 5.04%) range increase. This was an indication that although the metallic sites may not be performing at the same level as the fresh catalyst, the acidic sites on the support which promote the hydrocracking reactions are still fairly active. This is further supported by the increase in gas product yield as reaction temperature increases, suggesting a greater degree of cracking leading to smaller chain saturated n-alkanes.

Overall this regenerated Ru/Al₂O₃ catalyst has shown a considerable decrease in hydrotreating activity (poor conversion to liquid n-alkanes). However, it still seems to have a similar hydrocracking activity leading to similar yield distributions of the transportation fuels.

6.2.9 Results for experiments using commercially produced regenerated Ni/Al₂O₃ catalyst

The last set of experiments were performed using the commercially produced regenerated Ni/Al₂O₃ catalyst. The catalyst underwent in-situ regeneration via oxygen burning to remove any carbonaceous material formed during previous experimental runs. Thereafter in-situ sulphiding was performed. The same set of operating conditions used for the fresh catalyst were employed.

The results from these experiments would be compared to the performance of the regenerated Ru/Al₂O₃ catalyst as well as the fresh Ni/Al₂O₃ catalyst. Table 6-6 contains reactant and product data for experiments conducted using this catalyst. The figures that follow provide a graphical representation of calculated data based on Table 6-6.

Table 6-6 Product distribution & oil conversion for experiments over regenerated Ni/Al₂O₃ catalyst

Reaction temperature	[°C]	400.0	425.0	450.0
Total oil fed	[g]	11.040	11.040	11.040
Liquid product	[g]	6.368	5.824	7.018
Solid product	[g]	3.249	2.597	1.342
Gas product	[g]	1.423	2.619	2.680
n-Alkanes in liquid product	[g]	4.107	3.527	4.881
• Gasoline range	[g]	0.180	0.329	0.506
• Kerosene (Jet fuel) range	[g]	0.197	0.239	0.467
• Diesel range	[g]	3.730	2.959	3.908
Unreacted oil in liquid product	[g]	2.261	2.297	2.137
Oil conversion (%)	[%]	79.52	79.19	80.64

Table 6-6 shows relatively high and similar oil conversions for all three reaction temperatures. This is an early indication that this regenerated catalyst was able to maintain good hydrotreating activity, further suggesting that the metallic sites were still able to sufficiently promote hydrotreating reactions.

The earlier suggestion that the catalyst was able to maintain good hydrotreating activity is supported by the results presented in Figure 6-20, which show higher yields for liquid n-alkanes when compared to the solid residue. Although the expected trend for the yield of liquid n-alkanes with an increase in temperature is not met at 425 °C, this can be attributed to the large amount of gas product yield. This indicates a high rate of hydrocracking reactions from the liquid n-alkanes to the gaseous ones. The expected trends are observed for the solid (29.43, 23.52 and 12.16%) and gas (12.89, 23.72 and 24.28%) product yields with an increase in reaction temperature (400, 425 and 450 °C) validating that this catalyst was still performing well in hydroprocessing reactions.

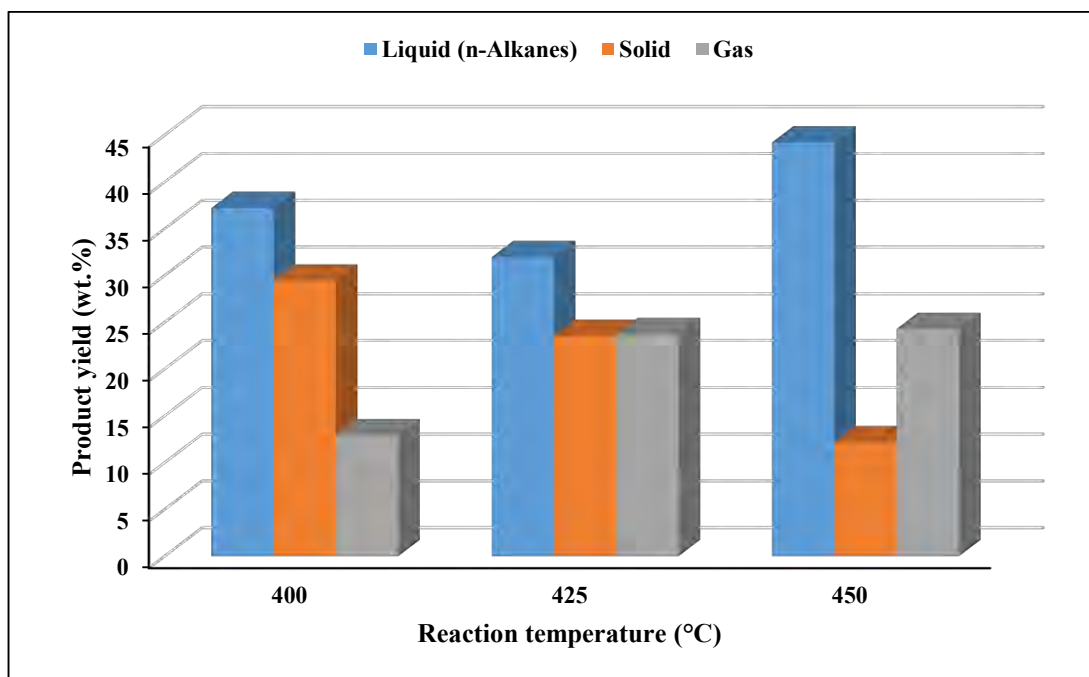


Figure 6-20 Product yields for experiments over regenerated Ni/Al₂O₃ catalyst at different temperatures

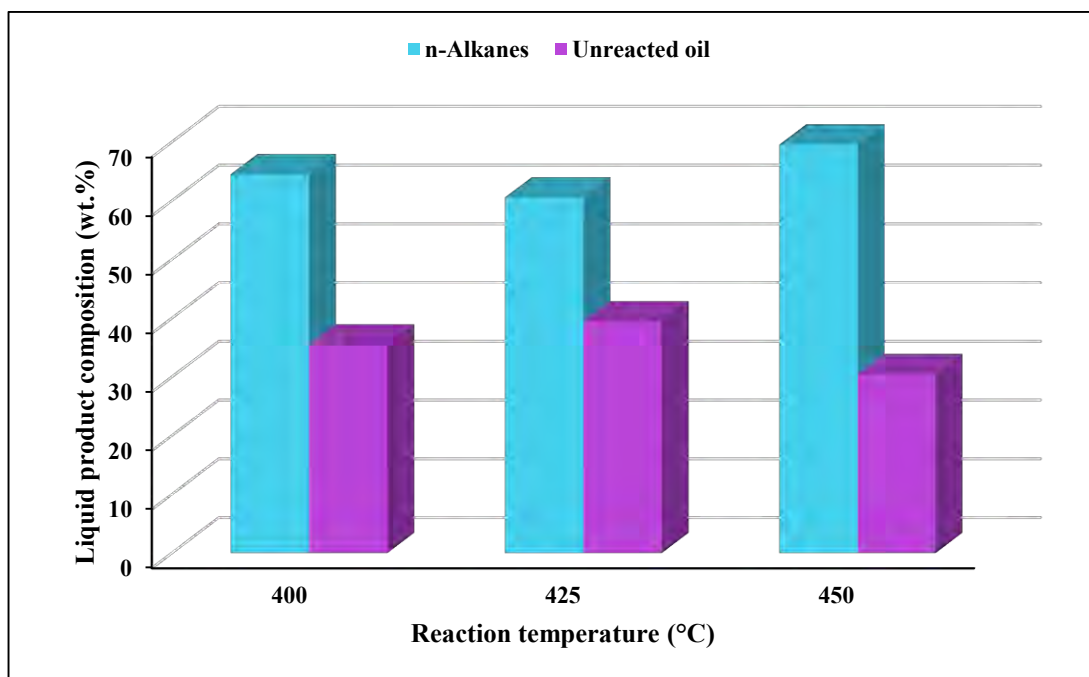


Figure 6-21 Composition of the liquid obtained from experiments over regenerated Ni/Al₂O₃ catalyst at different temperatures

Analysis of the liquid composition (Figure 6-21) further validates that this regenerated catalyst performed well in promoting hydroprocessing reactions since for all three experiments the n-alkane composition is greater than the composition of unreacted oil. The highest unreacted oil

composition was 39.44% (at 425 °C). This, coupled with the results seen in Figure 6-20 showing lower solid and higher liquid n-alkanes yields serves as proof that this regenerated catalyst was able to maintain its effectiveness in the hydroprocessing of waste cooking oil.

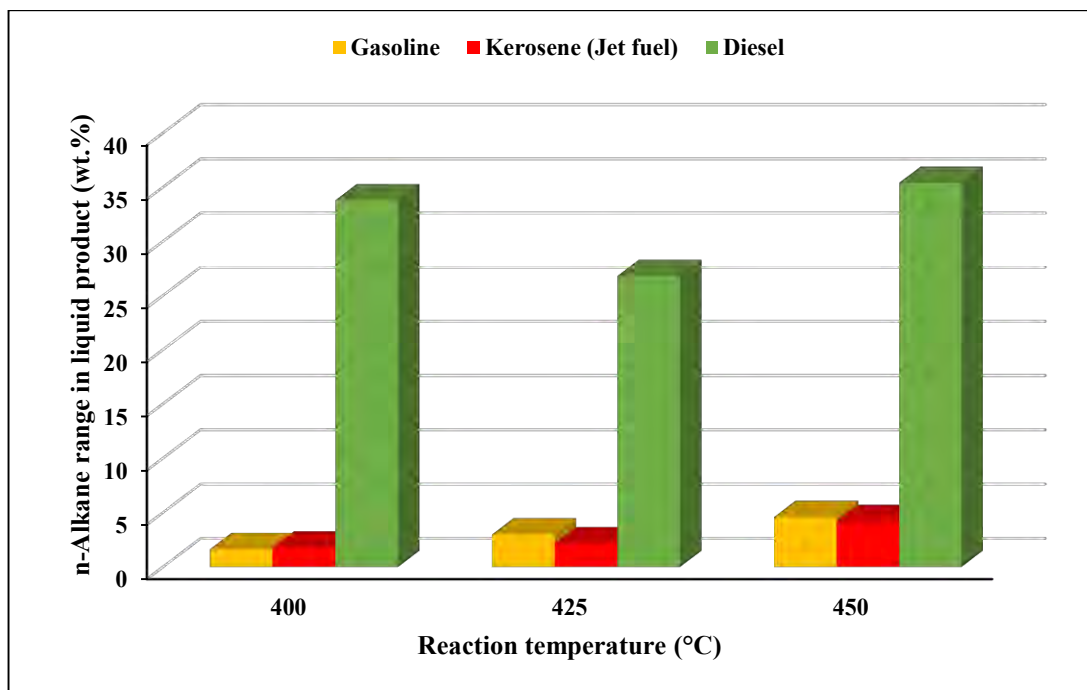


Figure 6-22 Yield of liquid n-alkanes in the transportation fuel range for experiments over regenerated Ni/Al₂O₃ catalyst at different temperatures

The distribution of the yields of the liquid n-alkanes for the different transportation fuels seen in Figure 6-22 show the expected trend for an increase in temperature (400, 245 and 450 °C), since the yield of n-alkanes in the gasoline (1.63, 2.98 and 4.59%) and kerosene (1.78, 2.17 and 4.23%) range increased. However, unlike in the fresh catalyst case, the yield of n-alkanes in the gasoline range is almost equal to or higher than the yield in the kerosene range for the three experiments. This suggests a better hydrocracking activity by the regenerated catalyst. While in theory this is unexpected, this result might be due to better sulphiding of the regenerated catalyst. Furthermore, the fresh catalyst was not new and maybe have had impurities on the surface which may have been burned off during regeneration causing the hydrocracking activity to improve. The high regeneration temperature (500 °C) may have also altered the catalyst exposing a greater active surface to the oil.

Overall the regenerated Ni/Al₂O₃ catalyst has performed well in promoting both the hydrotreating and hydrocracking reactions resulting in only a slight decrease in kerosene range n-alkane yield from the fresh counterpart.

6.2.10 Comparative study of the performance of the commercially produced regenerated Ru/Al₂O₃ and Ni/Al₂O₃ catalysts in the hydroprocessing of waste cooking oil

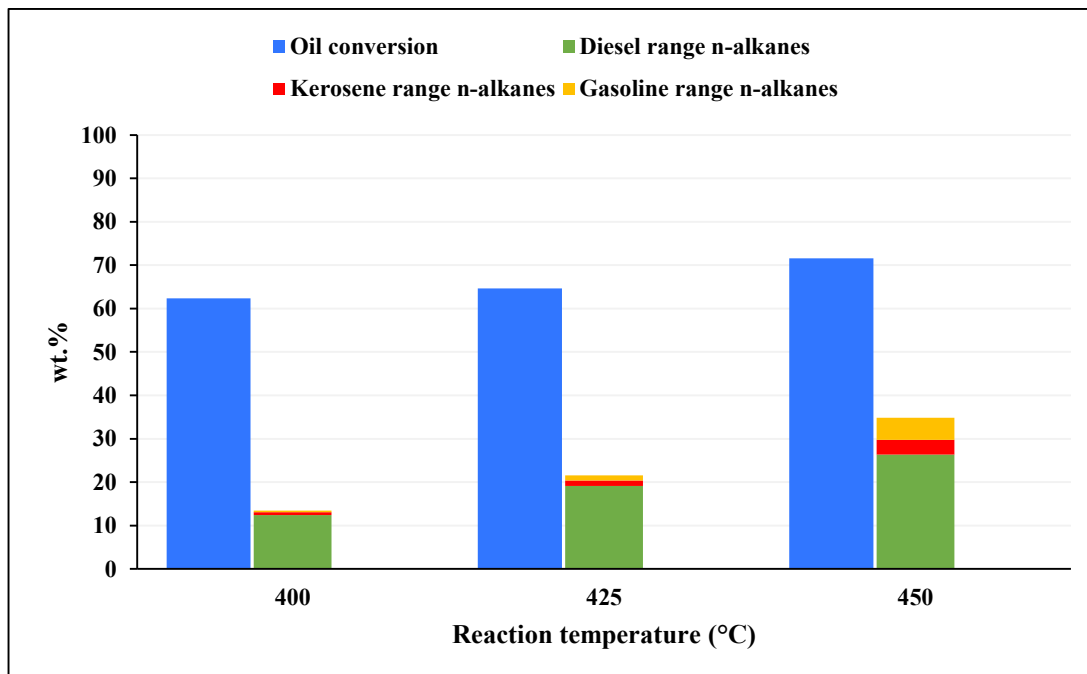


Figure 6-23 Oil conversion and liquid n-alkane product distribution for experiments over regenerated Ru/Al₂O₃ catalyst at different temperatures

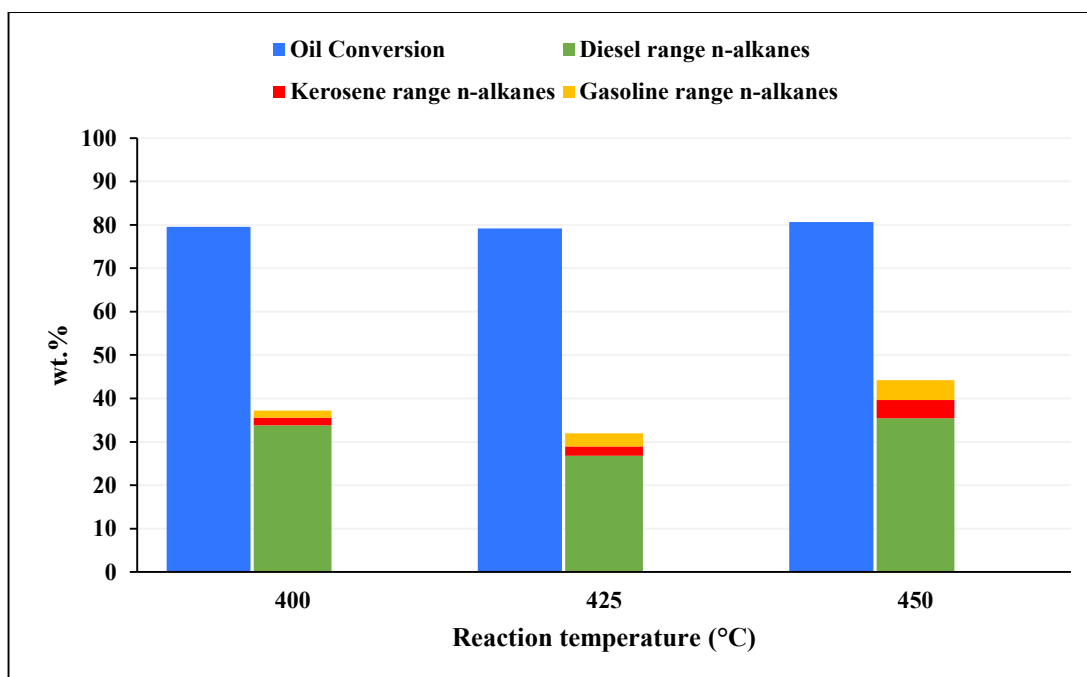


Figure 6-24 Oil conversion and liquid n-alkane product distribution for experiments over regenerated Ni/Al₂O₃ catalyst at different temperatures

A comparative study between the two commercially produced regenerated catalysts was performed in order to determine if the performance would be different from the corresponding fresh catalysts. The results of the fresh catalyst comparison was that while the Ru/Al₂O₃ catalyst was better at overall oil conversion, the Ni/Al₂O₃ performed better for hydrocracking reactions to yield kerosene range n-alkanes.

Figures 6-23 and 6-24 show the oil conversion and distribution of n-alkanes for transportation fuels produced from experiments with regenerated Ru/Al₂O₃ and Ni/Al₂O₃ catalyst, respectively. The Ni/Al₂O₃ catalyst had substantially higher oil conversion (79.52, 79.19 and 80.64%) when compared to the oil conversion for the Ru/Al₂O₃ catalyst (62.39, 64.66 and 71.54%) for all three experimental temperatures (400, 425 and 450 °C). This indicates that the metallic sites on the regenerated Ni/Al₂O₃ catalyst were more active than those on the regenerated Ru/Al₂O₃ catalyst in promoting hydrotreating reactions. In addition, it is evident from the figures that the Ni/Al₂O₃ catalyst produced a higher yield of liquid n-alkanes than the Ru/Al₂O₃ catalyst. Comparison of the n-alkanes in the kerosene range reveal that all experiments using the Ni/Al₂O₃ catalyst once again, performed better than the all experiments using the Ru/Al₂O₃ catalyst. This also suggests that the Ni/Al₂O₃ catalyst had a better hydrocracking activity than the Ru/Al₂O₃ catalyst.

In contrast to the fresh catalyst comparison, the regenerated Ni/Al₂O₃ catalyst has outperformed the regenerated Ru/Al₂O₃ catalyst in both hydrotreating and hydrocracking reactions resulting in higher yields of liquid n-alkanes in the jet fuel range. This was an indication that the Ni/Al₂O₃ catalyst had better maintained its effectiveness when compared to the Ru/Al₂O₃ catalyst for hydroprocessing waste cooking oil to produce jet fuel range n-alkanes.

6.2.11 Comparative study of the performance of the commercially produced fresh and regenerated Ru/Al₂O₃ catalysts in the hydroprocessing of waste cooking oil

In order to gain a true reflection of the catalyst's ability to sustain its effectiveness in the hydroprocessing of waste vegetable oil to jet fuel range n-alkanes, a comparison between the results from experiments using the fresh and regenerated catalyst was performed. In the case of the Ru/Al₂O₃ catalyst, comparisons were done for experiments at 425 and 450 °C only since at 400 °C, the fresh Ru/Al₂O₃ catalyst was not sulphided, while the regenerated one was sulphided.

Figure 6-7 and 6-23 show the oil conversion and distribution of n-alkanes for transportation fuels produced from experiments with fresh and regenerated Ru/Al₂O₃ catalyst respectively. It can be seen that oil conversion has decreased for the regenerated catalyst (64.66 and 71.54%) when compared to the fresh catalyst (99.16 and 98.79%) for experiments at 425 and 450 °C,

respectively. This is attributed to a loss in activity at the metallic sites resulting in a reduced effectiveness in promoting the initial hydrotreating reactions which initiate oil conversion. The total liquid n-alkane yield has also significantly decreased from the fresh catalyst (71.46 and 74.75%) to the regenerated catalyst (21.59 and 34.38%) for experiments at 425 and 450 °C, respectively. This further validates the reduction in activity at the metallic sites resulting in a decline in the promotion of hydrotreating reactions.

On the other hand, for the two reaction temperatures (425 and 450 °C), the yield for n-alkanes in the kerosene range using fresh catalyst (3.05 and 4.46%) does not differ drastically when compared to the regenerated catalyst (1.28 and 3.42%). This indicates that while the metallic sites may have lost activity, the acidic supports are still able to promote hydrocracking reactions close to the fresh catalyst.

In the focus of obtaining jet fuel range n-alkanes, the regenerated catalyst is able to maintain its effectiveness and achieve only a small decrease in yield when compared to the fresh catalyst. As such, in the case of Ru/Al₂O₃ catalyst, regeneration and re-use might be more economical than purchasing new catalyst to achieve only a very slight increase in yields. It also saves time and man power as it reduces the number of times the reactor needs to be unpacked and new catalyst loaded.

6.2.12 Comparative study of the performance of the commercially produced fresh and regenerated Ni/Al₂O₃ catalysts in the hydroprocessing of waste cooking oil

Figures 6-8 and 6-24 show the oil conversion and distribution of n-alkanes for transportation fuels produced from experiments with fresh and regenerated Ni/Al₂O₃ catalyst respectively. For all three reaction temperatures (400, 425 and 450 °C) it can be seen that oil conversion for the fresh catalyst (72.78, 78.38 and 78.38%) is similar to that for the regenerated catalyst (79.52, 79.19 and 80.86%). Although the regenerated catalyst has a slightly higher oil conversion, a potential reason for this is given in section 6.2.9 pertaining to possible impurities on the fresh catalyst that may have been burned off during regeneration processes resulting in an increased exposed surface area and therefore an increase in the catalyst activity. The similar oil conversion suggests that this catalyst has maintained its activity in hydrotreating reactions which suggests the metallic sites have maintained their effectiveness for these reactions. In addition there are small variations for the total liquid n-alkane yields for the three temperatures (400, 425 and 450 °C) for the fresh (35.79, 38.35 and 52.92%) and regenerated (37.20, 31.95 and 44.21%) catalyst. This further validates that the catalyst has sustained its activity for promoting hydrotreating reactions.

Furthermore, there is a marginal decrease in the yield of n-alkanes in the kerosene range from fresh (2.18, 2.52 and 5.18%) to regenerated catalyst (1.78, 2.17 and 4.23%) for all three reaction temperatures (400, 425 and 450 °C). This indicates the acidic sites on the catalyst support were able to maintain its hydrocracking activity in order to promote these reactions.

Overall, the regenerated Ni/Al₂O₃ catalyst has shown a very minute decrease in hydroprocessing activity. As a result, it is suggested that this catalyst be regenerated and re-used for hydroprocessing of waste cooking oil as it would be more economical than purchasing new catalyst. Furthermore, it also saves time and man power as it reduces the number of times the reactor needs to be unpacked and new catalyst loaded.

6.3 Reaction kinetic study

As mentioned in Chapter 2, the complexity of the reaction mechanisms involved in hydroprocessing reactions is high due to the variations in reactant composition and the behaviour and activity of different catalysts. As such, there is no general reaction rate expression which can predict results for a range of operating conditions regardless of the type of vegetable oil and catalyst employed. Research studies discussed in Chapter 2 provide kinetic results for reactions specific to their feedstock and catalyst. In the same way, this study aimed to determine the activation energy for each of the catalysts employed over the specified operating conditions.

In order to do this, the following assumption was made:

- The hydrogen gas was in large excess such that:

$$F_{BO} \approx F_B \quad (6-2)$$

Where F_{BO} and F_B are the initial and final hydrogen molar flow rates.

Starting with the reaction rate expression for a tubular packed-bed reactor:

$$r_A = \frac{dF_A}{dW} \quad (6-3)$$

Where: - r_A is the reaction rate with respect to species A (waste cooking oil),

– F_A is the final molar flow rate of species A,

– W is the mass of the catalyst.

The exit molar flow rate of species A can be determined from:

$$F_A = F_{AO}(1 - x) \quad (6-4)$$

Differentiating gives:

$$dF_A = -F_{A0} \cdot dx \quad (6-5)$$

Where: - F_{A0} is the initial molar flow rate of species A,

- x is the conversion.

Assuming a first-order reaction rate and that hydrogen is in excess:

$$-r_A = kC_A C_B \quad (6-6)$$

$$-r_A = k' C_A \quad (6-7)$$

$$k' = k C_B \quad (6-8)$$

Where: - k is the reaction rate constant,

- C_A and C_B are the exit molar concentrations of species A and B respectively.

Recalling:

$$C_A = \frac{F_A}{q} \quad (6-9)$$

Substituting (6-9) into (6-7) gives:

$$-r_A = k' \frac{F_A}{q} \quad (6-10)$$

Where q is the total volumetric flow rate.

Substituting equation (6-4) into (6-10) and equation (6-5) into (6-3) and combining equations (6-3) and (6-10) gives:

$$\frac{dX}{dW} = \frac{k'(1-x)}{q} \quad (6-11)$$

Let:

$$k'' = \frac{k'}{q} \quad (6-12)$$

Substituting equation (6-12) into (6-11), rearranging and integrating gives:

$$\int_0^x \frac{dX}{(1-X)} = k'' W$$

$$-\ln(1-X) = k'' W \quad (6-13)$$

Using known catalyst masses, measured conversions, total volumetric flow rates and species molar concentrations (see Appendix D for calculations) k'' , k' and k can be solved from equations (6-13), (6-12) and (6-8) respectively.

The activation energy is a variable in the Arrhenius equation:

$$k = A \exp\left(\frac{-E_a}{RT}\right) \quad (6-14)$$

Linearizing (6-14) gives:

$$\ln(k) = \ln(A) - \frac{E_a}{RT} \quad (6-15)$$

Where: - A is the pre-exponential factor,

- E_a is the activation energy,

- R is the universal gas constant,

- T is the reaction temperature.

By plotting $\ln(k)$ versus $\frac{1}{T}$ a straight line should be observed whose slope is $\frac{-E_a}{R}$ with intercept $\ln(A)$. From the equation of the line the pre-exponential factor and the activation energy can be determined. These plots were done for all tested catalysts as shown in the following figures. Table 6-7 contains information obtained from these figures. Sample calculations for the experimental points can be seen in Appendix D with all the calculated data available in Appendix F.

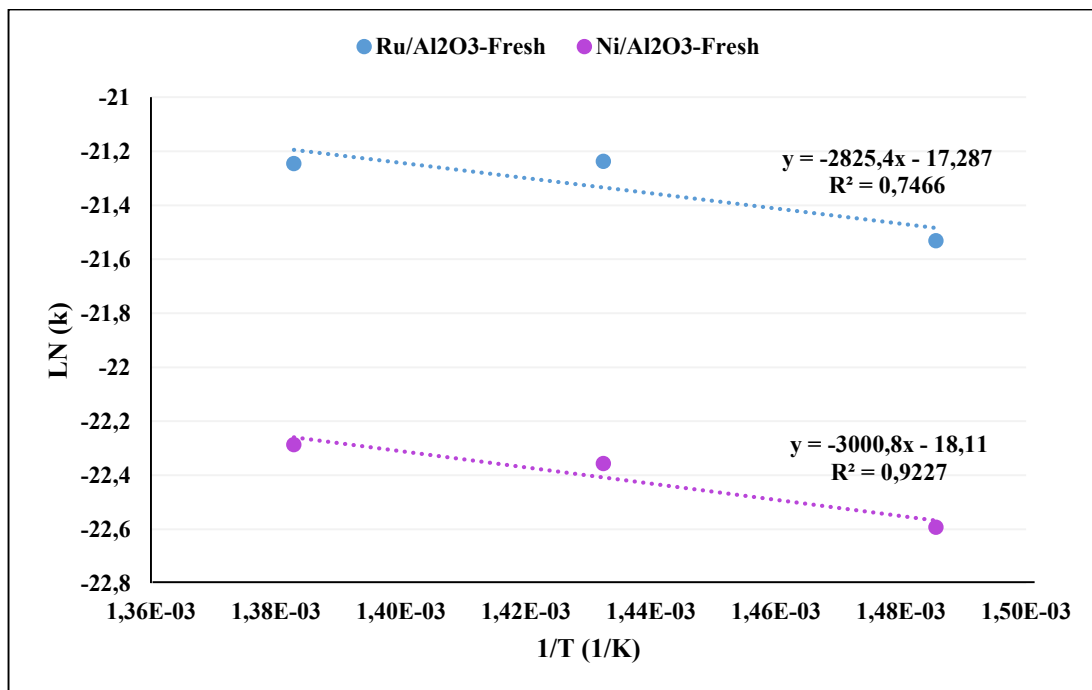


Figure 6-25: Linearized Arrhenius plots for the commercially produced fresh Ru/Al₂O₃ and Ni/Al₂O₃ catalysts

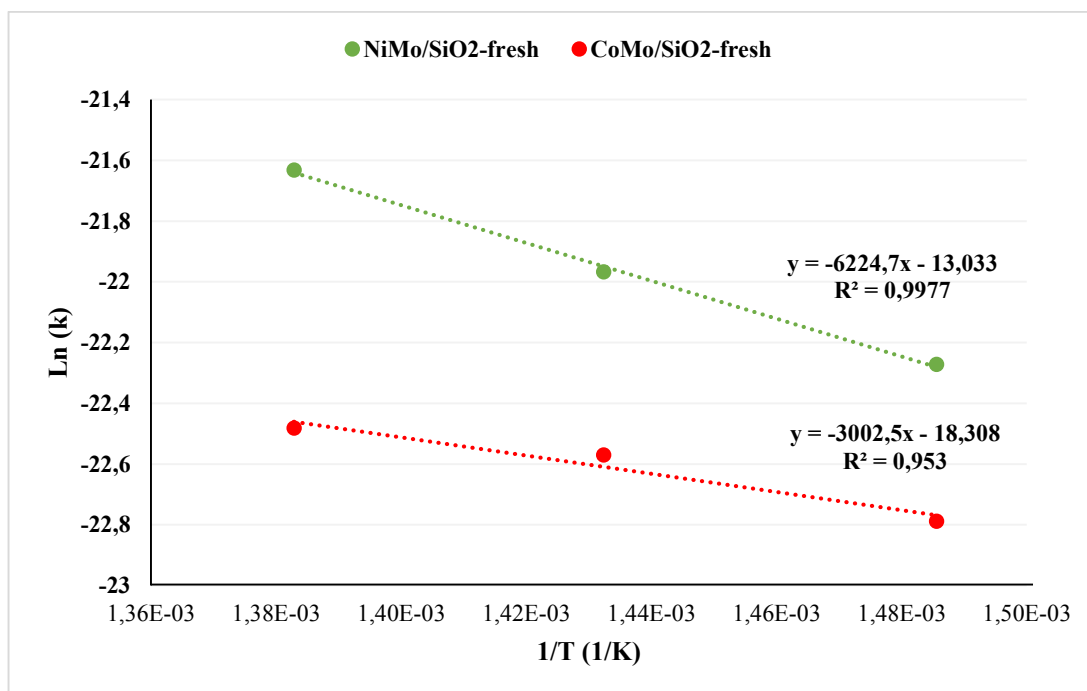


Figure 6-26: Linearized Arrhenius plots for the laboratory prepared fresh Ni-Mo/SiO₂ and Co-Mo/SiO₂ catalysts

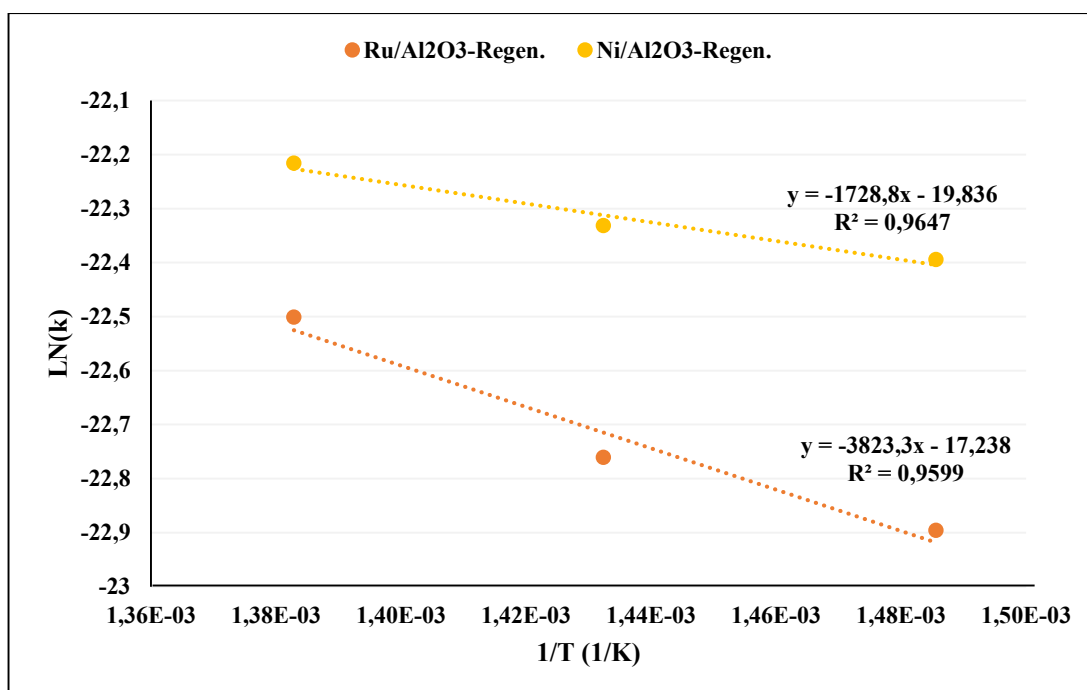


Figure 6-27: Linearized Arrhenius plots for the commercially produced regenerated Ru/Al₂O₃ and Ni/Al₂O₃ catalysts

Table 6-7 Data obtained from the linearized Arrhenius plots

Catalyst	Linearized trend line equation	R ²	A (pre-factor)	E _a (kJ.mol ⁻¹)
Ru/Al ₂ O ₃ (F) ^a	$y = -2825.4x - 17.287$	0.7466	3.11E-08	23.49
Ni/Al ₂ O ₃ (F)	$y = -3000.8x - 18.110$	0.9227	1.36E-08	24.95
Ni-Mo/SiO ₂ (F)	$y = -6224.7x - 13.033$	0.9977	2.19E-06	51.75
Co-Mo/SiO ₂ (F)	$y = -3002.5x - 18.308$	0.9530	1.12E-08	24.96
Ru/Al ₂ O ₃ (R) ^b	$y = -1728.8x - 19.836$	0.9647	3.26E-08	31.79
Ni/Al ₂ O ₃ (R)	$y = -3823.3x - 17.238$	0.9599	2.43E-09	14.37

[a] (F) – Indicates fresh catalyst

[b] (R) – Indicates regenerated catalyst

The linearized Arrhenius plots in Figure 6-25 for the fresh commercial catalysts show a good fit for the Ni/Al₂O₃ catalyst with an R² = 0.9227. From this fit, the pre-exponential factor was found to be 1.36E-08 and the activation energy was found to be 24.95 kJ.mol⁻¹.

On the other hand, the trend line has a R² = 0.7466 for the Ru/Al₂O₃ catalyst suggesting it does not fit the data very well. However, it must be remembered that for the experiment carried out at 400 °C, the Ru/Al₂O₃ catalyst was not sulphided. Section 6.2.1 provided substantial evidence on the importance of sulphiding due to its large influence on the catalyst activity for hydroprocessing reactions. Therefore, the poor fit can be attributed to the catalyst not being sulphided for one experiment, while it was sulphided for the remaining two. As such, all data obtained from this plot must be treated with caution. From the plot, as seen in Table 6-7, the pre-exponential factor was 3.11E-08 and the activation energy was estimated to be 23.49 kJ.mol⁻¹.

In the case of the laboratory prepared NiMo/SiO₂ and CoMo/SiO₂ catalysts (Arrhenius plots in Figure 6-26), both trend lines showed excellent fits to the experimental data with R² = 0.9977 and 0.9530 respectively. The NiMo/SiO₂ catalyst had both the highest pre-exponential factor of 2.19E-06 (approx. 100 times greater than the others) as well as the highest estimated activation energy of 51.75 kJ.mol⁻¹. The research study (Hanafi et al., 2015) reviewed in Chapter 2 used a NiW/SiO₂-Al₂O₃ catalyst and estimated the activation energy to be 56 kJ.mol⁻¹ over a temperature range of 325 to 450 °C. The closeness in the activation energies validates the results for both studies as both catalysts comprised of similar compounds and a similar reaction temperature range. The pre-exponential factor and activation energy for the CoMo/SiO₂ catalyst was found to be 1.12E-08 and 24.96 kJ.mol⁻¹ respectively.

Finally, the Arrhenius plots for the regenerated commercially produced catalysts can be seen in Figure 6-27. Both trend lines once again fit the experimental data well with $R^2 = 0.9599$ and 0.9647 for the $\text{Ru}/\text{Al}_2\text{O}_3$ and $\text{Ni}/\text{Al}_2\text{O}_3$ catalyst respectively. In the case of the regenerated $\text{Ru}/\text{Al}_2\text{O}_3$ catalyst, the pre-exponential factor was found to be $3.26\text{E-}08$ and the activation energy was determined to be $31.79 \text{ kJ.mol}^{-1}$. Compared to the fresh catalyst, the increased activation energy is expected since the used catalyst has a reduced activity and therefore requires a higher minimum amount of energy for the reactions to start. This increased activation energy further validates that the catalyst lost some of its hydroprocessing activity from the fresh to the regenerated catalyst.

In the case of the regenerated $\text{Ni}/\text{Al}_2\text{O}_3$ catalyst, the pre-exponential factor was found to be $2.43\text{E-}09$ and the activation energy was calculated to be $14.37 \text{ kJ.mol}^{-1}$. Interestingly, compared to the fresh catalyst, the activation energy has decreased for the regenerated catalyst. However, this is consistent with the fact that slightly better oil conversions were confirmed for the regenerated catalyst. The lower activation energy for the regenerated catalyst indicates a greater exposed active surface area of the catalyst, reasons for which were discussed in sections 6.2.9 and 6.2.12.

Chapter

7

Conclusion & recommendations

The performance of several transition metal-based catalysts was investigated for the hydroprocessing of waste cooking oil to produce kerosene (jet fuel) range n-alkanes in a laboratory-scale, fixed-bed tubular reactor. Preliminary tests revealed the initial operating parameters including a temperature range of 350–400 °C, operating pressure of 40 bar and a liquid oil volumetric flow rate of 0.2 ml/min were not suitable due to excess formation of waxy residue product resulting in line blockages. Final operating parameters were a temperature range of 400–450 °C, operating pressure of 120 bar and a liquid oil volumetric flow rate of 0.1 ml/min. Furthermore, spherical glass beads were found to be a more efficient form of packing material compared to glass wool. Oil conversion was found to range from 62.39 to 99.16% indicating that the metallic sites on all catalysts were active and able to sufficiently promote hydrotreating reactions. Experiments using the commercially produced catalysts resulted in some formation of a waxy residue. This suggests that these catalysts weren't able to promote complete hydrotreating of the converted oil. On the other hand, the laboratory prepared catalysts had no waxy residue present in the product, indicating that all converted oil underwent complete hydrotreating reactions. An increase in the reaction temperature was found to result in an increase in oil conversion, indicating that hydrotreating reactions were favoured at higher temperatures. For the commercial catalysts, an increase in the reaction temperature resulted in lower yields of waxy residue along with increased yields of liquid n-alkane and gaseous products. The reduced wax yield is further proof that hydrotreating reactions are favoured at higher temperatures.

Furthermore, the increased yields in liquid n-alkanes and gaseous products indicates that hydrocracking reactions are also favoured at higher temperatures resulting in longer straight chain n-alkanes breaking down to form shorter saturated n-alkane liquid and gas products. While the laboratory prepared catalysts had no solid product, an increase in reaction temperature resulted in a decrease in liquid n-alkanes and an increase in gaseous products. This too suggests that hydrocracking reactions are favoured at higher temperatures since the liquid n-alkanes are breaking down to form more gas products. The fact that the laboratory prepared catalysts produced higher liquid n-alkane yields and had no solid products indicated that the metallic sites (Ni-Mo and Co-Mo) had a greater activity toward hydrotreating reactions while the acidic support (SiO₂) had a greater activity toward hydrocracking when compared to the metallic sites (Ru and Ni) and acidic support (Al₂O₃) for the commercial catalyst. Results for all catalysts at all reaction temperatures revealed that majority ($\geq 67.69\%$) of the n-alkanes in the liquid product belonged to the diesel range. This suggested that hydrotreating reactions were occurring first and required a lower activation energy than hydrocracking reactions. The highest yields for kerosene and gasoline range n-alkanes were found at the highest reaction temperature further validating that hydrocracking reactions are favoured at higher temperatures. Comparative studies of the results indicated the best yield of kerosene range n-alkanes (5.84%) was obtained at a reaction temperature of 450 °C using the laboratory produced fresh Ni-Mo/SiO₂ catalyst. Catalyst regeneration was found to be a viable option as there was only a slight decrease in the yield of kerosene range n-alkanes. The Ni/Al₂O₃ was found to better sustain its activity with the greatest decrease in kerosene range n-alkanes from fresh to regenerated catalyst being only 0.95%. Sulphiding the catalyst was found to be a vital step in activating the catalyst as there was a drastic increase in hydroprocessing activity resulting in a substantial decrease in waxy residue and correspondingly, a large increase in liquid n-alkane product when compared to non-sulphided catalyst. A reaction kinetic study was performed whereby a model to determine activation energies was developed. The estimated activation energies ranged from 14.37 - 51.75 kJ/mol and was found to be consistent with literature. Improved oil conversion and kerosene range n-alkane yields may have been obtained by using fresh catalyst for every experimental temperature tested during the fresh catalyst study, as well as regenerating the catalyst after every experimental temperature tested during the regeneration study. A larger catalyst bed may be employed to increase residence time which will improve the yield of kerosene range n-alkanes as more hydrocracking reactions will occur. Furthermore, designing separate specialised catalysts to perform hydrotreating and then hydrocracking reactions in two different packed-beds may significantly improve oil conversion and the yield of kerosene range n-alkanes.

References

1. Abidin, S. Z., Patel, D., Saha, Basudeb., “Quantitative analysis of fatty acids composition in the used cooking oil (UCO) by gas chromatography-mass spectrometry (GC-MS)”, *Can. J. Chem. Eng.* **91** (2012) 1896-1903
2. Akande, A. J., Idem, R. O., Dalai, A. K., “Synthesis, characterization and performance evaluation of Ni/Al₂O₃ catalysts for reforming of crude ethanol for hydrogen production”, *Applied Catalysis A: General* **287** (2005) 159-175
3. Alouche, A., “Preparation and characterization of copper and/or cerium catalysts supported on alumina or ceria”, *Jordon Journal of Mechanical and Industrial Engineering* **2** (2008) 111-116
4. Anderson, J. R. and Pratt, K. C., “Introduction to characterisation and testing of catalysts”, Academic Press, Australia, 1985
5. Appleby, W. G., Gibson, J. W., Good, G. M., “Coke formation in catalytic cracking”, *Ind. Eng. Chem. Process. Des. Dev.* **1** (1962) 102-110
6. Barath, F., Turki, M., Keller, V., Maire, G., “Catalytic activity of reduced MoO₃/α-Al₂O₃ for hexanes reforming: 1. Preparation, characterization and X-ray photoelectron spectrometry studies”, *Journal of Catalysis* **185** (1991) 1-11
7. Bendz, K., “EU-25 oilseeds and products biofuels situation in the European Union”, 2005
8. Bezergianni, S., “Liquid, Gaseous and solid biofuels – Conversion techniques: Chapter 9 -Catalytic hydroprocessing of liquid biomass for biofuels production”, *Intech* (2013) 299-326
9. Bezergianni, S. and Kalogianni, A., “Hydrocracking of used cooking oil for biofuels production”, *Bioresource Technology* **100** (2009) 3927-3932
10. Bezergianni, S., Voutetakis, S., Kalogianni, A., “Catalytic hydrocracking of fresh and used cooking oil”, *Ind. Eng. Chem. Res.* **48** (2008) 8402-8406

11. Birchem, T., "Latest improvements in ACETM catalysts technology for ULSD production & deep cetane increase", *5th ERTC Annual Meeting: Conference proceedings*, Istanbul, Turkey, 2010
12. Charusiri, W. and Vitidsant, T., "Kinetic study of used vegetable oil to liquid fuels over sulphated zirconia", *Energy & Fuels* **19** (2005) 1783-1789
13. Chhetri, A. B., Watts, K. C., Islam, M. R., "Waste cooking oil as an alternate feedstock for biodiesel production", *Energies* (2008) 3-18
14. Choudhary, N. and Saraf, D. N., "Hydrocracking: A review" *Product R&D* **14** (1975) 74-83
15. da Rocha Filho, G. N., Brodzki, D., Djéga-Mariadassou, G., "Formation of alkanes, alkylcycloalkanes and alkylbenzenes during the catalytic hydrocracking of vegetable oils", *Fuel* **72** (1993) 543-549
16. de Klerk, A., "Environmentally friendly refining: Fischer-Tropsch versus crude oil", *Green Chemistry* **6** (2006) 560-565
17. DeCoursey, W. J., "Statistics and probability for engineering applications with Microsoft Excel", Elsevier Science, USA, 2003
18. Donnis, B., Egeberg, R. G., Blom, P., Knudsen, K., "Hydroprocessing of bio-oils and oxygenates to hydrocarbons: Understanding reaction routes", *Top. Catal.* **52** (2009) 229-240
19. Dunn, R. O., "Alternative jet fuels from vegetable-oils", *Transactions of the ASAE* **44** (2001) 1751-1757
20. Eberly, P. E., Kimberlin, C. N., Miller, W. H., Drushel, A. V., "Coke formation on silica-alumina cracking catalysts" *Ind. Eng. Chem. Process. Des. Dev.* **5** (1966) 193-198
21. Egeberg, R. G. and Knudsen, K., "Industrial-scale production of renewable diesel", *PTQ* **Q3** (2011) 59-65

22. Eijssbouts, S., "On the flexibility of the active phase in hydrotreating", *Applied Catalysis A: General* **158** (1997) 53-92
23. Freerks, R. L. and Muzzell, P. A., "Production and characterization of synthetic jet fuel produced from Fisher-Tropsch hydrocarbons", *Prepr. Pap.-Am. Chem. Soc. Div. Petrol. Chem.* **49** (2004) 407-410
24. Goering, A. S., Daugherty, M. J., Pryde, E. H., Heakin, A. J., "Fuel properties of eleven vegetable oils", *Trans. ASAE* **25** (1982) 1472-1477
25. Goldstein, J. I., Newbury, D. E., Echlin, P., Joy, D. C., Romig, A. D., Lyman, C. E., Fiori, C., Lifshin, E., "Scanning electron microscopy and X-ray microanalysis", 2nd Edition, Plenum Press, New York, 1992
26. Göröcs, N., Mudri, D., Mátyási, J., Balla, J., "The determination of GC-MS relative molar responses of some n-alkanes and their halogenated analogs", *Journal of Chromatographic Science* **51** (2013) 138-145
27. Guesta, F. J., Sanchez-Muniz, C., Polonio-Garrido, S., Varela-Lopez, A. R., "Thermoxidative and hydrolytic changes in sunflower oil using in frying with a fast turnover of fresh oil", *J. Am. Oil. Chem. Soc.* **70** (1993) 1069-1073
28. Haldeman, R. G., Botty, M. C., "On the nature of the carbon deposit of cracking catalysts", *J. Phys. Chem.* **63** (1959) 489-496
29. Hanafi, S. A., Elmelawy, M. S., El-Syed, H. A., Shalaby, N. H., "Hydrocracking of waste cooking oil as renewable fuel on NiW/SiO₂-Al₂O₃ catalyst", *Journal of Advanced Catalysis Science and Technology* **2** (2015) 27-37
30. Hancsók, J., Eller, Z., Pölczmann, G., Varga, Z., "Sustainable production of bioparaffins in a crude oil refinery", *Clean Technologies and Environmental Policy* **16** **9** (2014) 1445-1454
31. Heinemann, H., "A brief history of industrial catalysis", *Catalysis: Science and Technology Vol.1* (1981) 1-41

32. Huber, G. W. and Dumesic, J. A., "An overview of aqueous-phase catalytic processes for production of hydrogen and alkanes in biorefinery", *Catal. Today* **111** (2006) 119-132
33. Huber, G.W., O'Connor, P., Corma, A., "Processing biomass in conventional oil refineries: Production of high quality diesel by hydrotreating vegetable oils in heavy vacuum oil mixtures", *Applied Catalysis A: General* **329** (2007) 120-129
34. John, R., "Catalysis" *Science and Technology, Vol. 11* 1996
35. Knothe, G., "Dependence of biodiesel fuel properties on the structure of fatty acid alkyl esters", *Fuel Process. Technol.* **86** (2005) 1059-1070
36. Koivusalmi, E., Piilola, R., Aalto, P., "Process for producing branched hydrocarbons", *United States Patent Publication* **0302001** 2008
37. Kunkes, E. L., Simonetti, D. A., West, R. M., Serrano-Ruiz, J. C., Gartner, C. A., Dumesic, J. A., "Catalytic conversion of biomass to monofunctional hydrocarbons and targeted liquid-fuel classes", *Science* **322** (2008) 417-421
38. Leardi, R., "Experimental design in chemistry: A tutorial", *Analytica Chimica Acta.* **652** (2009) 161-172
39. Mäki-Arvela, P., Rozmysłowicz, B., Lestari, S., Simakova, O., Eränen, K., Salmi, T., Murzin, D. Y., "Catalytic deoxygenation of tall fatty acid over palladium supported on mesoporous carbon", *Energy & Fuels* **25** (2011) 2815-2825
40. Marckley, K. S., "Fatty acids, their chemistry and physical properties", 2nd Edition, Interscience, New York, 1960
41. Maxwell, I. E., "Zeolite catalysis in hydroprocessing technology", *Catalysis Today* **1** (1987) 385-413
42. Mills, G. A., Heinemann, H., Milliken, T. H., Oblad, A. G., "(Houdriforming reactions) Catalytic mechanism", *Ind. Eng. Chem.* **45** (1953) 134-137
43. Montgomery, D. C., "Engineering statistics", John Wiley and Sons, USA, 1998

44. Morel, F., Kressmann, S., Harle, V., Kasztelan, S., "Processes and catalysts for hydrocracking of heavy oil and residues", *Studies in surface science and catalysis* **106** (1997) 1-16
45. Murphree, E. V., Brown, C. L., Gohr, E. J., "Hydrogenation of petroleum", *Ind. Eng. Chem.* **32** (1940) 1203-1212
46. Nasikin, M., Susanto, B. H., Hirsaman, M. A., Wijanarko, A., "Biogasoline from palm oil by simultaneous cracking and hydrogenation reaction over NiMo/zeolite catalyst", *World Applied Sciences Journal* **5** (2009) 74-79
47. Peng, B., "Transformation of triglycerides and fatty acids into biofuels with sulfur-free catalysts", PhD Thesis – Technischen Universität München, 2012
48. Perego, C. and Villa, P., "Catalyst preparation methods", *Catalysis Today* **34** (1997) 281-305
49. Pinna, F., "Supported metal catalyst preparation", *Catalysis Today* **41** (1998) 129-137
50. Rahmes, T., "Status of sustainable biofuel efforts for aviation", *Boeing Management Company* 2004
51. Rekkab-Hammoumraoui, I., Benabadji-Soulimane, R., El Korso-Hamza Reguig, S., Choukchou-Brabam, A., Bachir, R., "Preparation and characterization of X wt-% Ru/Al₂O₃ catalysts for cyclohexane oxidation using tert-butyl hydroperoxide", *Research Journal of Pharmaceutical, Biological and Chemical Sciences* **1** (2010) 239-249
52. Satterfield, C. N., "Heterogeneous catalysis in industrial practice", McGraw-Hill, New York, 1991
53. Scherzer, J. and Gruia, A. J., "Hydrocracking science and technology", Mercel Dekker, Inc., New York, 1996

54. Silvy, R. P., Grange, P., Delannay, F., Delmon, B., "Influence of the nature of activating molecules on the catalytic activity of cobalt-molybdenum/alumina catalysts", *Applied Catalysis* **46** (1989) 113-129
55. Smejkal, Q., Smejkalova, L., Kubicka, D., "Thermodynamic balance in reaction system of total vegetable oil hydrogenation", *Chemical Engineering Journal* **146** (2009) 155-160
56. Sotel-Boyás, R., Liu, Y., Minowa, T., "Production of green diesel by hydrocracking of canola oil on Ni-Mo/ γ -Al₂O₃ and Pt-zeolitic based catalysts", *AIChE Paper* **P134226** 2008
57. Sotelo-Boyás, R., Trejo-Zárraga, F., de Jesús Hernández-Loyo, F., "Hydrogenation: Chapter 8 - Hydroconversion of triglycerides in green liquid fuels", *Intech* (2012) 187-226
58. Srivastha, A. and Prasad, R., "Triglycerides-based diesel fuels", *Renewable & Sustainable Energy Reviews* **4** (2000) 111-133
59. Stiles, A. B., "Catalyst supports and supported catalysts", *Theoretical and Applied Concepts*, Butterworth Publishers, United States, 1987
60. Sterba, M. J. and Watkins, C. H., "New hydrocracking process offers refiners more flexible gasoline-distillates output", *Oil and Gas Journal* **58** (1960) 102-106
61. Tiwari, R., Rana, B. S., Kumar, R., Verma, D., Joshi, R. K., Garg, M. O., Sinha, A. K., "Hydrotreating and hydrocracking catalysts for processing of waste soya-oil and refinery-oil mixtures", *Catalysis Communications* **12** (2011) 559-562
62. Thomas, H. C., "Heterogeneous ion exchange in a flowing system", *J. Am. Chem. Soc.* **66** (1944) 1664-1666
63. Van Gerpen. J., "Biodiesel processing and production", *Proc. Technol.* **86** (2004) 1097-1107
64. Voorhies, A., "Carbon formation in catalytic cracking", *Ind. Eng. Chem.* **37** (1945) 318-322

65. Vukovic, J., Neuman, D., Bouchagiar, L., "Reasons for ex-situ activation", Bitterfled-Wolfen, Germany, 2004
66. Wang, H., "Biofuels production from hydrotreating of vegetable oil using supported noble metals, and transition metal carbide and nitride", PhD Thesis – Wayne State University, 2012
67. Weisz, P. B., "Polyfunctional heterogeneous catalysts", *Advances in Catalysis* **13** (1962) 137-190
68. Zeuthen, P., Blom, P., "Temperature-programmed sulfidation and oxidation of Ni-Mo/alumina catalysts and reaction with ammonia", *Applied Catalysis* **68** (1991) 117-130

Appendix

A

Pump calibration

In order to ensure the amount of actual waste cooking oil being pumped into the reactor system was in agreement with the selected volumetric flow rate on the pump, two calibration tests were performed.

A.1 Pump calibration flow rate test

In the first test, waste cooking oil was pumped into a volumetric flask for 10 minutes, each time at a different flow rate. The amount collected was measured against the calculated amount based on the set flow rate. Table A-1 shows the data from this test.

Table A-1 Results from pump calibration flow rate test

Pump flow rate (ml/min)	Time (min)	Expected volume in flask (ml)	Actual volume in flask (ml)
0.10	20	2.00	2.00
0.20	20	4.00	4.00
0.30	20	6.00	6.00
0.40	20	8.00	8.00
0.50	20	10.00	10.00

A.2 Pump calibration time test

While the first test may have been sufficient, a second test was performed to identify if the pump was accurate over longer time periods. For this test, flow rates of 0.1 and 0.2 ml/min were selected and pumped for different time intervals. The amount collected was measured against the calculated amount based on the set flow rate. Table A-2 shows the data from this test.

Table A-2 Results from pump calibration time test

Pump flow rate (ml/min)	Time (min)	Expected volume in flask (ml)	Actual volume in flask (ml)
0.10	20	2.00	2.00
0.10	30	3.00	3.00
0.10	40	4.00	4.00
0.20	20	4.00	4.00
0.20	30	6.00	6.00
0.20	40	8.00	8.00

Both tests revealed that the pump setting corresponded accurately with the actual amount of oil being pumped.

Appendix

B

Catalyst characterisation

B.1 Laboratory prepared catalysts

Table B-1 BET surface area and Energy dispersive X-ray analysis results

Variable	Unit	Catalyst	
		Ni-Mo/SiO ₂	Co-Mo/SiO ₂
BET surface area	[m ² /g]	252	239
Pore volume	[cm ³ /g]	1.01	1.02
Pore width	[Å]	161	171
EDX analysis			
Al	[wt.%]	0.82 ± 0.06	1.01 ± 0.15
Si	[wt.%]	86.33 ± 0.78	86.67 ± 0.46
Co	[wt.%]	0.56 ± 0.03	2.31 ± 0.09
Mo	[wt.%]	10.20 ± 0.66	9.92 ± 0.73
Ni	[wt.%]	2.06 ± 0.08	-
Fe	[wt.%]	0.03 ± 0.01	0.09 ± 0.01

Table B-2 Composition of Fe-Mo precursor from supplier

Element	Content (wt.%)
Mo	67.11
C	0.03
Cu	0.36
P	0.042
S	0.03
Si	1.21
Fe	31.22

Table B-3 Composition of CoSO₄ precursor from supplier

Element	Minimum (%)	Maximum (PPM)
Co	21.0	
Ca		50
Cu		20
Fe		50
Mg		500
Mn		50
Na		50
Ni		100
SiO ₂		100
Zn		10

B-2 Commercially produced catalysts

Table B-4 Ru/Al₂O₃ characterisation data (Adapted from Rekkab-Hammoumraoui et al., 2010)

Catalyst	Ru	BET surface area	Particle size by XRD	Particle size by HRTEM
	[%]	[m ² /g]	[nm]	[nm]
Ru/Al ₂ O ₃	4.35	173.3	11.2	8.2

Table B-5 Ni/Al₂O₃ characterisation data (Adapted from Akande et al., 2005)

Catalyst	Ni	Al	O	BET surface area	Pore volume	Pore size
	[%]	[%]	[%]	m ² /g	cm ³ /g	nm
Ni/Al ₂ O ₃	25.00	39.69	35.31	68	0.19	12.0

Appendix

C

Waste cooking oil characterisation

Table C-1 Composition of waste cooking oil from GCMS analysis

Compound	Composition (wt.%)
Palmitic acid	6.41
Palmitoleic acid	0.01
Stearic acid	4.35
Oleic acid	21.02
Linoleic acid	68.14
Arachidic acid	0.07

Appendix

D

Sample calculations

D.1 Catalyst preparation calculations

The following is the sample calculations for the preparation of Ni-Mo/SiO₂ (2.3 wt.% Ni and 10.4 wt.% Mo) catalyst. The Co-Mo/SiO₂ was similarly prepared. The preparation description is provided in Chapter 5.

$$\text{Mass of Fe - Mo alloy (67.11\% Mo)} = 25 \text{ g}$$

$$\text{mass of Mo} = \text{Mass of Fe - Mo alloy} * 67.1\% \text{ Mo}$$

$$= 25 \text{ g} * 0.6711$$

$$= 16.778 \text{ g}$$

$$\text{mass of Fe} = \text{mass of alloy} - \text{mass of Mo}$$

$$= 25 - 16.778$$

$$= 8.222 \text{ g}$$

$$\text{molar mass of Mo} = 95.94 \text{ g/mol}$$

$$\text{molar mass of Fe} = 55.84 \text{ g/mol}$$

$$\text{moles of Mo (or Fe)} = \frac{\text{mass of Mo (or Fe)}}{\text{molar mass of Mo (or Fe)}}$$

$$= \frac{16.778}{95.940}$$

$$= 0.1749 \text{ moles}$$

$$\text{moles of Fe} = \frac{8.222}{55.840}$$

$$= 0.1473 \text{ moles}$$

$$\text{moles of HNO}_3 \text{ required} = (2 * \text{moles of Mo}) + (4 * \text{moles of Fe})$$

$$= (2 * 0.1749) + (4 * 0.1473)$$

$$= 0.9388 \text{ moles}$$

$$\text{moles of HNO}_3 \text{ used} = \text{excess ratio} * \text{moles of HNO}_3 \text{ required}$$

$$= 1.2 * 0.9388$$

$$= 1.127 \text{ moles}$$

$$\text{excess moles of HNO}_3 = \text{moles of HNO}_3 \text{ used} - \text{moles of HNO}_3 \text{ required}$$

$$= 1.127 - 0.9388$$

$$= 0.1876 \text{ moles}$$

$$\text{volume of HNO}_3 = \text{moles of HNO}_3 \text{ used} / \text{molarity of HNO}_3 \text{ used}$$

$$= \frac{1.127}{6}$$

$$= 0.1876 \text{ litres}$$

$$\text{moles of NH}_4\text{OH required for ammonium molybdate} = 2 * \text{moles of Mo}$$

$$= 2 * 0.1749$$

$$= 0.3496 \text{ moles}$$

$$\text{moles of NH}_4\text{OH required for iron nitrate} = 3 * \text{moles of Fe}$$

$$= 3 * 0.1473$$

$$= 0.4418 \text{ moles}$$

$$\text{moles of NH}_4\text{OH required to neutralize acid} = \text{excess moles of HNO}_3$$

$$= 0.1876 \text{ moles}$$

$$\begin{aligned} \text{total moles of } \text{NH}_4\text{OH required} &= 0.3496 + 0.4418 + 1876 \\ &= 0.9793 \text{ moles} \end{aligned}$$

$$\begin{aligned} \text{volume of } \text{NH}_4\text{OH} &= \text{total moles of } \text{NH}_4\text{OH required} * \text{molarity of } \text{NH}_4\text{OH} \\ &= 0.9793 * 6.498 \\ &= 0.1507 \text{ litres} \end{aligned}$$

$$\begin{aligned} \text{moles of ammonium molybdate} &= \text{moles of Mo} \\ &= 0.1749 \text{ moles} \end{aligned}$$

$$\begin{aligned} \text{total volume} &= \text{volume of } \text{HNO}_3 + \text{volume of } \text{NH}_4\text{OH} \\ &= 0.1876 + 0.1507 \\ &= 0.3385 \text{ litres} \end{aligned}$$

$$\begin{aligned} \text{Conc. of ammonium molybdate} &= \text{moles of ammonium molybdate} / \\ &\text{measured volume} \\ &= \frac{0.1749}{0.118} \\ &= 1.482 \text{ moles/litre} \end{aligned}$$

$$\begin{aligned} \text{mass of Mo required} &= \text{mass of } \text{SiO}_2 * \text{wt. \% of Mo} \\ &= 30.28 * 0.104 \\ &= 3.515 \text{ g} \end{aligned}$$

$$\begin{aligned} \text{moles of Mo required} &= \frac{3.515}{95.940} \\ &= 0.0366 \text{ moles} \end{aligned}$$

$$\begin{aligned} \text{moles of ammonium hydrate} &= \text{moles of Mo required} \\ &= 0.0366 \text{ moles} \end{aligned}$$

$$\begin{aligned} \text{volume ammonium hydrate} &= \text{moles ammonium hydrate} / \\ \text{Conc. of ammonium molybdate} \\ &= \frac{0.0366}{1.482} \\ &= 0.0247 \text{ litres} \end{aligned}$$

$$\text{mass of Ni required} = \text{mass of SiO}_2 * \text{wt. \% of Ni}$$

$$= 30.28 \times 0.023$$

$$= 0.713 \text{ g}$$

$$\text{moles of Ni required} = \frac{0.713}{58.710}$$

$$= 0.0121 \text{ moles}$$

$$\text{moles of Ni(NO}_3)_2 \text{ required} = \text{moles of Ni required}$$

$$= 0.0121 \text{ moles}$$

$$\text{volume of Ni(NO}_3)_2 \text{ required}$$

$$= \text{moles of Ni(NO}_3)_2 \text{ required} / \text{conc. of moles of Ni(NO}_3)_2$$

$$= \frac{0.0121}{1.022}$$

$$= 0.0119 \text{ litres}$$

D.2 Experimental analysis calculations

The following sample calculations demonstrate how the masses and yields of all the products are calculated. The calculations pertaining to the experimental run at 450 °C using fresh Co-Mo/SiO₂ are shown. Calculations for other experimental runs followed the same procedure.

$$\dot{V}_{\text{liquid oil}} = 0.1 \text{ ml/min}$$

$$\rho_{\text{liquid oil}} = 0.92 \text{ g/ml}$$

$$t_{\text{run}} = 10800 \text{ s}$$

$$m_{\text{total liquid oil fed}} = \rho_{\text{oil}} * \dot{V}_{\text{oil}} * t_{\text{run}}$$

$$= 0.1 * 0.92 * 10800$$

$$= 16.560 \text{ g}$$

$$m_{\text{liquid product}} = 9.240 \text{ g}$$

$$m_{\text{solid product}} = 0.000 \text{ g}$$

$$\begin{aligned}
 m_{\text{gas product}} &= m_{\text{total oil fed}} - m_{\text{liquid product}} - m_{\text{solid product}} \\
 &= 16.56 - 9.240 - 0.000 \\
 &= 7.140 \text{ g}
 \end{aligned}$$

GCMS analysis of a sample of liquid product generated a total ion chromatogram (TIC). Each peak on the TIC represented a compound and the area of the peak was found using the proprietary software. The calculations of pentane are shown below. Hexane through to Octadecane was calculated via the same method.

$$m_{\text{liquid sample}} = 0.166 \text{ g}$$

$$m_{\text{internal standard (Xylene)}} = 0.136 \text{ g}$$

$$\begin{aligned}
 n_{\text{internal standard (Xylene)}} &= \frac{m_{\text{internal standard (Xylene)}}}{MM_{\text{internal standard (Xylene)}}} \\
 &= \frac{0.136}{106.6} \\
 &= 0.0013 \text{ moles}
 \end{aligned}$$

$$A_{\text{pentane}} = 1.27E + 04$$

$$A_{\text{internal standard (Xylene)}} = 2.79E + 06$$

$$RMR_{\text{pentane}} = \frac{(0.171 \times N) - 0.405}{0.263}$$

$$\begin{aligned}
 RMR_{\text{pentane}} &= \frac{(0.171 \times 5) - 0.405}{0.263} \\
 &= 1.71
 \end{aligned}$$

$$\begin{aligned}
 n_{\text{pentane in liquid sample}} &= \frac{A_{\text{pentane}} * n_{\text{internal standard (Xylene)}}}{RMR_{\text{pentane}} * A_{\text{internal standard (Xylene)}}} \\
 &= \frac{1.27 \times 10^4 * 1.71 * 0.0013}{1.71 * 2.79 \times 10^6} \\
 &= 3.41 \times 10^{-6} \text{ moles}
 \end{aligned}$$

$$\begin{aligned}
 m_{\text{pentane in liquid sample}} &= n_{\text{pentane in liquid sample}} * MM_{\text{pentane}} \\
 &= 3.41 \times 10^{-6} * 72.15 \\
 &= 2.46 \times 10^{-4} \text{ g}
 \end{aligned}$$

$$\begin{aligned}
 x_{\text{pentane in liquid sample}} &= \frac{m_{\text{pentane in liquid sample}}}{m_{\text{liquid sample}}} \\
 &= \frac{2.46 \times 10^{-4}}{0.166} \\
 &= 0.0015
 \end{aligned}$$

Assuming: $x_{\text{liquid sample}} = x_{\text{total liquid product}}$

$$\begin{aligned}
 m_{\text{pentane in liquid product}} &= x_{\text{pentane in liquid sample}} * m_{\text{liquid product}} \\
 &= 0.0015 * 9.420 \\
 &= 0.014 \text{ g}
 \end{aligned}$$

$$\begin{aligned}
 m_{\text{n-alkanes in liquid product}} &= \sum m_{C_5-C_{18} \text{ n-alkanes in the liquid product}} \\
 &= 4.991 \text{ g}
 \end{aligned}$$

$$\begin{aligned}
 m_{\text{unreacted oil}} &= m_{\text{liquid product}} - m_{\text{n-alkanes in liquid product}} \\
 &= 9.420 - 4.991 \\
 &= 4.429 \text{ g}
 \end{aligned}$$

$$\begin{aligned}
 m_{\text{gasoline range n-alkanes}} &= \sum m_{C_5-C_{10} \text{ n-alkanes in the liquid product}} \\
 &= 0.014 + 0.018 + 0.168 + 0.200 + 0.228 + 0.293 \\
 &= 0.921 \text{ g}
 \end{aligned}$$

$$\begin{aligned}
 m_{\text{kerosene range n-alkanes}} &= \sum m_{C_{11}-C_{13} \text{ n-alkanes in the liquid product}} \\
 &= 0.200 + 0.228 + 0.199 \\
 &= 0.627 \text{ g}
 \end{aligned}$$

$$\begin{aligned}
 m_{\text{diesel range n-alkanes}} &= \sum m_{C_{14}-C_{18} \text{ n-alkanes in the liquid product}} \\
 &= 0.233 + 0.662 + 0.861 + 1.533 + 0.154 \\
 &= 3.443 \text{ g}
 \end{aligned}$$

$$\begin{aligned}
 \text{Yield}_{\text{liquid n-alkane product}} &= \frac{m_{\text{n-alkanes in liquid product}}}{m_{\text{total liquid oil fed}}} * 100 \\
 &= \frac{4.991}{16.560} * 100 \\
 &= 30.14 \text{ wt. \%}
 \end{aligned}$$

$$\begin{aligned}
 Yield_{solid\ product} &= \frac{m_{solid\ product}}{m_{total\ liquid\ oil\ fed}} * 100 \\
 &= \frac{0.000}{16.560} * 100 \\
 &= 0.00\ wt.\ \%
 \end{aligned}$$

$$\begin{aligned}
 Yield_{gas\ product} &= \frac{m_{gas\ product}}{m_{total\ liquid\ oil\ fed}} * 100 \\
 &= \frac{7.140}{16.560} * 100 \\
 &= 43.12\ wt.\ \%
 \end{aligned}$$

$$\begin{aligned}
 Yield_{gasoline\ product} &= \frac{m_{gasoline\ range\ n-alkanes}}{m_{total\ liquid\ oil\ fed}} * 100 \\
 &= \frac{0.921}{16.560} * 100 \\
 &= 5.56\ wt.\ \%
 \end{aligned}$$

$$\begin{aligned}
 Yield_{kerosene\ product} &= \frac{m_{kerosene\ range\ n-alkanes}}{m_{total\ liquid\ oil\ fed}} * 100 \\
 &= \frac{0.627}{16.560} * 100 \\
 &= 3.79\ wt.\ \%
 \end{aligned}$$

$$\begin{aligned}
 Yield_{diesel\ product} &= \frac{m_{diesel\ range\ n-alkanes}}{m_{total\ liquid\ oil\ fed}} * 100 \\
 &= \frac{3.443}{16.560} * 100 \\
 &= 20.79\ wt.\ \%
 \end{aligned}$$

$$\begin{aligned}
 Composition_{n-alkanes\ in\ liquid\ product} &= \frac{m_{n-alkanes\ in\ liquid\ product}}{m_{liquid\ product}} * 100 \\
 &= \frac{4.991}{9.420} * 100 \\
 &= 52.98\ wt.\ \%
 \end{aligned}$$

$$\begin{aligned}
 Composition_{unreacted\ oil\ in\ liquid\ product} &= \frac{m_{unreacted\ oil}}{m_{liquid\ product}} * 100 \\
 &= \frac{4.429}{9.420} * 100 \\
 &= 47.02\ wt.\ \%
 \end{aligned}$$

$$\begin{aligned}
 \text{Composition}_{\text{gasoline } n\text{-alkanes in liquid } n\text{-alkanes}} &= \frac{m_{\text{gasoline range } n\text{-alkanes}}}{m_{n\text{-alkanes in liquid product}}} * 100 \\
 &= \frac{0.921}{4.991} * 100 \\
 &= 18.46 \text{ wt. \%}
 \end{aligned}$$

$$\begin{aligned}
 \text{Composition}_{\text{kerosene } n\text{-alkanes in liquid } n\text{-alkanes}} &= \frac{m_{\text{kerosene range } n\text{-alkanes}}}{m_{n\text{-alkanes in liquid product}}} * 100 \\
 &= \frac{0.627}{4.991} * 100 \\
 &= 12.57 \text{ wt. \%}
 \end{aligned}$$

$$\begin{aligned}
 \text{Composition}_{\text{diesel } n\text{-alkanes in liquid } n\text{-alkanes}} &= \frac{m_{\text{diesel range } n\text{-alkanes}}}{m_{n\text{-alkanes in liquid product}}} * 100 \\
 &= \frac{3.443}{4.991} * 100 \\
 &= 68.98 \text{ wt. \%}
 \end{aligned}$$

$$\begin{aligned}
 X_{oil} &= \frac{m_{\text{total liquid oil fed}} - m_{\text{unreacted oil}}}{m_{\text{total liquid oil fed}}} * 100 \\
 &= \frac{16.560 - 4.429}{16.560} * 100 \\
 &= 73.25 \text{ wt. \%}
 \end{aligned}$$

D.3 Reaction kinetic calculations

The reaction kinetic calculations for the experiment at 450 °C using Co-Mo/SiO₂ catalyst is shown. The same calculations were carried out for all other experiments.

$$\begin{aligned}
 \dot{m}_{oil} &= \dot{V}_{oil} * \rho_{oil} \\
 &= 0.1 * 0.92 \\
 &= 0.092 \text{ g/min}
 \end{aligned}$$

The waste cooking oil was made up of different weight fractions of fatty acids (measured via SEM). The calculation for palmitic acid is shown while the balance of the data is shown in Table D-1.

$$\begin{aligned}
 \dot{m}_{\text{palmitic acid}} &= \dot{m}_{oil} * x_{\text{palmitic acid}} \\
 &= 0.092 * 0.0641
 \end{aligned}$$

$$= 5.897 \times 10^{-3} \text{ g/min}$$

$$\begin{aligned} \dot{n}_{\text{palmitic acid}} &= \frac{\dot{m}_{\text{palmitic acid}}}{MM_{\text{palmitic acid}}} \\ &= \frac{5.897 \times 10^{-3}}{256.43} \\ &= 2.300 \times 10^{-5} \text{ moles/min} \end{aligned}$$

Table D-1 Molar flow rate of feed oil constituents

Compound	Wt. fraction (x)	Mass flow rate (g/min)	Molar mass (g/mol)	Molar flow rate (mol/min)
Palmitic acid	0.0641	5.897E-03	256.43	2.300E-05
Palmitoleic acid	0.0001	9.200E-06	254.41	3.616E-08
Stearic acid	0.0435	4.002E-03	284.48	1.407E-05
Oleic acid	0.2102	1.934E-02	282.47	6.846E-05
Linoleic acid	0.6814	6.269E-02	280.45	2.235E-04
Arachidic acid	0.0007	6.440E-05	312.53	2.061E-07
Total	1	0.092		3.290E-04

$$\begin{aligned} \dot{n}_{\text{oil}} &= \sum \dot{n}_{\text{each constituent}} \\ &= 3.290 \times 10^{-4} \text{ moles/min} \end{aligned}$$

$$P = 120 \times 10^5 \text{ Pa}$$

$$T = 450 + 273.15$$

$$= 723.15 \text{ K}$$

$$R = 8.314 \text{ J/K/mol}$$

$$\begin{aligned} \dot{V}_{\text{gas oil}} &= \frac{\dot{n}_{\text{oil}} * R * T}{P} \\ &= \frac{3.290 \times 10^{-4} * 8.314 * 723.15}{120 \times 10^5} \\ &= 1.65 \times 10^{-7} \text{ m}^3/\text{min} \end{aligned}$$

$$\dot{V}_{\text{hydrogen gas}} (@ STP) = 0.0005 \text{ m}^3/\text{min}$$

$$\dot{V}_{\text{hydrogen gas}} = \frac{P_{STP} * \dot{V}_{STP}}{T_{STP}} * \frac{T}{P}$$

$$= \frac{1 \times 10^5 * 0.0005 * 723.15}{298.15 * 120 \times 10^5}$$

$$= 1.01 \times 10^{-5} \text{ m}^3/\text{min}$$

$$\dot{q} = \dot{V}_{gas \text{ oil}} + \dot{V}_{hydrogen \text{ gas}}$$

$$= 1.65 \times 10^{-7} + 1.01 \times 10^{-5}$$

$$= 1.03 \times 10^{-5} \text{ m}^3/\text{min}$$

$$\dot{n}_{hydrogen \text{ gas}} = \frac{P * \dot{V}_{hydrogen \text{ gas}}}{R * T}$$

$$= \frac{120 \times 10^5 * 1.01 \times 10^{-5}}{8.314 * 723.15}$$

$$= 2.017 \times 10^{-2} \text{ moles}/\text{min}$$

$$C_{hydrogen \text{ gas}} = \frac{\dot{n}_{hydrogen \text{ gas}}}{\dot{V}_{hydrogen \text{ gas}}}$$

$$= \frac{2.017 \times 10^{-2}}{1.01 \times 10^{-5}}$$

$$= 1.964 \times 10^3 \text{ moles}/\text{m}^3$$

$$W = m_{catalyst} = 40.000 \text{ g}$$

$$k'' = \frac{-\ln(1-X_{oil})}{W}$$

$$= \frac{-\ln(1-0.7325)}{40.000}$$

$$= 7.711 \times 10^{-2}$$

$$k' = k'' * \dot{q}$$

$$= 7.711 \times 10^{-2} \times 1.03 \times 10^{-5}$$

$$= 7.920 \times 10^{-7}$$

$$k = \frac{k'}{C_{hydrogen \text{ gas}}}$$

$$= \frac{7.920 \times 10^{-7}}{1.964 \times 10^3}$$

$$= 4.033 \times 10^{-10} \text{ m}^6/\text{mol}/\text{g}/\text{s}$$

$$\ln(k) = \ln(4.033 \times 10^{-10})$$

$$= 21.63$$

$$\frac{1}{T} = \frac{1}{723.15}$$

$$= 0.001383$$

Appendix

E

Experimental data

The tables contain the measured experimental data used for all calculations. For layout purposes the tables start on the next page.

Table E-1 Experimental data for fresh Ru/Al₂O₃ catalyst

Variable	Unit	Temperature [°C]		
		400	425	450
Mass of catalyst	[g]	38.905	38.905	38.905
Mass of liquid product	[g]	2.717	7.982	8.386
Mass of solid product	[g]	8.063	2.310	1.693
Mass of gas product	[g]	0.260	0.748	0.962
Mass of liquid product sample	[g]	0.080	0.067	0.100
Mass of xylene	[g]	0.301	0.304	0.251
Compound		Area (from total ion chromatogram)		
Pentane	C ₅	0.00E+00	0.00E+00	0.00E+00
Hexane	C ₆	0.00E+00	2.20E+05	2.33E+05
Heptane	C ₇	1.81E+05	9.48E+05	1.13E+06
Octane	C ₈	6.30E+05	2.34E+06	3.30E+06
Nonane	C ₉	1.15E+06	2.77E+06	6.08E+06
Decane	C ₁₀	1.83E+06	3.88E+06	8.79E+06
Undecane	C ₁₁	2.36E+06	4.61E+06	1.12E+07
Dodecane	C ₁₂	2.03E+06	4.10E+06	9.59E+06
Tridecane	C ₁₃	3.26E+06	5.48E+06	1.22E+07
Tetradecane	C ₁₄	1.02E+07	1.43E+07	1.41E+07
Pentadecane	C ₁₅	6.33E+07	6.37E+07	1.04E+08
Hexadecane	C ₁₆	3.94E+07	3.53E+07	6.36E+07
Heptadecane	C ₁₇	1.72E+08	1.55E+08	2.39E+08
Octadecane	C ₁₈	9.11E+07	6.22E+07	1.16E+08
Xylene		3.83E+08	3.93E+08	3.63E+08

Table E-2 Experimental data for fresh Ni/Al₂O₃ catalyst

Variable	Unit	Temperature [°C]		
		400	425	450
Mass of catalyst	[g]	38.221	38.221	38.221
Mass of liquid product	[g]	6.956	6.620	8.229
Mass of solid product	[g]	2.954	2.468	0.867
Mass of gas product	[g]	1.130	1.952	1.944
Mass of liquid product sample	[g]	0.160	0.159	0.166
Mass of xylene	[g]	0.300	0.290	0.366
Compound		Area (from total ion chromatogram)		
Pentane	C ₅	0.00E+00	0.00E+00	0.00E+00
Hexane	C ₆	3.35E+05	3.60E+05	3.50E+05
Heptane	C ₇	1.65E+06	1.96E+06	1.79E+06
Octane	C ₈	5.59E+06	4.71E+06	5.26E+06
Nonane	C ₉	4.19E+06	5.86E+06	7.75E+06
Decane	C ₁₀	5.29E+06	7.24E+06	1.08E+07
Undecane	C ₁₁	7.45E+06	8.06E+06	1.23E+07
Dodecane	C ₁₂	7.66E+06	6.79E+06	1.09E+07
Tridecane	C ₁₃	1.05E+07	8.67E+06	1.20E+07
Tetradecane	C ₁₄	1.12E+07	8.59E+06	1.29E+07
Pentadecane	C ₁₅	8.28E+07	7.06E+07	6.27E+07
Hexadecane	C ₁₆	4.16E+07	3.71E+07	4.58E+07
Heptadecane	C ₁₇	1.89E+08	1.47E+08	1.20E+08
Octadecane	C ₁₈	8.04E+07	7.18E+07	7.78E+07
Xylene		2.76E+08	2.62E+08	2.89E+08

Table E-3 Experimental data for fresh Ni-Mo/SiO₂ catalyst

Variable	Unit	Temperature [°C]		
		400	425	450
Mass of catalyst	[g]	30.280	30.280	30.280
Mass of liquid product	[g]	11.300	9.800	8.520
Mass of solid product	[g]	0.000	0.000	0.000
Mass of gas product	[g]	5.260	6.760	8.040
Mass of liquid product sample	[g]	0.132	0.137	0.146
Mass of xylene	[g]	0.121	0.125	0.130
Compound		Area (from total ion chromatogram)		
Pentane	C ₅	5.99E+04	1.10E+05	1.31E+05
Hexane	C ₆	1.25E+05	1.65E+05	2.21E+05
Heptane	C ₇	1.43E+05	1.92E+05	2.24E+05
Octane	C ₈	1.69E+05	2.01E+05	2.69E+05
Nonane	C ₉	2.06E+05	3.03E+05	3.81E+05
Decane	C ₁₀	2.22E+05	3.60E+05	4.35E+05
Undecane	C ₁₁	2.69E+05	3.54E+05	4.63E+05
Dodecane	C ₁₂	3.15E+05	4.34E+05	5.06E+05
Tridecane	C ₁₃	2.35E+05	4.41E+05	5.18E+05
Tetradecane	C ₁₄	2.56E+05	5.68E+05	6.83E+05
Pentadecane	C ₁₅	1.15E+06	1.31E+06	1.44E+06
Hexadecane	C ₁₆	1.80E+06	1.88E+06	1.87E+06
Heptadecane	C ₁₇	1.38E+06	2.18E+06	3.10E+06
Octadecane	C ₁₈	2.11E+06	9.29E+05	6.27E+05
Xylene		2.97E+06	3.01E+06	3.00E+06

Table E-4 Experimental data for fresh Co-Mo/SiO₂ catalyst

Variable	Unit	Temperature [°C]		
		400	425	450
Mass of catalyst	[g]	40.000	40.000	40.000
Mass of liquid product	[g]	11.340	10.250	9.420
Mass of solid product	[g]	0.000	0.000	0.000
Mass of gas product	[g]	5.220	6.310	7.140
Mass of liquid product sample	[g]	0.192	0.189	0.166
Mass of xylene	[g]	0.157	0.153	0.136
Compound		Area (from total ion chromatogram)		
Pentane	C ₅	8.86E+03	7.92E+03	1.27E+04
Hexane	C ₆	1.59E+04	1.43E+04	1.94E+04
Heptane	C ₇	2.52E+04	1.70E+04	1.94E+05
Octane	C ₈	2.19E+05	2.99E+05	2.46E+05
Nonane	C ₉	2.53E+05	2.73E+05	2.95E+05
Decane	C ₁₀	2.59E+05	2.63E+05	3.93E+05
Undecane	C ₁₁	2.79E+05	2.84E+05	2.76E+05
Dodecane	C ₁₂	3.35E+05	2.97E+05	3.22E+05
Tridecane	C ₁₃	3.01E+05	3.64E+05	2.84E+05
Tetradecane	C ₁₄	3.34E+05	3.46E+05	3.41E+05
Pentadecane	C ₁₅	1.21E+06	1.03E+06	9.84E+05
Hexadecane	C ₁₆	2.04E+06	1.96E+06	1.30E+06
Heptadecane	C ₁₇	1.58E+06	2.03E+06	2.33E+06
Octadecane	C ₁₈	7.25E+05	6.02E+05	2.36E+05
Xylene		2.93E+06	2.79E+06	2.79E+06

Table E-5 Experimental data for regenerated Ru/Al₂O₃ catalyst

Variable	Unit	Temperature [°C]		
		400	425	450
Mass of catalyst	[g]	38.905	38.905	38.905
Mass of liquid product	[g]	5.635	6.285	6.987
Mass of solid product	[g]	4.213	3.216	2.165
Mass of gas product	[g]	1.192	1.539	1.888
Mass of liquid product sample	[g]	0.067	0.065	0.072
Mass of xylene	[g]	0.328	0.327	0.331
Compound		Area (from total ion chromatogram)		
Pentane	C ₅	0.00E+00	0.00E+00	9.08E+05
Hexane	C ₆	0.00E+00	2.61E+05	1.83E+06
Heptane	C ₇	1.42E+05	1.03E+06	4.13E+06
Octane	C ₈	9.08E+05	2.33E+06	6.38E+06
Nonane	C ₉	1.05E+06	1.63E+06	4.33E+06
Decane	C ₁₀	2.19E+06	2.25E+06	4.91E+06
Undecane	C ₁₁	2.72E+06	2.85E+06	5.71E+06
Dodecane	C ₁₂	2.61E+06	2.72E+06	5.40E+06
Tridecane	C ₁₃	3.70E+06	3.63E+06	6.52E+06
Tetradecane	C ₁₄	1.68E+07	6.35E+06	9.00E+06
Pentadecane	C ₁₅	3.92E+07	3.02E+07	2.64E+07
Hexadecane	C ₁₆	2.33E+07	2.32E+07	3.87E+07
Heptadecane	C ₁₇	7.50E+07	5.80E+07	4.11E+07
Octadecane	C ₁₈	3.02E+07	3.03E+07	3.08E+07
Xylene		4.17E+08	3.90E+08	3.86E+08

Table E-6 Experimental data for regenerated Ni/Al₂O₃ catalyst

Variable	Unit	Temperature [°C]		
		400	425	450
Mass of catalyst	[g]	38.221	38.221	38.221
Mass of liquid product	[g]	6.368	5.824	7.018
Mass of solid product	[g]	3.249	2.597	1.342
Mass of gas product	[g]	1.423	2.619	2.680
Mass of liquid product sample	[g]	0.158	0.161	0.159
Mass of xylene	[g]	0.337	0.330	0.356
Compound		Area (from total ion chromatogram)		
Pentane	C ₅	0.00E+00	0.00E+00	0.00E+00
Hexane	C ₆	2.69E+05	1.53E+06	1.06E+06
Heptane	C ₇	1.57E+06	4.59E+06	4.17E+06
Octane	C ₈	3.43E+06	7.97E+06	8.92E+06
Nonane	C ₉	3.41E+06	6.45E+06	9.12E+06
Decane	C ₁₀	4.45E+06	7.18E+06	1.14E+07
Undecane	C ₁₁	5.22E+06	7.95E+06	1.25E+07
Dodecane	C ₁₂	3.87E+06	6.34E+06	1.08E+07
Tridecane	C ₁₃	6.88E+06	8.41E+06	1.22E+07
Tetradecane	C ₁₄	5.05E+06	7.39E+06	1.23E+07
Pentadecane	C ₁₅	7.98E+07	7.51E+07	7.34E+07
Hexadecane	C ₁₆	2.16E+07	2.56E+07	3.58E+07
Heptadecane	C ₁₇	1.76E+08	1.51E+08	1.45E+08
Octadecane	C ₁₈	4.28E+07	4.32E+07	5.34E+07
Xylene		2.82E+08	2.92E+08	3.07E+08

Appendix

F

Calculated data

This appendix contains data calculated from the experimental data seen in Appendix E. The data herein were calculated following the method outlined in the sample calculations in Appendix D.

Table F-1 Calculated data at three reaction temperatures independent of catalysts

Variable	Unit	Temperature [°C]		
		400	425	450
Liquid oil mass flow rate	[g/min]	0.092	0.092	0.092
Liquid oil molar flow rate	[mol/min]	3.29E-04	3.29E-04	3.29E-04
Gas oil volumetric flow rate	[l/min]	1.54E-04	1.59E-04	1.65E-08
Hydrogen gas volumetric flow rate	[l/min]	9.41E-03	9.76E-03	1.01E-02
Hydrogen gas molar flow rate	[mol/min]	2.02E-02	2.02E-02	2.02E-02
Total gas volumetric flow rate	[l/min]	9.56E-03	9.92E-03	1.03E-02
Hydrogen gas concentration	[mol/m ³]	2.11E+03	2.03E+03	1.96E+03

Table F-2 Calculated data for fresh Ru/Al₂O₃ at 400 °C

Variable	Unit	Value		Unit	Value		Unit	Value
n-Alkanes in product	[g]	2.476	Diesel range product	[g]	2.396	Diesel range yield	[%]	21.70
Unreacted oil	[g]	0.241	n-Alkane product yield	[%]	22.43	Solid product yield	[%]	73.03
Gasoline range product	[g]	0.028	Gasoline range yield	[%]	0.26	Gas product yield	[%]	2.36
Kerosene range product	[g]	0.052	Kerosene range yield	[%]	0.48	Oil conversion	[%]	97.82

Compound	Ratio _{Area}	Moles _{sample}	Mass _{sample}	Mass Fraction _{sample}	Mass _{liquid product}
Pentane	0.000	0.00E+00	0.00E+00	0.0000	0.000
Hexane	0.000	0.00E+00	0.00E+00	0.0000	0.000
Heptane	0.000	4.44E-07	4.45E-05	0.0006	0.002
Octane	0.002	1.27E-06	1.45E-04	0.0018	0.005
Nonane	0.003	1.97E-06	2.52E-04	0.0032	0.009
Decane	0.005	2.73E-06	3.89E-04	0.0049	0.013
Undecane	0.006	3.11E-06	4.87E-04	0.0061	0.017
Dodecane	0.005	2.40E-06	4.09E-04	0.0051	0.014
Tridecane	0.008	3.49E-06	6.50E-04	0.0081	0.022
Tetradecane	0.027	9.99E-06	1.98E-03	0.0248	0.067
Pentadecane	0.165	5.70E-05	1.21E-02	0.1515	0.412
Hexadecane	0.103	3.29E-05	7.45E-03	0.0932	0.253
Heptadecane	0.448	1.34E-04	3.21E-02	0.4014	1.091
Octadecane	0.238	6.63E-05	1.69E-02	0.2109	0.573

Table F-3 Calculated data for fresh Ru/Al₂O₃ at 425 °C

Variable	Unit	Value		Unit	Value		Unit	Value
n-Alkanes in product	[g]	7.889	Diesel range product	[g]	7.286	Diesel range yield	[%]	66.00
Unreacted oil	[g]	0.093	n-Alkane product yield	[%]	71.46	Solid product yield	[%]	20.92
Gasoline range product	[g]	0.266	Gasoline range yield	[%]	2.41	Gas product yield	[%]	6.78
Kerosene range product	[g]	0.337	Kerosene range yield	[%]	3.05	Oil conversion	[%]	99.16
Compound		Ratio _{Area}	Moles _{sample}		Mass _{sample}	Mass Fraction _{sample}		Mass _{liquid product}
Pentane		0.000	0.00E+00		0.00E+00	0.0000		0.000
Hexane		0.001	6.79E-07		5.85E-05	0.0009		0.007
Heptane		0.002	2.30E-06		2.30E-04	0.0034		0.027
Octane		0.006	4.66E-06		5.32E-04	0.0079		0.063
Nonane		0.007	4.68E-06		6.00E-04	0.0090		0.072
Decane		0.010	5.70E-06		8.11E-04	0.0121		0.097
Undecane		0.012	5.99E-06		9.36E-04	0.0140		0.112
Dodecane		0.010	4.78E-06		8.13E-04	0.0121		0.097
Tridecane		0.014	5.78E-06		1.08E-03	0.0161		0.128
Tetradecane		0.036	1.38E-05		2.73E-03	0.0407		0.325
Pentadecane		0.162	5.65E-05		1.20E-02	0.1792		1.430
Hexadecane		0.090	2.90E-05		6.57E-03	0.0981		0.783
Heptadecane		0.394	1.19E-04		2.85E-02	0.4254		3.396
Octadecane		0.158	4.46E-05		1.14E-02	0.1695		1.353

Table F-4 Calculated data for fresh Ru/Al₂O₃ at 450 °C

Variable	Unit	Value		Unit	Value		Unit	Value
n-Alkanes in product	[g]	8.252	Diesel range product	[g]	7.442	Diesel range yield	[%]	67.41
Unreacted oil	[g]	0.133	n-Alkane product yield	[%]	74.75	Solid product yield	[%]	15.34
Gasoline range product	[g]	0.317	Gasoline range yield	[%]	2.88	Gas product yield	[%]	8.71
Kerosene range product	[g]	0.493	Kerosene range yield	[%]	4.46	Oil conversion	[%]	98.79
Compound	Ratio _{Area (Xylene)}		Moles _{sample}		Mass _{sample}	Mass Fraction _{sample}		Mass _{liquid product}
Pentane	0.000		0.00E+00		0.00E+00	0.0000		0.000
Hexane	0.001		6.43E-07		5.54E-05	0.0006		0.005
Heptane	0.003		2.44E-06		2.45E-04	0.0024		0.021
Octane	0.009		5.86E-06		6.70E-04	0.0067		0.056
Nonane	0.017		9.17E-06		1.18E-03	0.0118		0.099
Decane	0.024		1.15E-05		1.64E-03	0.0164		0.138
Undecane	0.031		1.30E-05		2.04E-03	0.0204		0.171
Dodecane	0.026		9.96E-06		1.70E-03	0.0170		0.142
Tridecane	0.034		1.15E-05		2.14E-03	0.0214		0.179
Tetradecane	0.039		1.22E-05		2.41E-03	0.0241		0.202
Pentadecane	0.287		8.26E-05		1.75E-02	0.1754		1.471
Hexadecane	0.175		4.67E-05		1.06E-02	0.1057		0.886
Heptadecane	0.657		1.63E-04		3.93E-02	0.3929		3.295
Octadecane	0.320		7.44E-05		1.89E-02	0.1893		1.588

Table F-5 Calculated data for fresh Ni/Al₂O₃ at 400 °C

Variable	Unit	Value		Unit	Value		Unit	Value	
n-Alkanes in product	[g]	3.951	Diesel range product	[g]	3.533	Diesel range yield	[%]	32.00	
Unreacted oil	[g]	3.005	n-Alkane product yield	[%]	35.79	Solid product yield	[%]	26.76	
Gasoline range product	[g]	0.178	Gasoline range yield	[%]	1.61	Gas product yield	[%]	10.24	
Kerosene range product	[g]	0.240	Kerosene range yield	[%]	2.18	Oil conversion	[%]	72.78	
Compound		Ratio _{Area}			Moles _{sample}		Mass _{sample}	Mass Fraction _{sample}	Mass _{liquid product}
Pentane		0.000			0.00E+00		0.00E+00	0.0000	0.000
Hexane		0.001			1.45E-06		1.25E-04	0.0008	0.004
Heptane		0.006			5.62E-06		5.63E-04	0.0035	0.019
Octane		0.020			1.56E-05		1.79E-03	0.0112	0.060
Nonane		0.015			9.94E-06		1.27E-03	0.0080	0.043
Decane		0.019			1.09E-05		1.55E-03	0.0097	0.052
Undecane		0.027			1.36E-05		2.12E-03	0.0133	0.071
Dodecane		0.028			1.25E-05		2.13E-03	0.0133	0.071
Tridecane		0.038			1.56E-05		2.91E-03	0.0182	0.098
Tetradecane		0.040			1.51E-05		3.00E-03	0.0188	0.101
Pentadecane		0.300			1.03E-04		2.19E-02	0.1372	0.735
Hexadecane		0.151			4.80E-05		1.09E-02	0.0681	0.365
Heptadecane		0.686			2.04E-04		4.90E-02	0.3066	1.642
Octadecane		0.291			8.09E-05		2.06E-02	0.1289	0.690

Table F-6 Calculated data for fresh Ni/Al₂O₃ at 425 °C

Variable	Unit	Value		Unit	Value		Unit	Value
n-Alkanes in product	[g]	4.233	Diesel range product	[g]	3.692	Diesel range yield	[%]	33.44
Unreacted oil	[g]	2.387	n-Alkane product yield	[%]	38.35	Solid product yield	[%]	22.36
Gasoline range product	[g]	0.263	Gasoline range yield	[%]	2.38	Gas product yield	[%]	17.68
Kerosene range product	[g]	0.279	Kerosene range yield	[%]	2.52	Oil conversion	[%]	78.38

Compound	Ratio _{Area}	Moles _{sample}	Mass _{sample}	Mass Fraction _{sample}	Mass _{liquid product}
Pentane	0.000	0.00E+00	0.00E+00	0.0000	0.000
Hexane	0.001	1.59E-06	1.37E-04	0.0009	0.006
Heptane	0.007	6.78E-06	6.80E-04	0.0043	0.028
Octane	0.018	1.34E-05	1.53E-03	0.0096	0.064
Nonane	0.022	1.42E-05	1.82E-03	0.0114	0.075
Decane	0.028	1.52E-05	2.16E-03	0.0136	0.090
Undecane	0.031	1.50E-05	2.34E-03	0.0147	0.097
Dodecane	0.026	1.13E-05	1.92E-03	0.0121	0.080
Tridecane	0.033	1.31E-05	2.44E-03	0.0153	0.101
Tetradecane	0.033	1.18E-05	2.35E-03	0.0147	0.098
Pentadecane	0.269	8.96E-05	1.90E-02	0.1195	0.791
Hexadecane	0.141	4.36E-05	9.88E-03	0.0621	0.411
Heptadecane	0.561	1.61E-04	3.88E-02	0.2436	1.613
Octadecane	0.274	7.36E-05	1.87E-02	0.1177	0.779

Table F-7 Calculated data for fresh Ni/Al₂O₃ at 450 °C

Variable	Unit	Value		Unit	Value		Unit	Value
n-Alkanes in product	[g]	5.843	Diesel range product	[g]	4.810	Diesel range yield	[%]	43.57
Unreacted oil	[g]	2.386	n-Alkane product yield	[%]	52.92	Solid product yield	[%]	7.85
Gasoline range product	[g]	0.461	Gasoline range yield	[%]	4.17	Gas product yield	[%]	17.61
Kerosene range product	[g]	0.572	Kerosene range yield	[%]	5.18	Oil conversion	[%]	78.38

Compound	Ratio _{Area}	Moles _{sample}	Mass _{sample}	Mass Fraction _{sample}	Mass _{liquid product}
Pentane	0.000	0.00E+00	0.00E+00	0.0000	0.000
Hexane	0.001	1.77E-06	1.53E-04	0.0009	0.008
Heptane	0.006	7.09E-06	7.10E-04	0.0043	0.035
Octane	0.018	1.71E-05	1.96E-03	0.0118	0.097
Nonane	0.027	2.15E-05	2.75E-03	0.0166	0.137
Decane	0.037	2.60E-05	3.70E-03	0.0223	0.184
Undecane	0.043	2.62E-05	4.09E-03	0.0247	0.204
Dodecane	0.038	2.08E-05	3.54E-03	0.0214	0.176
Tridecane	0.042	2.07E-05	3.87E-03	0.0234	0.192
Tetradecane	0.045	2.03E-05	4.03E-03	0.0244	0.200
Pentadecane	0.217	9.11E-05	1.93E-02	0.1169	0.962
Hexadecane	0.158	6.16E-05	1.40E-02	0.0843	0.694
Heptadecane	0.415	1.50E-04	3.62E-02	0.2185	1.798
Octadecane	0.269	9.13E-05	2.32E-02	0.1405	1.156

Table F-8 Calculated data for fresh NiMo/SiO₂ at 400 °C

Variable	Unit	Value		Unit	Value		Unit	Value
n-Alkanes in product	[g]	7.301	Diesel range product	[g]	5.593	Diesel range yield	[%]	33.77
Unreacted oil	[g]	3.999	n-Alkane product yield	[%]	44.09	Solid product yield	[%]	0.00
Gasoline range product	[g]	0.972	Gasoline range yield	[%]	5.87	Gas product yield	[%]	31.76
Kerosene range product	[g]	0.736	Kerosene range yield	[%]	4.44	Oil conversion	[%]	75.85
Compound	Ratio _{Area}		Moles _{sample}		Mass _{sample}	Mass Fraction _{sample}		Mass _{liquid product}
Pentane	0.020		1.34E-05		9.69E-04	0.0073		0.083
Hexane	0.042		2.02E-05		1.74E-03	0.0132		0.149
Heptane	0.048		1.83E-05		1.83E-03	0.0139		0.157
Octane	0.057		1.77E-05		2.02E-03	0.0153		0.173
Nonane	0.069		1.83E-05		2.35E-03	0.0178		0.201
Decane	0.075		1.72E-05		2.44E-03	0.0185		0.209
Undecane	0.091		1.84E-05		2.88E-03	0.0218		0.246
Dodecane	0.106		1.93E-05		3.29E-03	0.0249		0.282
Tridecane	0.079		1.30E-05		2.43E-03	0.0184		0.208
Tetradecane	0.086		1.30E-05		2.58E-03	0.0196		0.221
Pentadecane	0.387		5.37E-05		1.14E-02	0.0864		0.976
Hexadecane	0.606		7.79E-05		1.76E-02	0.1336		1.510
Heptadecane	0.466		5.59E-05		1.34E-02	0.1018		1.150
Octadecane	0.710		7.97E-05		2.03E-02	0.1536		1.736

Table F-9 Calculated data for fresh NiMo/SiO₂ at 425 °C

Variable	Unit	Value		Unit	Value		Unit	Value			
n-Alkanes in product	[g]	7.039	Diesel range product	[g]	4.904	Diesel range yield	[%]	29.62			
Unreacted oil	[g]	2.761	n-Alkane product yield	[%]	42.51	Solid product yield	[%]	0.00			
Gasoline range product	[g]	1.195	Gasoline range yield	[%]	7.22	Gas product yield	[%]	40.82			
Kerosene range product	[g]	0.940	Kerosene range yield	[%]	5.67	Oil conversion	[%]	83.33			
Compound		Ratio _{Area}			Moles _{sample}		Mass _{sample}		Mass Fraction _{sample}		Mass _{liquid product}
Pentane		0.037			2.51E-05		1.81E-03		0.0132		0.130
Hexane		0.055			2.74E-05		2.36E-03		0.0172		0.169
Heptane		0.064			2.50E-05		2.51E-03		0.0183		0.179
Octane		0.067			2.15E-05		2.45E-03		0.0179		0.175
Nonane		0.101			2.75E-05		3.53E-03		0.0258		0.252
Decane		0.120			2.84E-05		4.04E-03		0.0295		0.289
Undecane		0.118			2.47E-05		3.86E-03		0.0282		0.276
Dodecane		0.144			2.71E-05		4.62E-03		0.0337		0.331
Tridecane		0.147			2.50E-05		4.65E-03		0.0340		0.333
Tetradecane		0.189			2.94E-05		5.83E-03		0.0426		0.417
Pentadecane		0.435			6.24E-05		1.33E-02		0.0967		0.948
Hexadecane		0.626			8.32E-05		1.88E-02		0.1375		1.348
Heptadecane		0.723			8.95E-05		2.15E-02		0.1572		1.540
Octadecane		0.309			3.58E-05		9.11E-03		0.0665		0.652

Table F-10 Calculated data for fresh NiMo/SiO₂ at 450 °C

Variable	Unit	Value		Unit	Value		Unit	Value
n-Alkanes in product	[g]	6.917	Diesel range product	[g]	4.682	Diesel range yield	[%]	28.27
Unreacted oil	[g]	1.603	n-Alkane product yield	[%]	41.77	Solid product yield	[%]	0.00
Gasoline range product	[g]	1.268	Gasoline range yield	[%]	7.65	Gas product yield	[%]	48.55
Kerosene range product	[g]	0.967	Kerosene range yield	[%]	5.84	Oil conversion	[%]	90.32
Compound	Ratio _{Area}		Moles _{sample}		Mass _{sample}	Mass Fraction _{sample}		Mass _{liquid product}
Pentane	0.044		3.13E-05		2.26E-03	0.0155		0.132
Hexane	0.074		3.82E-05		3.29E-03	0.0225		0.192
Heptane	0.075		3.03E-05		3.04E-03	0.0208		0.177
Octane	0.090		2.99E-05		3.42E-03	0.0234		0.200
Nonane	0.127		3.60E-05		4.62E-03	0.0316		0.270
Decane	0.145		3.58E-05		5.09E-03	0.0349		0.297
Undecane	0.154		3.37E-05		5.26E-03	0.0360		0.307
Dodecane	0.169		3.30E-05		5.62E-03	0.0385		0.328
Tridecane	0.173		3.06E-05		5.70E-03	0.0390		0.332
Tetradecane	0.227		3.68E-05		7.31E-03	0.0500		0.426
Pentadecane	0.478		7.13E-05		1.52E-02	0.1038		0.884
Hexadecane	0.621		8.58E-05		1.94E-02	0.1331		1.134
Heptadecane	1.032		1.33E-04		3.19E-02	0.2187		1.864
Octadecane	0.209		2.51E-05		6.40E-03	0.0438		0.373

Table F-11 Calculated data for fresh CoMo/SiO₂ at 400 °C

Variable	Unit	Value		Unit	Value		Unit	Value		
n-Alkanes in product	[g]	5.935	Diesel range product	[g]	4.486	Diesel range yield	[%]	27.09		
Unreacted oil	[g]	5.405	n-Alkane product yield	[%]	35.84	Solid product yield	[%]	0.00		
Gasoline range product	[g]	0.703	Gasoline range yield	[%]	4.25	Gas product yield	[%]	31.52		
Kerosene range product	[g]	0.745	Kerosene range yield	[%]	4.50	Oil conversion	[%]	67.36		
Compound		Ratio _{Area}			Moles _{sample}		Mass _{sample}	Mass Fraction _{sample}		Mass _{liquid product}
Pentane		0.003			2.62E-06		1.89E-04	0.0010		0.011
Hexane		0.005			3.40E-06		2.93E-04	0.0015		0.017
Heptane		0.009			4.24E-06		4.25E-04	0.0022		0.025
Octane		0.075			3.02E-05		3.45E-03	0.0180		0.204
Nonane		0.086			2.96E-05		3.80E-03	0.0198		0.224
Decane		0.088			2.64E-05		3.75E-03	0.0195		0.222
Undecane		0.095			2.51E-05		3.92E-03	0.0204		0.232
Dodecane		0.114			2.70E-05		4.60E-03	0.0240		0.272
Tridecane		0.103			2.20E-05		4.10E-03	0.0213		0.242
Tetradecane		0.114			2.23E-05		4.42E-03	0.0230		0.261
Pentadecane		0.413			7.44E-05		1.58E-02	0.0823		0.934
Hexadecane		0.699			1.17E-04		2.64E-02	0.1375		1.559
Heptadecane		0.539			8.38E-05		2.02E-02	0.1049		1.190
Octadecane		0.248			3.60E-05		9.17E-03	0.0478		0.542

Table F-12 Calculated data for fresh CoMo/SiO₂ at 425 °C

Variable	Unit	Value		Unit	Value		Unit	Value		
n-Alkanes in product	[g]	5.714	Diesel range product	[g]	4.254	Diesel range yield	[%]	25.69		
Unreacted oil	[g]	4.536	n-Alkane product yield	[%]	34.50	Solid product yield	[%]	0.00		
Gasoline range product	[g]	0.738	Gasoline range yield	[%]	4.46	Gas product yield	[%]	38.10		
Kerosene range product	[g]	0.722	Kerosene range yield	[%]	4.36	Oil conversion	[%]	72.61		
Compound		Ratio _{Area}			Moles _{sample}		Mass _{sample}	Mass Fraction _{sample}		Mass _{liquid product}
Pentane		0.003			2.39E-06		1.72E-04	0.0009		0.009
Hexane		0.005			3.11E-06		2.68E-04	0.0014		0.015
Heptane		0.006			2.91E-06		2.92E-04	0.0015		0.016
Octane		0.107			4.22E-05		4.82E-03	0.0255		0.261
Nonane		0.098			3.26E-05		4.18E-03	0.0221		0.227
Decane		0.094			2.73E-05		3.89E-03	0.0206		0.211
Undecane		0.101			2.61E-05		4.07E-03	0.0215		0.221
Dodecane		0.106			2.45E-05		4.17E-03	0.0221		0.226
Tridecane		0.130			2.72E-05		5.06E-03	0.0268		0.274
Tetradecane		0.124			2.36E-05		4.68E-03	0.0248		0.254
Pentadecane		0.367			6.44E-05		1.37E-02	0.0724		0.742
Hexadecane		0.700			1.14E-04		2.58E-02	0.1364		1.398
Heptadecane		0.727			1.10E-04		2.65E-02	0.1402		1.437
Octadecane		0.215			3.06E-05		7.77E-03	0.0411		0.422

Table F-13 Calculated data for fresh CoMo/SiO₂ at 450 °C

Variable	Unit	Value		Unit	Value		Unit	Value
n-Alkanes in product	[g]	4.991	Diesel range product	[g]	3.443	Diesel range yield	[%]	20.79
Unreacted oil	[g]	4.429	n-Alkane product yield	[%]	30.14	Solid product yield	[%]	0.00
Gasoline range product	[g]	0.921	Gasoline range yield	[%]	5.56	Gas product yield	[%]	43.12
Kerosene range product	[g]	0.627	Kerosene range yield	[%]	3.79	Oil conversion	[%]	73.25
Compound	Ratio _{Area}		Moles _{sample}		Mass _{sample}	Mass Fraction _{sample}		Mass _{liquid product}
Pentane	0.005		3.41E-06		2.46E-04	0.0015		0.014
Hexane	0.007		3.77E-06		3.25E-04	0.0020		0.018
Heptane	0.069		2.95E-05		2.95E-03	0.0178		0.168
Octane	0.088		3.08E-05		3.52E-03	0.0212		0.200
Nonane	0.106		3.14E-05		4.02E-03	0.0242		0.228
Decane	0.141		3.63E-05		5.16E-03	0.0311		0.293
Undecane	0.099		2.25E-05		3.52E-03	0.0212		0.200
Dodecane	0.115		2.36E-05		4.02E-03	0.0242		0.228
Tridecane	0.102		1.89E-05		3.51E-03	0.0212		0.199
Tetradecane	0.122		2.07E-05		4.10E-03	0.0247		0.233
Pentadecane	0.352		5.49E-05		1.17E-02	0.0703		0.662
Hexadecane	0.464		6.70E-05		1.52E-02	0.0914		0.861
Heptadecane	0.834		1.12E-04		2.70E-02	0.1627		1.533
Octadecane	0.084		1.06E-05		2.71E-03	0.0163		0.154

Table F-14 Calculated data for regenerated Ru/Al₂O₃ at 400 °C

Variable	Unit	Value		Unit	Value		Unit	Value		
n-Alkanes in product	[g]	1.482	Diesel range product	[g]	1.373	Diesel range yield	[%]	12.44		
Unreacted oil	[g]	4.153	n-Alkane product yield	[%]	13.43	Solid product yield	[%]	38.16		
Gasoline range product	[g]	0.037	Gasoline range yield	[%]	0.34	Gas product yield	[%]	10.80		
Kerosene range product	[g]	0.072	Kerosene range yield	[%]	0.65	Oil conversion	[%]	62.39		
Compound		Ratio _{Area}			Moles _{sample}		Mass _{sample}	Mass Fraction _{sample}		Mass _{liquid product}
Pentane		0.000			0.00E+00		0.00E+00	0.0000		0.000
Hexane		0.000			0.00E+00		0.00E+00	0.0000		0.000
Heptane		0.000			3.50E-07		3.50E-05	0.0005		0.001
Octane		0.002			1.84E-06		2.10E-04	0.0031		0.008
Nonane		0.003			1.80E-06		2.31E-04	0.0035		0.009
Decane		0.005			3.27E-06		4.65E-04	0.0069		0.018
Undecane		0.007			3.59E-06		5.61E-04	0.0084		0.022
Dodecane		0.006			3.09E-06		5.26E-04	0.0078		0.021
Tridecane		0.009			3.96E-06		7.38E-04	0.0110		0.029
Tetradecane		0.040			1.65E-05		3.27E-03	0.0488		0.129
Pentadecane		0.094			3.53E-05		7.50E-03	0.1119		0.296
Hexadecane		0.056			1.94E-05		4.40E-03	0.0657		0.174
Heptadecane		0.180			5.83E-05		1.40E-02	0.2094		0.554
Octadecane		0.072			2.20E-05		5.59E-03	0.0834		0.221

Table F-15 Calculated data for regenerated Ru/Al₂O₃ at 425 °C

Variable	Unit	Value		Unit	Value		Unit	Value
n-Alkanes in product	[g]	2.383	Diesel range product	[g]	2.113	Diesel range yield	[%]	19.14
Unreacted oil	[g]	3.902	n-Alkane product yield	[%]	21.59	Solid product yield	[%]	29.13
Gasoline range product	[g]	0.129	Gasoline range yield	[%]	1.17	Gas product yield	[%]	13.94
Kerosene range product	[g]	0.141	Kerosene range yield	[%]	1.28	Oil conversion	[%]	64.66
Compound	Ratio _{Area}		Moles _{sample}		Mass _{sample}	Mass Fraction _{sample}		Mass _{liquid product}
Pentane	0.000		0.00E+00		0.00E+00	0.0000		0.000
Hexane	0.001		8.73E-07		7.52E-05	0.0012		0.005
Heptane	0.003		2.70E-06		2.71E-04	0.0042		0.019
Octane	0.006		5.02E-06		5.73E-04	0.0088		0.041
Nonane	0.004		2.99E-06		3.83E-04	0.0059		0.027
Decane	0.006		3.57E-06		5.08E-04	0.0078		0.036
Undecane	0.007		4.01E-06		6.27E-04	0.0096		0.045
Dodecane	0.007		3.43E-06		5.83E-04	0.0090		0.042
Tridecane	0.009		4.14E-06		7.71E-04	0.0119		0.055
Tetradecane	0.016		6.63E-06		1.31E-03	0.0202		0.094
Pentadecane	0.077		2.90E-05		6.16E-03	0.0948		0.438
Hexadecane	0.060		2.07E-05		4.69E-03	0.0721		0.333
Heptadecane	0.148		4.81E-05		1.16E-02	0.1779		0.823
Octadecane	0.078		2.35E-05		5.98E-03	0.0921		0.426

Table F-16 Calculated data for regenerated Ru/Al₂O₃ at 450 °C

Variable	Unit	Value		Unit	Value		Unit	Value
n-Alkanes in product	[g]	3.845	Diesel range product	[g]	2.911	Diesel range yield	[%]	26.37
Unreacted oil	[g]	3.142	n-Alkane product yield	[%]	34.83	Solid product yield	[%]	19.61
Gasoline range product	[g]	0.557	Gasoline range yield	[%]	5.04	Gas product yield	[%]	17.11
Kerosene range product	[g]	0.377	Kerosene range yield	[%]	3.42	Oil conversion	[%]	71.54
Compound	Ratio _{Area}		Moles _{sample}		Mass _{sample}	Mass Fraction _{sample}		Mass _{liquid product}
Pentane	0.002		4.28E-06		3.09E-04	0.0043		0.030
Hexane	0.005		6.26E-06		5.39E-04	0.0075		0.052
Heptane	0.011		1.11E-05		1.11E-03	0.0154		0.108
Octane	0.017		1.41E-05		1.61E-03	0.0223		0.156
Nonane	0.011		8.10E-06		1.04E-03	0.0144		0.101
Decane	0.013		7.98E-06		1.14E-03	0.0158		0.110
Undecane	0.015		8.22E-06		1.28E-03	0.0178		0.125
Dodecane	0.014		6.96E-06		1.19E-03	0.0165		0.115
Tridecane	0.017		7.61E-06		1.42E-03	0.0197		0.138
Tetradecane	0.023		9.60E-06		1.90E-03	0.0265		0.185
Pentadecane	0.068		2.59E-05		5.51E-03	0.0765		0.534
Hexadecane	0.100		3.52E-05		7.98E-03	0.1108		0.774
Heptadecane	0.106		3.49E-05		8.39E-03	0.1165		0.814
Octadecane	0.080		2.44E-05		6.22E-03	0.0863		0.603

Table F-17 Calculated data for regenerated Ni/Al₂O₃ at 400 °C

Variable	Unit	Value		Unit	Value		Unit	Value
n-Alkanes in product	[g]	4.107	Diesel range product	[g]	3.730	Diesel range yield	[%]	33.79
Unreacted oil	[g]	2.261	n-Alkane product yield	[%]	37.20	Solid product yield	[%]	29.43
Gasoline range product	[g]	0.180	Gasoline range yield	[%]	1.63	Gas product yield	[%]	12.89
Kerosene range product	[g]	0.197	Kerosene range yield	[%]	1.78	Oil conversion	[%]	79.52
Compound	Ratio _{Area}		Moles _{sample}		Mass _{sample}		Mass Fraction _{sample}	Mass _{liquid product}
Pentane	0.000		0.00E+00		0.00E+00		0.0000	0.000
Hexane	0.001		1.28E-06		1.10E-04		0.0007	0.004
Heptane	0.006		5.88E-06		5.89E-04		0.0037	0.024
Octane	0.012		1.05E-05		1.20E-03		0.0076	0.048
Nonane	0.012		8.89E-06		1.14E-03		0.0072	0.046
Decane	0.016		1.01E-05		1.43E-03		0.0090	0.058
Undecane	0.018		1.04E-05		1.63E-03		0.0103	0.066
Dodecane	0.014		6.94E-06		1.18E-03		0.0075	0.048
Tridecane	0.024		1.12E-05		2.08E-03		0.0132	0.084
Tetradecane	0.018		7.50E-06		1.49E-03		0.0094	0.060
Pentadecane	0.283		1.09E-04		2.32E-02		0.1464	0.932
Hexadecane	0.077		2.74E-05		6.21E-03		0.0392	0.250
Heptadecane	0.622		2.07E-04		4.99E-02		0.3148	2.005
Octadecane	0.152		4.73E-05		1.20E-02		0.0760	0.484

Table F-18 Calculated data for regenerated Ni/Al₂O₃ at 425 °C

Variable	Unit	Value		Unit	Value		Unit	Value
n-Alkanes in product	[g]	3.527	Diesel range product	[g]	2.959	Diesel range yield	[%]	26.80
Unreacted oil	[g]	2.297	n-Alkane product yield	[%]	31.95	Solid product yield	[%]	23.52
Gasoline range product	[g]	0.329	Gasoline range yield	[%]	2.98	Gas product yield	[%]	23.72
Kerosene range product	[g]	0.239	Kerosene range yield	[%]	2.17	Oil conversion	[%]	79.19

Compound	Ratio _{Area}	Moles _{sample}	Mass _{sample}	Mass Fraction _{sample}	Mass _{liquid product}
Pentane	0.000	0.00E+00	0.00E+00	0.0000	0.000
Hexane	0.005	6.90E-06	5.95E-04	0.0037	0.022
Heptane	0.016	1.62E-05	1.62E-03	0.0101	0.059
Octane	0.027	2.32E-05	2.65E-03	0.0164	0.096
Nonane	0.022	1.59E-05	2.04E-03	0.0127	0.074
Decane	0.025	1.54E-05	2.19E-03	0.0136	0.079
Undecane	0.027	1.51E-05	2.36E-03	0.0146	0.085
Dodecane	0.022	1.08E-05	1.83E-03	0.0114	0.066
Tridecane	0.029	1.29E-05	2.41E-03	0.0150	0.087
Tetradecane	0.025	1.04E-05	2.06E-03	0.0128	0.075
Pentadecane	0.257	9.72E-05	2.07E-02	0.1284	0.748
Hexadecane	0.088	3.07E-05	6.96E-03	0.0433	0.252
Heptadecane	0.517	1.69E-04	4.05E-02	0.2520	1.468
Octadecane	0.148	4.53E-05	1.15E-02	0.0716	0.417

Table F-19 Calculated data for regenerated Ni/Al₂O₃ at 450 °C

Variable	Unit	Value		Unit	Value		Unit	Value	
n-Alkanes in product	[g]	4.881	Diesel range product	[g]	3.908	Diesel range yield	[%]	35.40	
Unreacted oil	[g]	2.137	n-Alkane product yield	[%]	44.21	Solid product yield	[%]	12.16	
Gasoline range product	[g]	0.506	Gasoline range yield	[%]	4.59	Gas product yield	[%]	24.28	
Kerosene range product	[g]	0.467	Kerosene range yield	[%]	4.23	Oil conversion	[%]	80.64	
Compound		Ratio _{Area}			Moles _{sample}		Mass _{sample}	Mass Fraction _{sample}	Mass _{liquid product}
Pentane		0.000			0.00E+00		0.00E+00	0.0000	0.000
Hexane		0.003			4.92E-06		4.24E-04	0.0027	0.019
Heptane		0.014			1.51E-05		1.52E-03	0.0095	0.067
Octane		0.029			2.66E-05		3.04E-03	0.0191	0.134
Nonane		0.030			2.31E-05		2.96E-03	0.0186	0.130
Decane		0.037			2.50E-05		3.56E-03	0.0223	0.157
Undecane		0.041			2.44E-05		3.81E-03	0.0239	0.168
Dodecane		0.035			1.88E-05		3.19E-03	0.0200	0.141
Tridecane		0.040			1.93E-05		3.60E-03	0.0226	0.158
Tetradecane		0.040			1.77E-05		3.52E-03	0.0221	0.155
Pentadecane		0.239			9.77E-05		2.07E-02	0.1302	0.913
Hexadecane		0.117			4.41E-05		9.99E-03	0.0627	0.440
Heptadecane		0.471			1.66E-04		3.99E-02	0.2504	1.757
Octadecane		0.174			5.74E-05		1.46E-02	0.0916	0.643

Table F-20 Calculated kinetic data

Catalyst	Variable	Temperature [°C]		
		400	425	450
Ru/Al ₂ O ₃ (F)	k''	9.83E-02	1.23E-01	1.14E-01
	k'	9.40E-07	1.22E-06	1.17E-06
	k (m ⁶ /mol/g/s)	4.46E-10	5.99E-10	5.94E-10
	Ln (k)	-21.53	-21.24	-21.24
Ni/Al ₂ O ₃ (F)	k''	3.40E-02	4.01E-02	4.01E-02
	k'	3.26E-07	3.97E-07	4.12E-07
	k (m ⁶ /mol/g/s)	1.54E-10	1.95E-10	2.10E-10
	Ln (k)	-22.59	-22.36	-22.29
NiMo/SiO ₂ (F)	k''	4.69E-02	5.92E-02	7.71E-02
	k'	4.49E-07	5.87E-07	7.92E-07
	k (m ⁶ /mol/g/s)	2.13E-10	2.88E-10	4.03E-10
	Ln (k)	-22.27	-21.97	-21.63
CoMo/SiO ₂ (F)	k''	2.80E-02	3.24E-02	3.30E-02
	k'	2.68E-07	3.21E-07	3.39E-07
	k (m ⁶ /mol/g/s)	1.27E-10	1.58E-10	1.72E-10
	Ln (k)	-22.79	-22.57	-22.48
Ru/Al ₂ O ₃ (R)	k''	2.51E-02	2.67E-02	3.23E-02
	k'	2.40E-07	2.65E-07	3.32E-07
	k (m ⁶ /mol/g/s)	1.14E-10	1.30E-10	1.69E-10
	Ln (k)	-22.90	-22.76	-22.50
Ni/Al ₂ O ₃ (R)	k''	4.15E-02	4.11E-02	4.30E-02
	k'	3.97E-07	4.07E-07	4.41E-07
	k (m ⁶ /mol/g/s)	1.88E-10	2.00E-10	2.25E-10
	Ln (k)	-22.39	-22.33	-22.22